Ancile 0

Design Synthesis Exercise Autumn 2012

Final Report

Version 2

Internal Structure and Composition of Mars

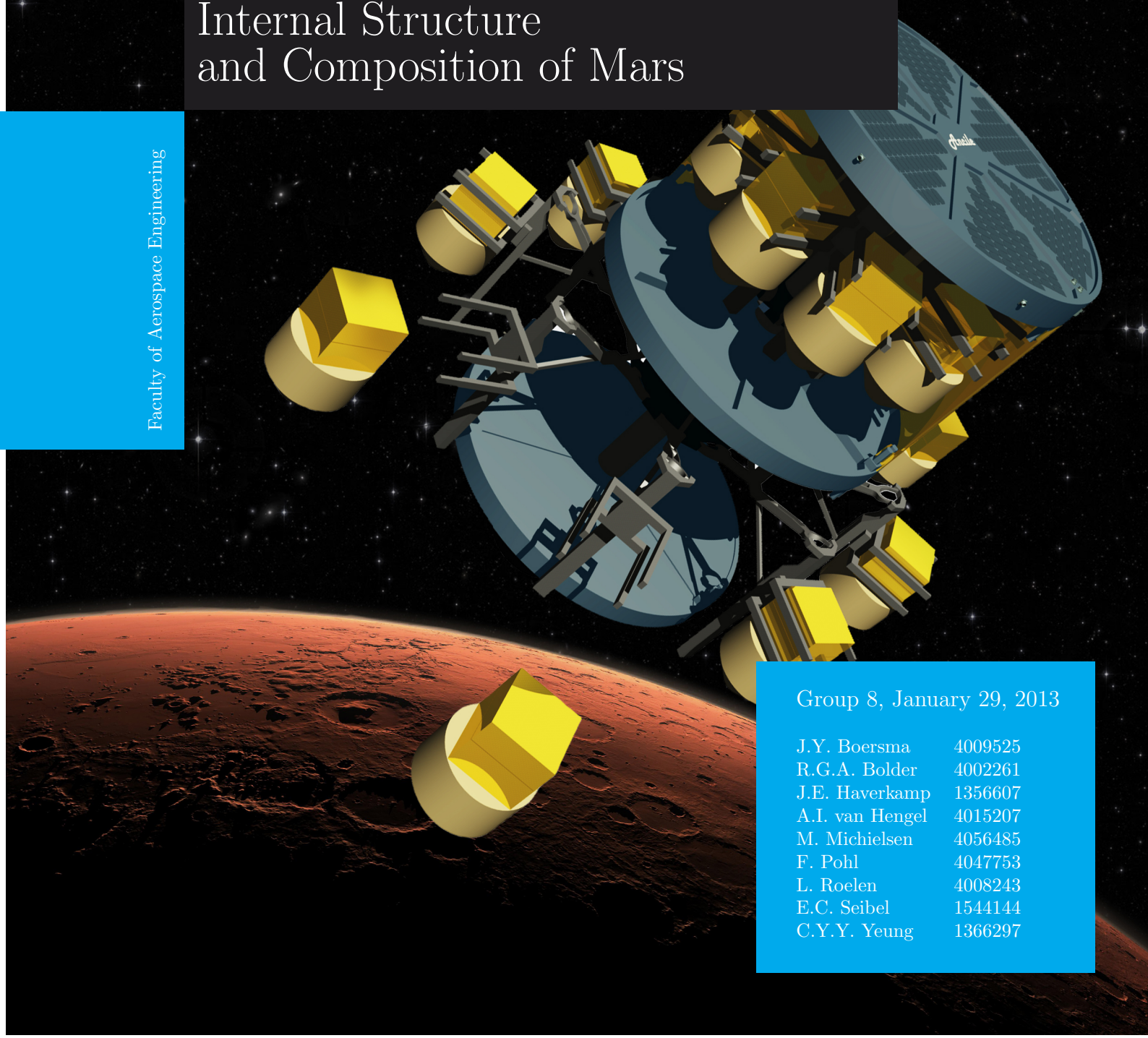

Faculty of Aerospace Engineering

Group 8, January 29, 2013

J.Y. Boersma	4009525
R.G.A. Bolder	4002261
J.E. Haverkamp	1356607
A.I. van Hengel	4015207
M. Michielsen	4056485
F. Pohl	4047753
L. Roelen	4008243
E.C. Seibel	1544144
C.Y.Y. Yeung	1366297

TU Delft Delft University of Technology

Challenge the future

Preface

This report describes the detailed design phase for tectonics-movement measuring on Mars as part of the Design Synthesis Exercise (DSE). It is initiated as final project of the BSc. by the faculty of Aerospace Engineering at Delft University of Technology. In this report the design will be defined, verified and validated within their subsystems. The analysis includes performance, risk, secondary objectives and sustainability. Finally, the fully integrated system is presented in more detail.

This report has been completed with the help of the entire project team during ten weeks of work, deliberation and writing. We would like to thank sincerely our supervisor E. Schrama and two coaches J. Melkert and A. Cervone for their help in answering questions and for participating enthusiastically and constructively in this project. In addition, many thanks to E. Mooij for his support regarding the analysis of 'Entry, Descent and Landing phase' on Mars, G. Drijkoningen for providing his expertise on seismic measurements, C. Verhoeven for his advice on antennas, solar panels and electronics, W. Broere for providing information about soil penetration and L. Gurvitz for his contribution to radio astronomy. We also pronounce our thanks to NASA, department for flight vehicle atmospheric environments for making the software 'Mars GRAM' available for our investigation of the Mars atmosphere. Finally, we thank C. Kassapoglou for his expert opinion on damping systems and structural integrity.

Summary

The goal of this project is to design a mission that can investigate plate tectonics on Mars and give insight into the internal structure of Mars. Here a design including 16 probes, landing in a grid on Mars and measuring both relative movement and seismic activities, was chosen. The measurement techniques used are *near-field VLBI*, *seismic interferometry* and the basic principle of seimology; *Ray's theory* respectively.

The 16 probes will be launched at once with the Ariane 5G on the 1st of May in 2018. After launch the space bus will be in a low earth orbit at 200 km height. After a change in velocity of 3.6 km/s the space bus will begin its transfer to Mars. During which the batteries of the probes will be charged by the solar panels attached to the bus. Near Mars the velocity and spin rate will be adjusted to meet the probe release conditions. The outer shell that covered the probes during their transfer will be ejected into space. The first circular clamping mechanism will increase in radius and spin up. The probes are attached to the release system by a magnetic and mechanical clamping system. First the mechanical clamping system is retracted, after which the magnetic clamps will be cut from power releasing the first eight probes towards Mars. The probe bus will be slowed down and the second bunch of probes will be released in the same fashion. The probes will experience a 10 to 15 rpm spin rate induced at release. This spin rate will need to be decreased to 0.1 rpm. This is done by a *stretch YoYo* system attached to each probe. After de spinning the *stretch YoYos* will be released. The heat shield will then be inflated before entering the Martian atmosphere. The entry angles of the landers range between 11^{circ} to 29^{circ}. The average velocity at entering is 5.6 km/s. At Mach 1.77 the parachutes will be deployed, slowing the probes down to subsonic velocities. The inflatable heat shields will have to be adjusted in shape, in order to keep the probe stable, when the velocity is decreased to the subsonic zone. At approximately 100 m above the ground the parachutes will be released. Each probe will penetrate the surface with an average speed of 100 m/s. The pin will penetrate the inflatable and the ground and come to a stand still, having penetrated the crust of Mars at least 45 cm. When the probes have landed on Mars the solar panel will be deployed and the measurements can start.

The deep space network will send radio waves at a constant frequency into space. These waves are received by each probe individually. The received signal is mixed-down with a constant signal produced by a local oscillator in the probe. The resulting signal will be stored. A down link through the MRO is created which regularly sends the data back to Earth. On Earth, the data can be analyzed.

Table of Contents

1 Introduction **1**

2 Mission Description **2**
2.1 Scientific goals . . . 2
2.2 Functional Flow Diagram . . . 3
2.3 Functional Breakdown Structure . . . 4
2.4 Market Analysis . . . 5
2.5 Mission description . . . 9

3 Mission Operations **11**
3.1 Measurement techniques . . . 11
3.2 Scenario analysis for the required amount of landers . . . 21
3.3 Accuracy . . . 22

4 Probe **26**
4.1 Probe Design Description . . . 26
4.2 Communications . . . 26
4.3 Payload . . . 32
4.4 Penetration Depth and Pin Design . . . 36
4.5 Power . . . 39
4.6 Crushable Honeycomb Structure . . . 48
4.7 Thermal Control . . . 51
4.8 Command and Data Handling . . . 55
4.9 Layout . . . 56
4.10 Instrument Box . . . 58

5 Earth-Mars Transfer **63**
5.1 Launch . . . 63
5.2 Transfer Module . . . 67
5.3 Transfer Orbit . . . 74
5.4 Approach . . . 81
5.5 Entry, Descent and Landing . . . 95

6 System Analysis **107**
6.1 Risk Assessment . . . 107
6.2 Sensitivity Analysis . . . 109
6.3 Resource Allocation . . . 109
6.4 Sustainable Development Strategy . . . 110
6.5 Compliance Matrix . . . 113

7 Conclusion **116**
7.1 Conclusion . . . 116
7.2 Recommendations . . . 116

Appendix A: Project Organization and Design & Development Logic **117**

Appendix B: Gantt Chart **118**

Appendix C: Who did what **120**

List of Figures

2.1 Functional Flow Diagram . . . 3
2.2 Functional Breakdown structure . . . 4
2.3 Functional Breakdown structure . . . 5
2.4 Business environment with the stakeholders . . . 6
2.5 Accomplished Mars missions of ESA and NASA per century . . . 7
2.6 SWOT analysis of the Mars mission . . . 8
2.7 Annual budget of ESA and NASA in the last Century . . . 9

3.1 Baseline calculation using radio interferometry (from [87]) . . . 11
3.2 Recievers surrounded by enery sources . . . 15
3.3 Recievers surrounded by joined noise sources . . . 15
3.4 Impact Velocities vs Entry Velocities [31] . . . 17
3.5 Ratio vs Entry Velocities [31] . . . 18
3.6 List of Mars entering meteoroids [31] . . . 19
3.7 Martian meteroids, their occurance and impacts [31] . . . 19
3.8 Plane waves and spherical waves [84] . . . 19
3.9 Changes due to refraction of a wave front [84] . . . 20
3.10 Wavefront reaching a material boundary [84] . . . 20
3.11 The forming of headwaves [84] . . . 20
3.12 Baselines . . . 21
3.13 Sampling pattern phased array antenna and the resulting frequencies . . . 24

4.1 Cross-section of the probe, showing all of its components . . . 27
4.2 A general (8 by 8) phased array antenna . . . 27
4.3 The phased array antenna mounted on the instrument box . . . 29
4.4 A Chip-Sized Atomic Clock . . . 33
4.5 The principle of the VBB seismometer [75] . . . 34
4.6 The VBB seismometer [75] . . . 35
4.7 Model based performances [75] . . . 35
4.8 Results of the performance tests [75] . . . 35
4.9 Penetration Depth as a function of Soil Penetrability . . . 37
4.10 Penetration Depth as a function of Velocity . . . 38
4.11 Penetration Depth as a function of Soil Penetrability . . . 39
4.12 Example of a rollable solar panel [13] . . . 42
4.13 Schematic drawing of solar roll . . . 42
4.14 Unrolling solar panel . . . 43
4.15 Dust shield with dust [1] . . . 46
4.16 Dust shield after dust removal [1] . . . 46
4.17 Unregulated bus using linear charge, current control and recharge control . . . 47
4.18 Electrical block diagram . . . 47
4.19 Crushable aluminum honeycomb structures and their loading pattern . . . 48
4.20 Ballistic air-gun shock test for dynamically testing the performance of many kinds of crushable honeycomb structures [34]. . . . 49
4.21 Probe dimensions . . . 50
4.22 Probe components . . . 50
4.23 G-loads, velocity and depth of penetration . . . 52
4.24 Thermal conditions on Mars depending on latitude during aphelion (figure taken from NASA's Mars Transportation Environment Definition Document [14]) . . . 53

4.25 Thermal conditions on Mars depending on latitude during perihelion (figure taken from NASA's Mars Transportation Environment Definition Document [14]) 54
4.26 The Hardware - Software block diagram 56
4.27 The Data Handling block diagram 57
4.28 Internal layout of the instrument box 57
4.29 Top view of the external layout of the instrument box 58
4.30 The deceleration experienced by the instrument box for landing in soft and hard soil. . 59
4.31 An illustration of the normal forces acting on the instrument box during the first phase of the impact 59
4.32 An illustration of the area on which the shear stress acts on the instrument box, due to the penetrator in the first phase 60
4.33 An illustration of the area on which the shear stress acts on the instrument box, due to the OCHS in the second phase 60
4.34 The maximum normal and shear stresses experienced by the bottom plate of the instrument box. 61
4.35 The highest bending stress in the cross-section of the instrument box. 62

5.1 Structural mass fraction of Ariane 5. The total dry mass is 35,200 kg 64
5.2 Ariane 5 payload capsule [78] 65
5.3 Ancile space-bus dimensions 65
5.4 Required Escape velocity with respect to launch-year [43] 65
5.5 Required travel time with respect to launch-year [43] 66
5.6 Launch sequence of the Ariane 5 [78] 67
5.7 Layout of the transfer module 68
5.8 Q_{in} of the transfer module from Earth to Mars 70
5.9 Temperature of the transfer module from Earth to Mars with insulation and a radiator area of 0.86 m^2 without louvers and heaters 71
5.10 Electronic block diagram of the transfer module 75
5.11 A spiral trajectory with electric propulsion [94] 75
5.12 Venus gravity assist trajectory [73] 76
5.13 Moon gravity assist trajectory [77] 77
5.14 Hohmann transfer [36] 77
5.15 Direct transfer [73] 78
5.16 Optimal planet constellation during mission time-line 80
5.17 The transfer module with both a stowed and extended probe mechanism 82
5.18 Two kinetic diagrams showing the movement of the transfer module and the probes before and after the release procedure, note the change in scale 83
5.19 Influence of release timing on landing area 85
5.20 Influence of first release angular velocity on landing area 85
5.21 Influence of second release angular velocity on landing area 86
5.22 Influence of release timing on entry angles 86
5.23 Influence of first release angular velocity on entry angles 86
5.24 Influence of second release angular velocity on entry angles 86
5.25 An overview of the approach trajectory inside the sphere of influence 87
5.26 The trajectories of the transfer module and probes during the release phase, not to scale 87
5.27 The individual probe trajectories during the entry in the atmosphere of Mars 88
5.28 The landing area of the probes, including the rotational drift on the surface of Mars due to their different arrival times 89
5.29 Typical designs of stretch YoYos [41] 90
5.30 Estimation for the MOI for the heat shield 91
5.31 Top view of the outer crushables 91
5.32 The instrument box including its de-spinning mechanism 94
5.33 Probe with inflated heat shield 95
5.34 Packed probe 97
5.35 Free Body Diagram 99
5.36 Kinetic Diagram 99
5.37 Free Body Diagram 100
5.38 Kinetic Diagram 100

5.39 Vertical Distance to Height . . . 105
5.40 Velocity to Height . . . 105
5.41 Acceleration to Height . . . 105
5.42 Acceleration to time . . . 105
5.43 Heating Rate to Height . . . 106
5.44 Entry, Descent and Landing . . . 106

6.1 Risk map for the Ancile mission . . . 107
6.2 Budget spent per year . . . 111
6.3 Compliance Matrix . . . 114
6.4 Compliance Matrix . . . 115

7.1 Gantt chart, part 1 . . . 118
7.2 Gantt chart, part 2 . . . 119

List of Tables

4.1 Dimensions and masses of the components installed on the probe . . . 26
4.2 Calculated values regarding the DSN transmissions . . . 30
4.3 Calculated values regarding probe transmissions . . . 31
4.4 Calculated values for the receiving antenna on the orbiter . . . 32
4.5 Chip-Scaled Atomic Clock specifications . . . 33
4.6 Initial values to calculate Penetration Depth . . . 36
4.7 Penetration Depth for various Cone Shapes . . . 37
4.8 Final values to calculate Penetration Depth . . . 39
4.9 Probe power distribution. This table shows the average power used by the probes subsystems during nominal operation . . . 40
4.10 Daily solar irradiance on Mars (W-hrs/m^2), for latitude and longitude around Valles Marineris [80] . . . 40
4.11 Parameters for existing rolled solar panels produced by PowerFilm Solar [13] . . . 42
4.12 Solar roll dimensions . . . 43
4.13 Thermal requirements for probe components. . . . 53
4.14 Typical command and data handling parameters for combined systems [94] . . . 56

5.1 Payload dimensions . . . 63
5.2 Launchers [78] [95] [15] . . . 63
5.3 Thruster characteristics [78] . . . 64
5.4 Launch mass fraction . . . 64
5.5 Launch Windows [43] [24] [62] . . . 66
5.6 Launch sequence . . . 67
5.7 Star and Sun sensors used in the transfer module . . . 69
5.8 Operational temperature rage of subsystems in the transfer module [53] [54] [94] . . . 70
5.9 Values regarding the transmitting transfer module antenna . . . 72
5.10 Transmission losses . . . 72
5.11 Values regarding the receiving DSN antenna . . . 73
5.12 Final link budget values . . . 73
5.13 Power consumption of subsystems in the transfer module . . . 74
5.14 Summary of Transfer Orbits . . . 78
5.15 Parameters for calculations [72] . . . 79
5.16 Initial conditions and requirements for release procedure . . . 83
5.17 Approach parameter summary . . . 84
5.18 Structure Dimensions . . . 94
5.19 Previous missions [23] . . . 102
5.20 Changeable Inputs of the System . . . 103
5.21 Changeable Inputs of the System . . . 104

List of Abbreviations

AC	Alternating Current
BER	Bit Error Rate
BW	Bandwidth
C&DH	Command and Data Handling
COPUOS	Committee on the Peaceful Usages of Outer Space
DSN	Deep Space Network
EAP	Solid Rocket Booster
EDL	Entry Descent and Landing
EIRP	Equivalent Isotropic Radiated Power
EOL	End of Life
EPC	Cryogenic Main Core Stage
ESA	European Space Agency
FY	Fiscal Year
GPS	Global Positioning System
JIVE	Joint Institute for VLBI in Europe
LEO	Low Earth Orbit
LO	Local Oscillator
MATLAB	Matrix laboratory
MLI	Multilayer Insulation
MNS	Mission Need Statement
MSL	Mars Science Laboratory
MRO	Mars Reconnaissance Orbiter
NASA	National Aeronautics and Space Administration
OCHS	Outer Crushable Honeycomb Structure
RTG	Radioisotope Thermoelectric Generator
SCHS	Seismometer Crushable Honeycomb Structure
SI	Seismic Interferometry
SWOT	Strengths, Weaknesses, Opportunities and Threats
TU Delft	Delft University of Technology
UCLA	University of California, Los Angeles
UN	United Nations
US	United States
VBB	Very Broad Band
VLBI	Very Long Baseline Interferometry
VPM	Venus Pioneer Multiprobe

Version History

Final Report v2.1, 29-January-2013

Improved Subsection 4.5.2 Deployment

Improved Figures 5.17 and 5.18 black and white version

Corrected Figure 5.11

Final Report v2.0, 25-January-2013

Improved Citations and references

Improved Sections

Improved Chapter 1 Introduction

Improved Section 2.1 Scientific goals

Improved Subsection 3.1.1 Primary measurement technique

Improved Section 3.2 Scenario analysis

Improved Section 4.1 Probe description

Improved Subsection 4.3.1 Frequency standard

Improved Subsection 4.3.2 Seismometer

Improved Section 4.6 Crushable honeycomb structure

Improved Section 4.9 Figures

Improved Section 4.10 Instrument box and figure

Improved Section 5.1 Launch

Improved Subsection 5.2.2 Attitude determination

Improved Subsection 5.2.5 Link budget

Improved Section 5.3 Transfer orbit

Improved Section 6.1 Risk assessment

Improved Section 6.2 Sensitivity analysis

Improved Section 6.4 Sustainable development

Added Coverpage

Added Subsection 3.3.1 Primary accuracy

Added Section 4.2 Pictures, references and explanations

Added Subsection 4.5.2 Calculation for solar roll diameter

Added Subsection 4.6.4 Figure

Added Subsection 4.8.2 HW/SW diagram

Added Subsection 4.8.3 Data handling diagram

Added Subsection 5.2.1 Transfer module layout picture

Added Subsection 5.2.3 Equations

Added Subsection 5.2.4 References

Added Subsection 5.4.1 Main figures, model verification and velocity vector explanation

Added Subsection 5.5.4 Verification and validation of descending tool

Added Section 6.5 Compliance matrix

Final Report v1.1, 22-January-2013

Improved Subsection 3.1.1 Primary mission

Added Section 3.2 Scenario analysis for the required amount of landers

Added Section 5.4 Approach

Final Report v1, 21-January-2013

Created Draft version of the Final Report.

Chapter 1

Introduction

Only 50 years ago, plate tectonics was accepted as a phenomenon on Earth by the geoscientific community. However, not all questions about plate tectonics have been resolved. Does it only exist on Earth or do planets like our neighbour Mars also know the phenomenon? If it could be proven that plate tectonics exist on Mars, other planets in the Milky Way and far beyond are more likely to also have plate tectonics. This will lead to a better understanding of the planets surrounding us and those millions of light-years away.

Long ago the god Mars sent an ancient shield called Ancile to Earth, declaring Rome the mistress of the world. Many identical copies were made, called Ancilia and it is time to send them back from where they came. The Ancile mission will send 16 probes to the surface of Mars to detect if plate tectonics exist. They will penetrate the ground in two circles around *Valles Marineris*, which is believed to be a geological feature indicating plate boundaries. If any movement occurs around this large canyon during the 5 operational mission years, the probes will detect it. Wind noise and natural meteoroid impacts will allow the probes to map the crust of Mars.

Chapter 2 will present a quick overview of the mission, state the scientific goals and the market analysis. In chapter 3, the missions operations are discussed, followed by an in depth description of the probes that land on Mars in chapter 4. Chapter 5 explains the Earth-Mars transfer, including the entry, descend and landing of the probes. The system analysis, which includes risk assessment, resource allocation and sustainable development strategy, is discussed in chapter 6 and finally chapter 7 contains the conclusion and recommendations.

Chapter 2

Mission Description

2.1 Scientific goals

The primary goal of this mission is to determine whether plate tectonics exist on Mars. This question is one of the most disputed by scientist in the fields of planetary geosciences. It was flared up again after a publication of geologist Prof. An Yin of UCLA on the possible role of plate tectonics in the formation of Valles Marineris [97]. Investigating this will provide a substantial step towards understanding the geological history of the planet Mars and the formation of our solar system and its planets.

For plate tectonics to be present, an active liquid core is required underneath a planet's mantle. Strong convection flows can force parts of the lithosphere to move or deform, thus creating tectonic movement. In general plate tectonics can directly be related to seismic events. Due to the forces that are released when two plates move along side each other, energy is set free.

However, only little is known about the internal structure of Mars. From the fact that Mars does not have a strong magnetosphere, scientists deduce that the internal dynamics are less than on Earth. Whether or not it generates forces strong enough to sustain plate tectonics is simply not known. The only seismometer that was ever in operation on the surface of Mars did not give any conclusive evidence of the existence of Marsquakes [16].

Therefore, this mission will send sixteen probes to Mars, penetrating the surface around Valles Marineres, the biggest suspected fault line on the planet. These landers consist of a primary payload that will measure plate tectonics and a secondary payload, consisting of seismometers, to further investigate the structure of the subsurface of Mars.

2.2 Functional Flow Diagram

In figure 2.1 the *Function flow diagram* of the final design is illustrated.

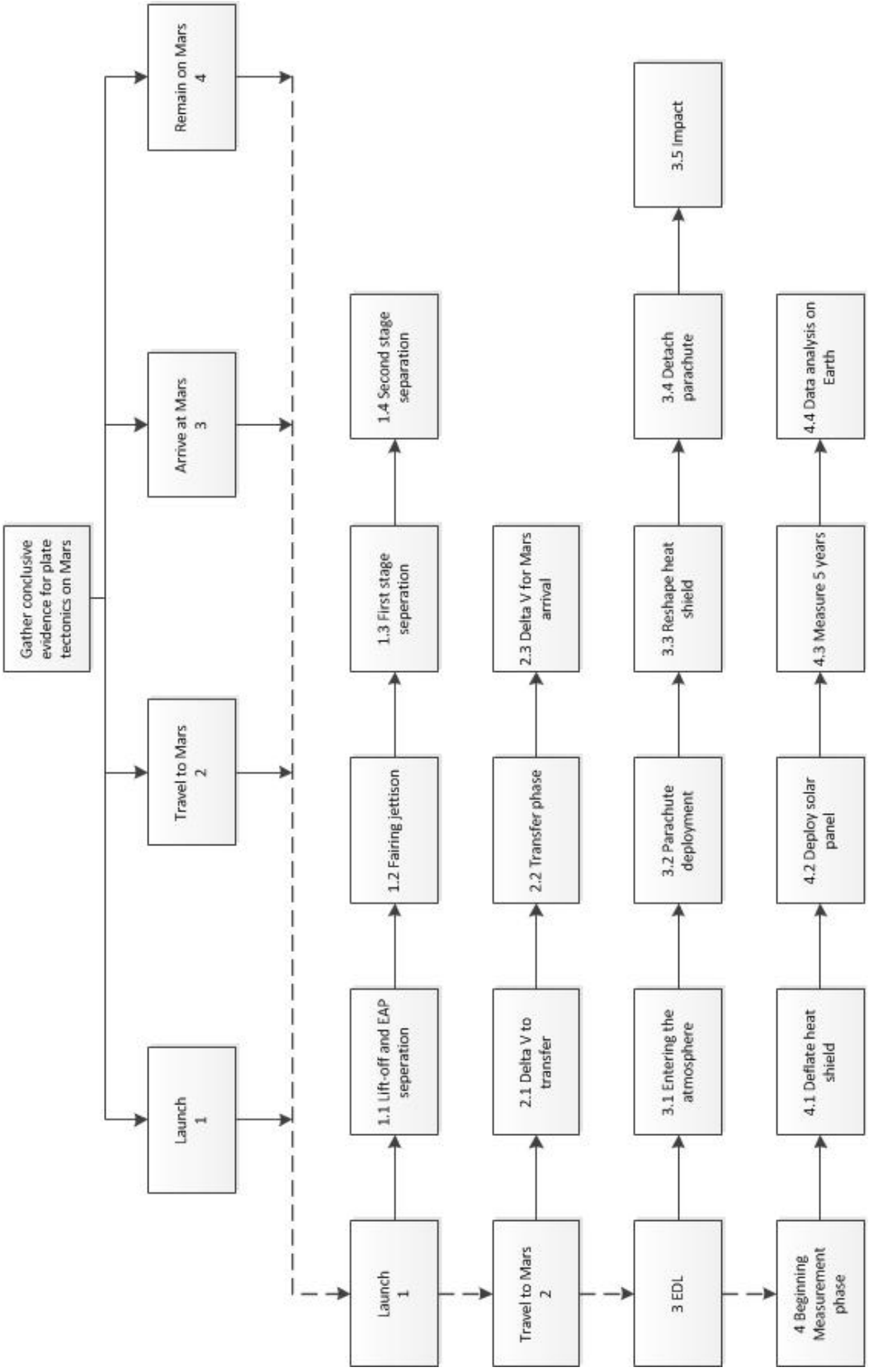

Figure 2.1: Functional Flow Diagram

2.3 Functional Breakdown Structure

In figure 2.2 and 2.3 the *Function breakdown structure* of the final design is illustrated.

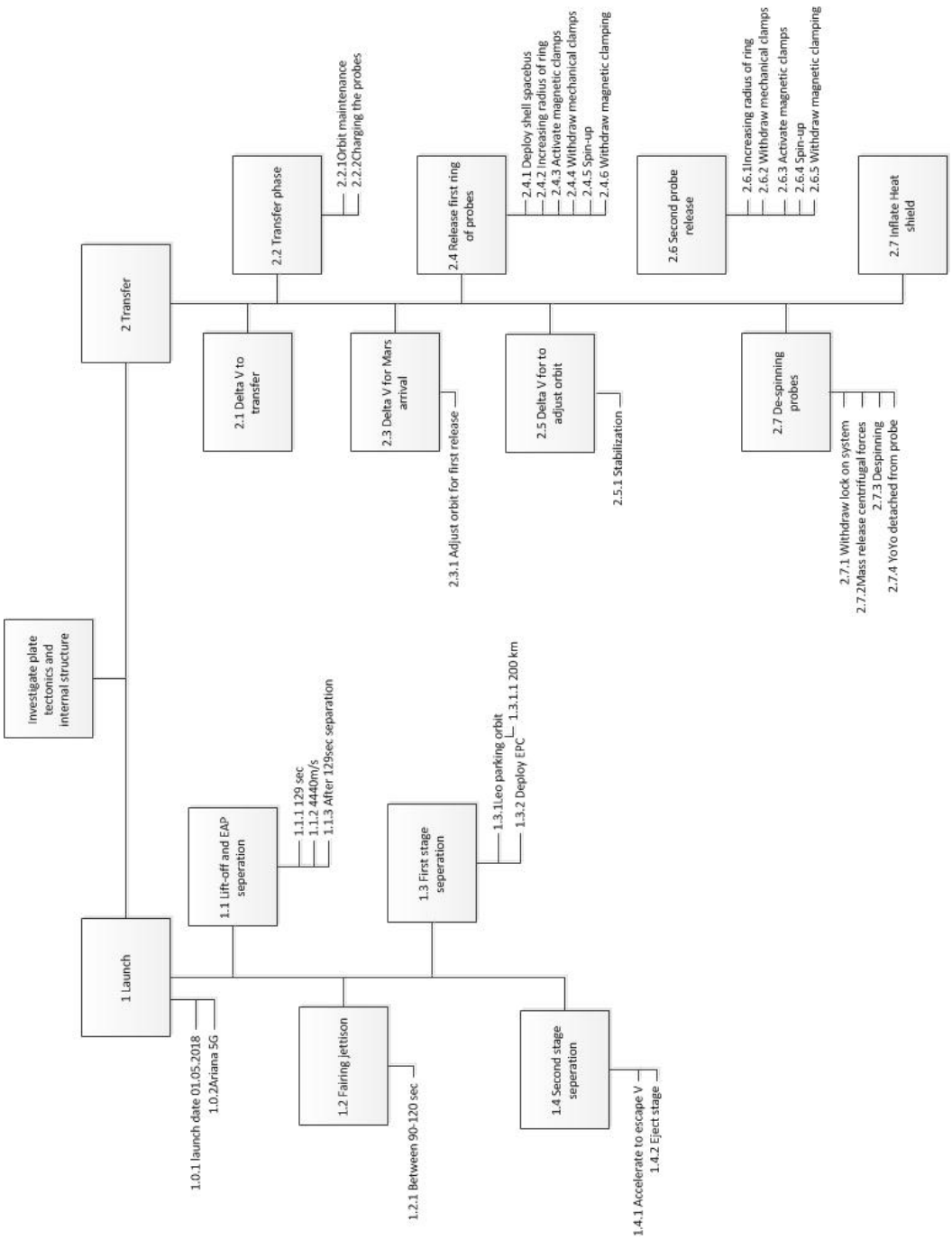

Figure 2.2: Functional Breakdown structure

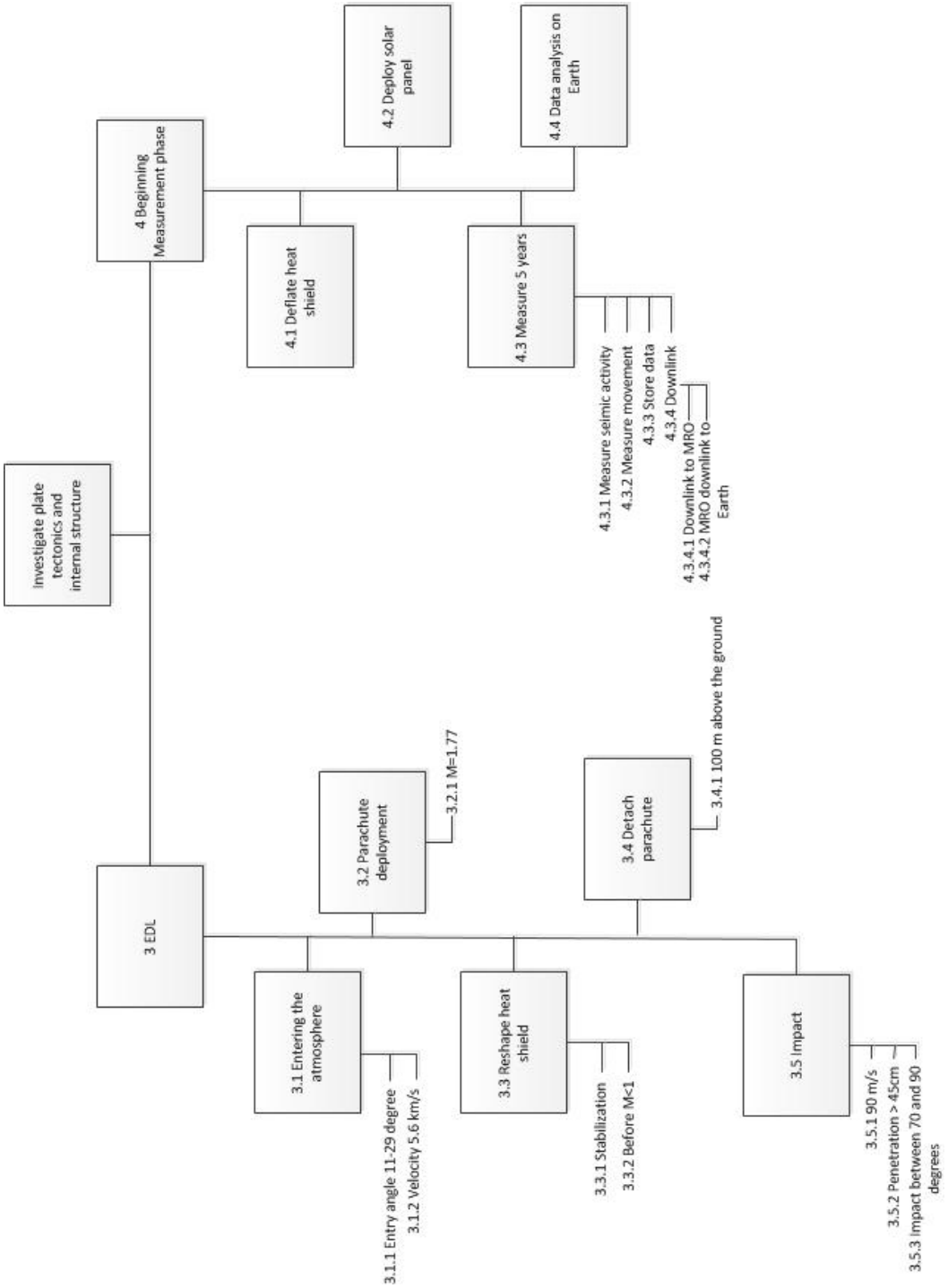

Figure 2.3: Functional Breakdown structure

2.4 Market Analysis

This chapter contains the market analysis for the mission, and identifies the stakeholders and their roles within this environment. Different tools are used to illustrate this, e.g. a business environment visualization, a SWOT analysis and a market dynamics graph. In addition, the Market attractiveness is described.

2.4.1 Market environment

The market consists of stakeholders, which could have influence on, or conversely, be influenced by the mission. The environment in which these stakeholders are in respect to the mission is visualized in figure 2.4.

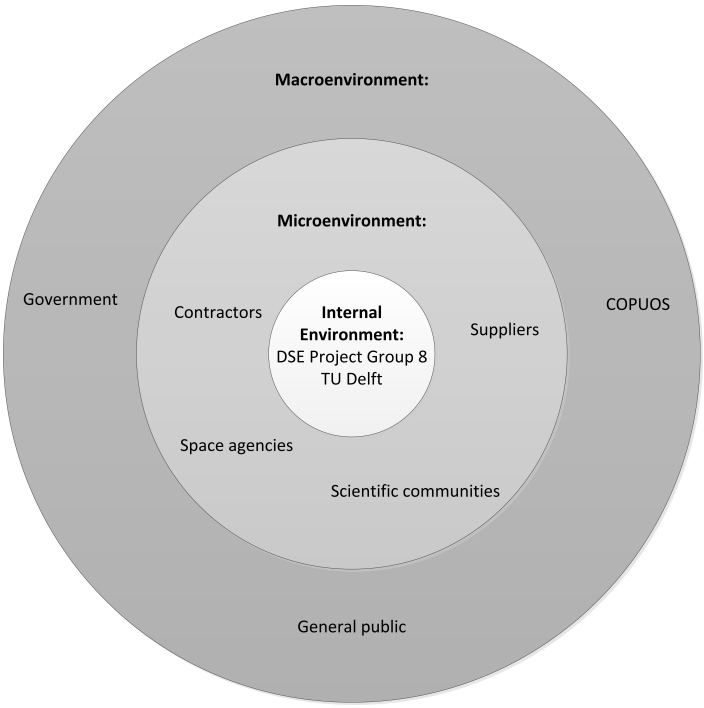

Figure 2.4: Business environment with the stakeholders

Scientific community

The interest of the scientific community defines the mission, hence the results will used by the community to further increase understanding of Earth's neighboring planet. In addition, the used instruments and Data collection may be used by future researchers to achieve their own intentions.

Space agencies

As the potential investors these agencies have invaluable expertise throughout the decades of dedicated space missions. With launching sites, well-equipped facilities for operation, experienced personnel and highly acclaimed reputation, they form a good base to transform a good idea into a final product. Examples of said agencies are NASA and ESA.

Government

The most important space agencies, namely ESA and NASA, are funded by a governmental budget. In the case of ESA the funding comes even from multiple governments. The elected-nature of these political organs have varied consequences on the mission. They can lead the attention to certain projects. However, possible economic issues or other events might affect this space mission. Therefore, the time to present the design concept should be observed before.

General public

The source of the funding is governmental, i.e. tax money from citizens. The public will have an opinion about the mission, and with the press as amplification, this could affect the political support. Within this group there are the environmentalists with creative outcries against the usage of fossil fuels for rockets and radioactive material for power generation.

Technical University Delft

Working as a group of student-scientists educated by TU Delft, the university puts its mark on the project. The guidance of the tutors, the list of adviser, the library and the facilities determine the overall quality of the final design.

COPUOS

Committee on the Peaceful Usages of Outer Space, a branch of the UN, is the international organization that supervises the process of using outer space, according to five treaties and agreements signed in the past century. The treaty is signed by 74 countries [69]. The mission has to be compliant with these legal restrictions.

Contractors

The final design concept could stimulate certain industries, initiating new developments thus increasing the amount of jobs. In addition, new instruments could be developed which can be marketed to earn back revenue.

2.4.2 Market Attractiveness

The scientific observations in space focus more and more on planet Mars. Discovering the existence of water, examining the atmospheric components and investigating the martian surface by taking ground samples or visual observations has been done in the last centuries. However, in order to fully understand the planet, the internal structure has to be examined as well. Observing the existence of plate tectonics is an important milestone and leads to further scientific investigations. The interest in Mars increases, not only within the space agencies but also in public. In figure 2.5 the total number of missions to Mars that were accomplished by NASA and ESA is shown with respect to century. Up to 1990, NASA and the Soviet union were the only active investigators on Mars. Since 1990 also other parties like Japan (Nozomi mission) and China (Yinghuo-1) got involved. In 2003 the first European missions were performed successfully (Mars express and Beagle 2) and in 10 years time ESA executed in total three substantial missions to Mars. Furthermore, in 2002 the Aurora program was introduced. This program is an alliance of multiple countries to support and motivate manned and unmanned missions to Mars and Moon. Several missions are already in process of planning for 2016 and future [22]. To conclude, there is still a lot to discover on Mars. The public interest increases and more budget is allocated especially for Mars missions.

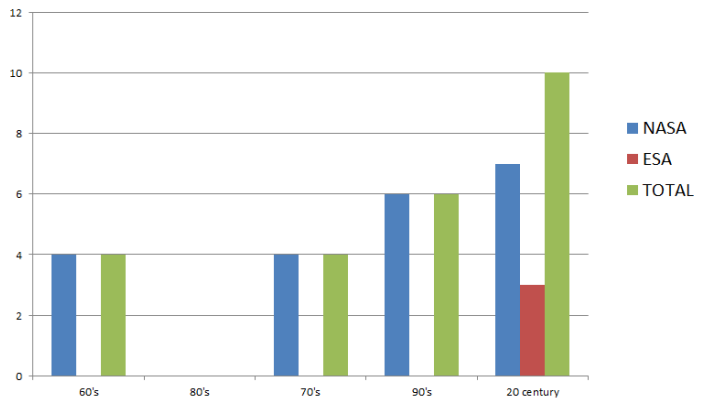

Figure 2.5: Accomplished Mars missions of ESA and NASA per century

2.4.3 SWOT analysis

Within this business environment, the mission needs a self-analysis, i.e. identifying its strengths and weaknesses, opportunities and threats in this environment as defined in section 2.4. Figure 2.6 shows this SWOT analysis. The image shows the positive and the negative factors in the columns, and the internal and external factors in the rows.

Strengths

As a design project, with the aim of designing an innovative solution to an existing problem and with a design team made up off student-scientists from the TU Delft, it has the freedom to explore all possible design options and do so unbiased. Also with the support from the Technical University of Delft: reliable testing facilities (when considering a conceptual design), and experts in the field of Aerospace engineering, the team has all the tools required to come up with an innovative design. Also

Strengths: - New product and innovation - TU Delft reputation - Access to testing facilities - Specialists in Aerospace engineering - Database and knowledge of preceding space missions	**Weaknesses:** - Lack of work experience in industry - High cost of project - Nonprofit project
Opportunities: - Generating public interest in space exploration - Spin-off technology - Loosing of regulations - Expanding Mars exploration	**Threats:** - Budget cut - Unknown competitors - Stricter regulations - Public dissatisfaction

Figure 2.6: SWOT analysis of the Mars mission

TU Delft's international reputation of providing high quality studies will help the team contact and communicate with different experts from all over the globe. At this moment there are five missions active on Mars, and more preceding Martian missions upon which this project can build. From both successful and non-successful missions there is much to be learned.

Weaknesses

As a group of students, lack of work-experience is an issue. A scientific mission to Mars is not aimed to be profitable in terms of finance. Its main goal is to gather new insights that are in the interest of science rather than making profit. Based on preceding Mars exploration missions, the estimated cost is around 2.5 billion euro which is a high amount of funds that need to be requested for.

Opportunities

Earlier this year, NASA scientists confirmed the existence of an ancient streambed where water had once "flown vigorously". This had caused a commotion among the public. This illustrates that the general public does have interest in the knowledge of Mars, especially when there are hints of habitability. In legal terms, regulations can change, it could loosen which will have a beneficial effect on certain performance criterion of the design. Another opportunity is having a spin-off product from the development, which can generate some revenue when marketed.

Threats

The market for space missions consists of the space agencies. Many space missions do not get funding, only a select few do. This also means that many of these are not made public, so it is hard to gauge the competitors. The agencies have a strict budget, determined by their respective governments, so a budget cut is always a threat. Just as the COPUOS can loosen regulations, they can also stricten them.

Dynamics of markets

The market is changing continuously and depends on certain factors which are described by the macro environment of a business. It is therefore important to establish a rough estimate of market development in the past years in order to verify possible investments in the future. Figure 2.7 shows

the yearly budget of ESA and NASA respectively since 2002. The figure clearly shows that NASA generally has a higher budget than ESA and therefore can be seen as a more reliable customer in financial perspective. NASA spent about 3.7 to 3.8 billion dollars on Space exploration in 2011, which is about 20% of the total budget. In addition, about 4 to 5 billion dollar was invested in general space operations. Compared to that, the financial resources of ESA are much less, namely around 4 billion euro in total per year (roughly 5.1 billion dollar). However, it has to be noted that fluctuations in funds are relatively big such that a drastic budget cut (for example due to governmental issues) would endanger the execution of this mission. In general these agencies are financed by public funds. Private companies are usually not able to accomplish enough assets to finance such a project. SpaceX has operated a total funding of approximately 1 billion US Dollar in 2012. However, incorporate possible investors might lead to a basis for financing the project [11] [39] [37] [52] [38] [70] [60] [3].

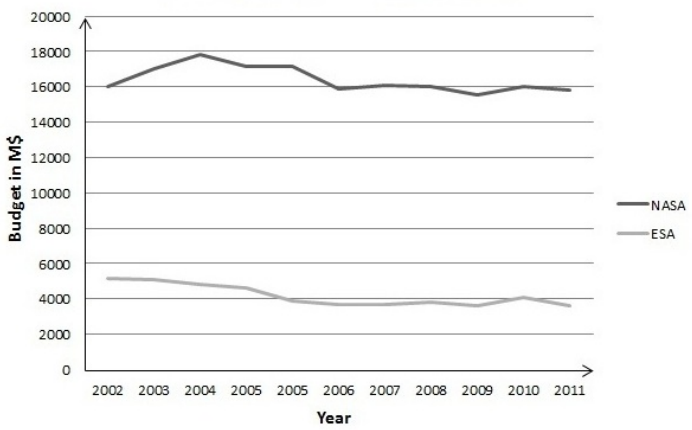

Figure 2.7: Annual budget of ESA and NASA in the last Century

Conclusion

The project contains many opportunities and might lead to important discoveries for future science application. The public interest on this topic is increasing and more missions are executed each year. However the concept has a high demand on financial resources. Threats and weaknesses have to be defined and precautionary measures to be taken. Regarding the dynamics of the market, NASA seems to be most likely the possible costumer due to their higher amount of budget. Their funds amounts to about 16 billion dollar every year. Furthermore, regarding the mission time-line NASA performed about 70% of all Mars missions within the last century.

2.5 Mission description

This mission is designed *to gather conclusive evidence for the possible existence of plate tectonics on Mars*. The secondary objectives of this mission were to investigate the internal structure of Mars. Plate tectonics is a phenomenon known only on Earth. Due to its dynamic inner structure, Earth's crustal plates move with respect to each other, creating geological features like mountains and canyons. Scientists are wondering if only Earth knows this phenomenon or do other planets like Mars also have them? Mars has been investigated for decades and shows many geological features comparable to Earth's. One of these geological features is *Valles Marineris*, a vast canyon, hundreds of kilometres wide, 4000 kilometres long and upto 7 kilometres deep, near the equatorial plane of Mars. It is assumed that this canyon is a transform fault. Transform faults are faults that indicate the boundary between two, lateral sliding plates, which would indicate plate tectonics. Therefore focus of this mission design is concentrated around Valles Marineris

In order to detect tectonic movement a grid of landers will be placed around Valles Marineris. Then the relative distance between the landers will be measured, using the principle of *near-field VLBI*.

Moreover a seismometer is added to every lander in the penetrating pin, which will measure the energy, created by natural impacts or wind, traveling through the ground to investigate the Martian crust.
Tectonic movement is detected in the range of a few millimetres per year. On Earth the fastest movement is measured to be approximately $17mm$ in one year. Mars is expected to have less tectonic movement, if any.In order to have a high chance of detecting plate tectonics on Mars the system needs to be accurate enough to detect in the range of $mm/year$. In order to assure a high seismic accuracy, the latest space application seismometer is used, which is expected to detect energies from natural impacts and wind noise, which are sources used in this design.

After launch the space bus will be in a low earth orbit at 200 km height. After a change in velocity of 3.6 km/s the space bus will begin its transfer to Mars. During which the batteries of the probes will be charged by the solar panels attached to the bus. Near Mars the velocity and spin rate will be adjusted to meet the probe release conditions. The outer shell that covered the probes during their transfer will be ejected into space. The first circular clamping mechanism will increase in radius and spin up. The probes are attached to the release system by a magnetic and mechanical clamping system. First the mechanical clamping system is retracted, after which the magnetic clamps will be cut from power releasing the first eight probes towards Mars. The probe bus will be slowed down and the second bunch of probes will be released in the same fashion. The probes will experience a 10 to 15 rpm spin rate induced at release. This spin rate will need to be decreased to 0.1 rpm. This is done by a *stretch YoYo* system attached to each probe. After de spinning the *stretch YoYos* will be released. The heat shield will then be inflated before entering the Martian atmosphere. The entry angles of the landers range between 11 deg to 29 deg. The average velocity at entering is 5.6 km/s. At Mach 1.77 the parachutes will be deployed, slowing the probes down to subsonic velocities. The inflatable heat shields will have to be adjusted in shape, in order to keep the probe stable, when the velocity is decreased to the subsonic zone. At approximately 100 m above the ground the parachutes will be released. Each probe will penetrate the surface with an average speed of 100 m/s. The pin will penetrate the inflatable and the ground and come to a stand still, having penetrated the crust of Mars at least 45 cm. When the probes have landed on Mars the solar panel will be deployed and the measurements can start.

The deep space network will send radio waves at a constant frequency into space. These waves are received by each probe individually. The received signal is mixed-down with a constant signal produced by a local oscillator in the probe. The resulting signal will be stored. A down link through the MRO is created which regularly sends the data back to Earth. On Earth, the data can be analyzed.

Chapter 3

Mission Operations

3.1 Measurement techniques

In this section the methods used for the measurements are discussed, including the basic theories used and the applications to this mission. This is done for both the primary (section 3.1.1) as for the secondary mission objectives (section 3.1.2).

3.1.1 Primary mission

The primary objective will be satisfied by displacement measurements between probes on the Martian surface. These landers, placed along two sides of a suspected fault line, will measure the relative distances between one another over a timespan of five years to determine if there is any tectonic movement. The method used for these measurements is derived from the principle of *Very Long Baseline Interferometry* (VLBI). The basics of VLBI will be discussed before the application to this mission is described.

Formulation of the problem

This measurement technique uses the propagation of electromagnetic signals to determine distances. A single signal, transmitted by a distant source in space, is received by multiple antennae placed around the globe. The path length of the signal from the source to each antenna differs slightly, due to the geometry of the system. This difference in path length causes both a difference in arrival time of the signal and in phase of the incoming signal, as shown in figure 3.1.

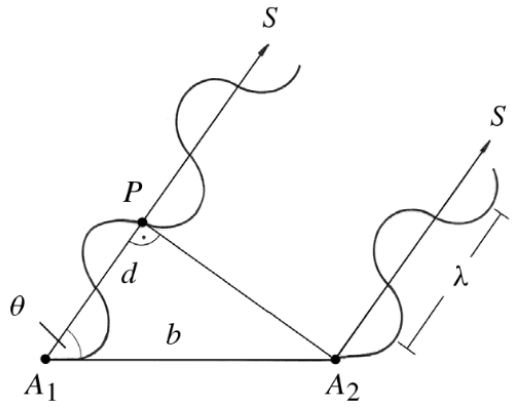

Figure 3.1: Baseline calculation using radio interferometry (from [87])

In this figure, the radio source is assumed to be at an infinite distance, which means that the incoming signal paths are parallel. (This is of course impossible, but for the radio sources generally used in VLBI, the distances are large enough for this assumption to be acceptable) The distance between the antennae is called the baseline (b). The angle of incidence relative to the baseline is θ and d is the difference in path length or *pseudorange*. The relation of the pseudorange to the geometric time offset (τ_g) described above and the baseline is described in equation 3.1, where c is the propagation velocity of electromagnetic waves, better known as the "speed of light".

$$d = \tau_g \cdot c = b \cos\theta \tag{3.1}$$

However, this is only one equation, with two unknowns (not regarding d). So, to be able to solve the system, an extra equation needs to be developed. This is done by describing the phase difference observed at station $A1$, relative to $A2$ in terms of b and θ as shown in equation 3.2. This so-called phase offset depends on the frequency of the signal f.

$$\Delta\varphi = \frac{2\pi f b \cos\theta}{c} \tag{3.2}$$

By measuring $\Delta\varphi$, f and τ_g, the equations can be solved for the baseline. However, measuring these values is not as straightforward as it sounds.

Interferometry

The total phase offeset $\delta\varphi$, as described in equation 3.2 is the total phase difference, which will allmost always have a value greater than 2π (i.e. d longer than one wavelength). But since the signal is a single frequency, continuous signal only the fractional difference in phase can be measured. The part of the phase offset consisting of full revolutions (an integer number of 2π) can not be determined. To find the total $\Delta\varphi$, the value from equation 3.2 can be compared with the relation between φ and τ_g, given in equation 3.3.

$$\Delta\varphi = 2\pi f \tau_g \tag{3.3}$$

However, τ_g can never be found exactly, because the time measured by the probes will suffer from instrumental delays and clock offsets. The inaccuracy of τ_g can be solved by applying a least square estimation over multiple measurements. An accurate solution for the baseline and θ can then be obtained. By performing multiple measurements and applying the least squares theorem, an accurate solution for b and θ can still be found.

Phase offset

The phase offset is actually the main measurable in VLBI, or radio interferometry measurements in general. This is also where the name interferometry comes from.
If the phases of the received signals would perfectly overlap (i.e. if θ is exactly 90° or d is an integer number of wavelengths), the source signal would simply be amplified. However, any phase difference will create electromagnetic interference between these signals. This interference can be visualised in a so-called *fringe pattern*. A voltage spike occurs for the points where both signals amplify each other and a minimum occurs where the signals attenuate. This fringe pattern is described by the fringe function, given in equation 3.5 (equation from Thompson, Moran & Swenson 2004, chapter 2 [93]).

$$F(t) = cos(2\pi f t) \tag{3.4}$$

$$F(\tau_g) = cos(2\pi f \tau_g) = \cos\left(\frac{2\pi b \sin\theta}{\lambda}\right) \tag{3.5}$$

$$\tag{3.6}$$

Fringe rate

However, when performing measurements as accurate as this, one has to account for the change in θ due to the rotation of the planet. During a measurement series, this change in θ will follow a change in phase, which in turn means a change in fringe pattern. Since the angular velocity of the planet can be assumed constant (at least over the short timeframe of one measurement set), this can be used as another measurable. The rate at which the fringe function changes is called the fringe rate or fringe frequency ν_f.

$$\nu_f = \frac{1}{2\pi}\frac{d\varphi}{dt} = -\omega b_\lambda \cos d \cos\delta \sin(H - h) + \nu_{in} \tag{3.7}$$

Equation 3.7, from [93] chapter 12, gives the fringe frequency in terms of the angular velocity of the planet ω, the baseline vector in units of the wavelength b_λ and the position vectors of the baseline. The component $\nu_i n$ results from instrument errors and frequency offsets between the local oscillators (described later).

Measurement techniques

To measure the fringes, both signals need to be processed and combined. For interferometry systems with large baselines, such as VLBI, it is generally not possible to do this in real-time. This would require expensive low-latency, high bandwidth datalinks between both antenna facilities. Therefore

the data is generally stored separately at each station, to be analysed at a later time. The data is sent to the processing facility via a slower data link or even by way of mail delivery.
In the following paragraphs, the entire data flow will be described from the antenna to the least-mean-squares fit.

Data generation
The sinusoidal signal that is received is converted into an electrical current by the antennae, producing output in volts. This signal is then converted down to a more convenient signal by down-mixing it with a very stable reference signal generated by a local oscillator (LO). A very good explanation of this is given by Campbell: "You can see how mixing works by multiplying two sinusoids together. Lets say we want to look at a bandwidth in our cosmic signal $\omega_0 \rightarrow \omega_0 + BW$. If we multiply the cosmic signal, $\cos \omega t$, by the output of a LO, $\cos \omega_0 t$, trig identities allow us to express the product as $[\cos(\omega + \omega_0)t + \cos(\omega - \omega_0)t]$. If we low-pass filter this result to save the $\omega - \omega_0$ term, our desired bandwidth now lives in frequencies $0 \rightarrow BW$. We can have multiple LOs set to different frequencies operating in parallel. These are typically called Video or Base-band Channels." [28]. This way, all noise frequencies are filtered out right at the source.
The down-mixed signals are then digitised and stored locally. To get the most stable signal, the LO is controlled by a very accurate frequency standard (an atomic clock). Almost as a byproduct, this atomic clock will generate a time reference. This time is also recorded and can be used to find a first estimate of τ_g. This time reference tends to drift over time and is not precise enough to be used right-away, as will be further described in section 3.3.1.
Another thing that has to be done before the data can be processed is the generation of so-called *a priori* estimates of the parameters. The baseline length, for example, can be estimated using other (less accurate) measurement techniques, such as GPS locations or even satellite imaging. τ_g can be approached by modelling the atomic clock drift.

Data processing
In the data processing facility, the data from all stations is played back and sent into the *correlator*. On the data that was received first, a time delay (τ) is applied (in this case, the data from station *A2*). The correlator tries to match both signals by iteratively shifting *tau* by small amounts until it finds the value of τ that yields the highest correlation.
This correlation is calculated by summing or *superpositioning* the two signals (after the time delay has been added) and squaring the resulting wave. This will result in the fringe pattern given by $F(\tau_g - \tau)$ (from equation 3.4). As described above, when the phase offset is reduced to zero, the two wave patterns will perfectly overlap and amplify. This results in the fringe pattern with the highest amplitude. The value of τ that yields the highest correlations is therefore the best estimate for τ ($\tau_g - \tau \overrightarrow{lim} 0 \Rightarrow F(0) = 1$). The same is done for fringe rate ν_f. The correlator will then give the best estimate for θ. From these values, an estimate of the baseline length can be calculated.
Executing this measurement multiple times over a relatively small timespan and calculating a least squares fit of the results, even better estimates for the input parameters can be found. Repeating these measurements over long timespans, the accuracy of the estimates can be increased enough to find trends and changes in the input parameters. For a more complete explanation of the basics of VLBI, it is recommended to read the lecture by Bob Campbell from JIVE [28], the book by Thompson, Moran & Swenson [93] for a complete explanation of everything VLBI or chapter 2 of [82] for a complete explanation of correlators.

Measurements Primary Objective

The goal of the proposed mission is to prove the existence of plate tectonics. This is done by applying radio interferometry as described above. Multiple landers are scattered on the Martian surface, all consisting of an antenna and a very accurate oscillator. But instead of using a natural radio source situated lightyears away in space, a man-made signal is used, originating from Earth. This has the advantage that the signal can be much stronger than that from a natural source, thus requiering a significantly smaller receiving antennae.
This approach does introduce some extra challenges. The assumption of a source at infinite distance does no longer apply, which means that an extra trigonometric factor and relativistic effects have to be taken into account. This variant of radio interferometry is called *near-field VLBI*.

Another factor that needs to be taken into account is the effect of both the atmosphere on Earth and the atmosphere of Mars on the propagation. Finally, the function of the fringe rate has to be expanded to take into account the axial rotations of both Earth and Mars and the heliocentric orbits of both planets. This means that considerable time has to be invested in expanding the governing equations, modelling the problems and finding the *a priori* parameters. However, similar models already exist for other proposed missions and building one should not throw up any problems [49].

3.1.2 Secondary Objectives

In order to fulfill the secondary objectives of this mission; investigating the internal composition of Mars, the basic principle of seismometry is used. Mars is one of the four terrestrial planets of our solar system. It has many features which are comparable to Earth's; volcanoes, valleys, deserts, and polar ice caps. It is assumed that there are Marsquakes but no legitimate proof has been found up until today. Thus other sources of waves need to be used. Hereby two sources are chosen; wind and natural impacts. The theories used are called *seismic interferometry* and *ray theory* respectively.

Natural Sources

In order to use the seismometers, implanted in the Martian surface, natural sources that generate seismic waves need to be used. In the following the two natural sources used for the seismic measures are presented and the principles used are explained.

Wind

Wind is a source that is often used as a source in ambient noise tomography, which is based on the principle of *seismic interferometry* (SI). It has been applied to map sub surfaces from regions who are "seismically quiescent", like the British isles [71]. It is predictable and has a certain regularity. Measurements can be taken over a long period of time, which is a criteria, when using SI. Wind is a phenomena that results from air pressure differences over a specified horizontal distance. These changes in pressure cause air molecules to rush from the area of high pressure to flow to the area of low pressure. Local temperature differences can cause such changes in pressure. Dependent on how high the differences in pressure and over which horizontal distance these differences occur, the strength of the wind will alter.
Noise sources in general are not uniform. There are many sources that produce noise and will be seen in the measurements. Dependent on their frequency they can be filtered out. Wind and other meteorological conditions create seismic noise at around 1 Hz; frequencies above that are mostly due to human activities and lower frequencies result from oceanic activity. On Mars the atmosphere is a lot thinner but still winds and/or storms occur [9].

Global dust storms

These huge storms are the result of airborne dust particles that absorb sunlight and warming the Martian atmosphere in their vicinity. These warm pockets of air flow toward colder regions, which generates winds. Strong winds will cause more dust getting into the air, which in turn heats the atmosphere, raising more wind and thus getting more dust into the atmosphere. [5] Global dust storms are a phenomenon occurring on Mars when it is closest to the sun, e.g. late spring of the southern hemisphere. Global storms are rare but increase in occurrence, as can be seen from records [18].

Local dust storms

Local dust storms occur frequently on Mars and are most likely comparable to those on Earth. Previous mission recorded many smaller dust storms [83]. These storms may occur from slope winds due to temperature differences of the surface layer of the atmosphere. "The deep canyon region of the equatorial zone are also sites of local dust storms and , although this region also has frequent condensate clouds, he dust clouds can usually be identified by their color and structural morphology." [83]

Seismic interferometry

In this section the principle of *seismic interferometry* will be explained.

Principle

Wind is a property that is considered as ambient seismic noise. Int the past noise resulting from e.g. wind, was filtered out of seismic data. In the last 10 to 15 years a technique called *seismic interferometry* uses the ambient seismic noise, that is caused due to so called micro-seismic events like wind, in order to gain knowledge about the upper layers of a surface (subsurface). The principle is based on cross-correlation of this passive noise, generated by wind for example, over a long period of time. These cross-correlations reproduce the subsurface impulse response. Thus, it is possible to obtain information about the subsurface with no need for an active seismic source [30].

The theory behind *seismic interferometry* is based on the cross-correlation of waves. For explanation it is assumed that there are two receivers (seismometers) within a surface that is surrounded by energy sources, as can be seen in figure 3.2. Each of the two receivers will record the propagating waves from each source. These signals can then be cross correlated. This is done by adding the signals together, after which the signals that have traveled between the two receivers will add constructively and signals that did not travel between the two seimometers will add destructively.

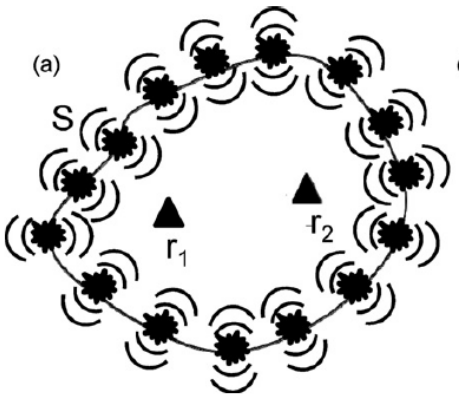

Figure 3.2: Recievers surrounded by enery sources

For the case of random noise, it can imagined that a surface S exists and all the noise sources are joint up together. It is known that energy sources can either fire at the same time or at overlapping times. In case of overlapping times the recorded signals do not need to be added anymore. They are already stacked. The principle can be visualized in figure 3.3. Some general assumptions are that the surface is large, the noise source has a certain regularity and that the noise is recorded for a sufficiently long time period. "While it is usually unclear whether all of these conditions are met in practise, experience shows that the results are nevertheless useful" [71].

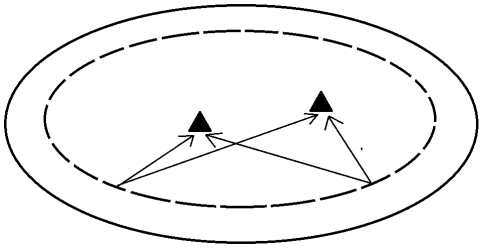

Figure 3.3: Recievers surrounded by joined noise sources

Conclusion

From the two sections *Global dust storms* and *Local dust storms* it can be seen that wind as a source can be used to investigate the subsurface of the Martian crust where the grid of probes is applied. The source has a certain regularity and the measurements are taken over 5 years. Other noise sources, e.g. regolith moving over the subsurface, will need to be taken into account and will have to be filtered out.

Natural impacts

Investigations

All information fount on the topic of *Natural impacts* are found from literature [31]. In the past there have been different missions that investigated the internal structure of planets by seismometers or geophones. The Apollo mission implanted seismometers on the moon in order to gain more information about impacts on the moon. It was investigated that there are approximately three meteoroid impacts per five days. These impacts were classified into different categories. Dependent on how many of the four planted long-term seimometers detected seismic waves, the impacts were classified to be large impacts, intermediate impacts or small impacts. The Viking missions to Mars included seimometers to investigate Marsquakes. Only on the Viking 2 mission the seismometer worked. It mainly recorded wind noise and one possible Marsquake. From this data Marsquakes could not been proven since the data was not explicit enough.

Meteoroid flux

Many planets/Moons suffer from impacts due to meteoroids on a frequent base. Dependent on the distance from the asteroid belt and the feature of the planet/moon, the impact flux will differ. Mars is closer to the asteroid belt than for example Earth whereas its atmosphere is less dense than that of Earth. The ablation due to the atmosphere will result in less meteoroids actually reaching the surface. The initial mass of each meteoroid will decrease with resulting in less energy available for conversion to seismic energy. Masses smaller than 1 kg will actually burn in the atmosphere and other micro meteoroids will also be too small for conversion to seismic energy. These features will influence the meteoroid flux on each planet individually. Moreover active and inactive comets might also contribute to the cratering flux on Mars. Initially it was assumed that the cratering rate was four times the one on Earth, taking this into account, the cratering size reduces to twice that on Earth. In order to find how many of the meteoroids will actually arrive at the Martian surface the formula from Halliday et al (1984) to estimate the influx on Earth is rewritten for Martian conditions. Hereby it is assumed that the impact ratio on Mars is 2.6. This value was estimated by Shoemaker in 1977 and also used in a study by Flynn and McKay on micrometeoroid ablation in 1990. The initial equation for Earth conditions

$$\log N = -0.689 \cdot \log m + 3.76 \tag{3.8}$$

where N is the Number of Meteoroids per Year and m is the Mass. Equation 3.8 was rewritten to Martian conditions, thus including the factor of 2.6 and taking the Martian surface area.

$$\log N = -0.689 \cdot \log m + 6.34 \tag{3.9}$$

Hereby it needs to be stated that only meteoroids reaching the surface are taken into account in the formulas 3.8 and 3.9. This is done because Halliday et al. estimated that only one third of all fireballs actually reach the planets surface.

Entry velocities

There are two mechanisms present that let asteroids drift from the asteroid belt onto a planetary-crossing orbit. These are either due to "secular resonances in the asteroid belt" or due to "chaotic motion near orbit resonances with Jupiter" [Meteroid Impacts as Seismic sources on Mars]. The chaotic motion near orbit resonances are about four times stronger than the secular resonances in the asteroid belt thus these are used to estimate the Mars crossing velocities. These chaotic motion near

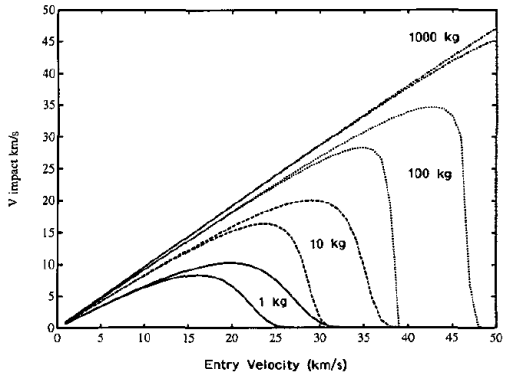

Figure 3.4: Impact Velocities vs Entry Velocities [31]

orbit resonances are mainly due to the a fact that bodies, that are within a so called 3/1 Kirkwood gap, will experience fluctuations in eccentricity, as a result of their interaction with Jupiter and the Sun. Kirkwood gaps are gaps in the asteroid belt where asteroids undergo violent variations in their orbits. The number 3/1 refers to the location of the Kirkwood gap [63]. The Mars crossing velocity for 3/1 asteroids was calculated to be 28.4 km/sec and its entry velocity was found to be 6.9 km/sec. These velocities were estimated from equation3.10 [31].

$$V = \sqrt{G \cdot M_s(\frac{2}{r} - \frac{1}{a})} \tag{3.10}$$

Where m is the mass, G is the gravitational constant, a is the semi major axis, r is the radius and M_s is the mass of the Sun. The results are lower than the actual entry velocities. This is due to the fact that the formula assumes orbits of 1 AU pericenter of 1 AU and zero inclination. The estimations for asteroids with a lower pericenter than 1 AU have an estimated entry velocity of 11.7 km/sec. After estimating the atmospheric entry distribution of meteoroids in 1990 the actual average entry velocity was found to be approximately 10.2 km/sec.

Ablation

Each body that enters the Martian atmosphere will undergo ablation due to friction and heat. The ablation factors are found from Revelle (1979) and are $2 \cdot 10^{-8}[\frac{s^2}{m^2}]$ to $3 \cdot 10^{-8}[\frac{s^2}{m^2}]$. In the calculations a value of $2 \cdot 10^{-8}[\frac{s^2}{m^2}]$
is used within a factor of 2. This is done due to "the agreement with the meteor observatory dynamical analysis, agreement with the cosmic ray data, and agreement with laboratory estimates of ablation". [31] Graphs of the decrease in entry velocities and the ratio can be found in the following graphs 3.4 and 3.5

From the outcome of the calculations it was found that for meteoroids with an initial mass of 1 kg to 1000 kg, entering at an average velocity of 10 km/sec, more than 50 percent of the mass remains. The velocity of each body will remain relatively high and thus 25 percent up to 80 percent of the incident energy will be available at impact.

Seismic energy

The seismic detectability is dependent on the mass and velocity as well as the surface structure the energy travels through. The conversion to seismic energy on Mars is unknown. The only given data can be found from the Moon. There a meteoroid of 0.1 kg with a velocity of 22.5 km/sec was detectable by a seismometer at 50 km distance. Here it is assumed that the same is possible and at bigger distances the energy will decay by 1/distance. Which implies that a meteoroid with an energy greater than 10^{12} Joules will be detectable around the whole planet.
Thus in table 3.6 the number of meteoroids entering the Martian atmosphere including there weight

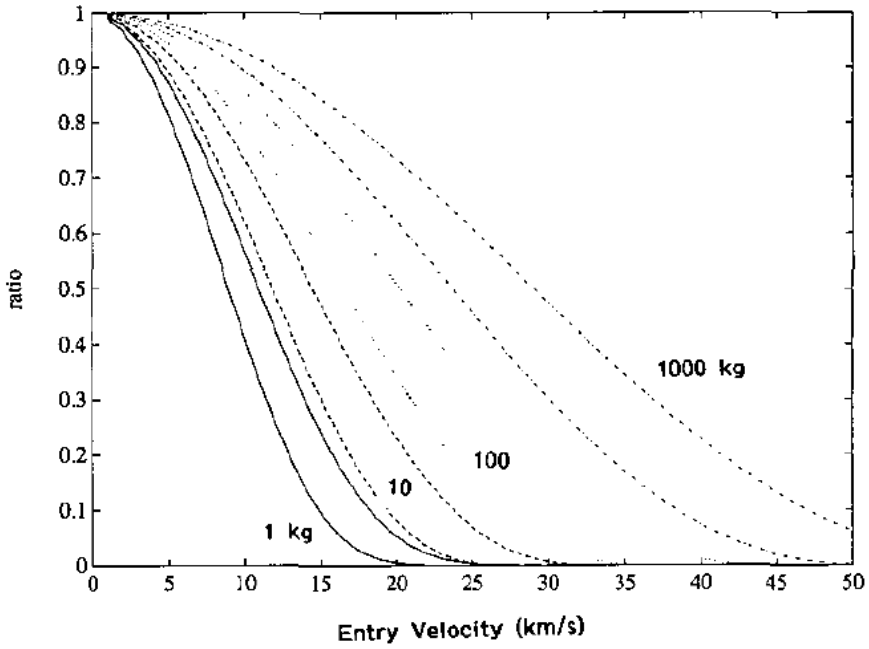

Figure 3.5: Ratio vs Entry Velocities [31]

are listed.

Finally the table of the expected number of detected meteoroid impacts on Mars per year of one seismometer are listed in table 3.7:

3.1.3 Ray theory - The principle

The contents of this chapter is based on literature [84]The *Ray principle* is used to investigate the deeper sub-surfaces of Earth. This principle is part of the reflection and refraction seismology. Energy that travels through a medium, like the surface, will travel in so called waves. Waves, or so called wave fronts, are per definition a set of points, that undergoes the same motion with respect to time. The propagation of wave fronts is found from *rays*. These are normal to the wave fronts and thus will always indicate the direction of propagation. An example of plane and spherical wave fronts, including *rays* can be seen in figure 3.8.
From optics the two main principles, behind the *Ray theory*, are found. *Huygens'* principle states that if the propagation and direction of a wave front is known, at one point in time, it can be predicted to a future point in time. It is based on the geometry of wave fronts. *Fermats'* principle deals with the time-travel conditions of wave fronts. It is built on the geometry of *ray*-paths and states that a *ray* will always follow a minimum *time path*.
Wave fronts that travel through one medium will propagate uniformly. A medium is considered of one material and one velocity. A medium boundary implies the same material but different velocities. If a wave front reaches a boundary, between two mediums , the wave will be refracted. Another medium implies an alter in velocity, which is why a wave front refracts. The basic idea of refraction can be seen in figure3.9.
If a wave front reaches a boundary, of two different materials the boundary is called a boundary between two half spaces. In that case there will be a refracted wave and a reflected wave. A drawing of a wave front reaching a boundary is found in figure 3.10.
If the velocity of the underlying half space is higher that the velocity of the upper medium, the refracted angle (j) is higher than the reflected angle (i). At some point the velocity differences can be so high that the refracted wave propagates parallel to the boundary, which happens under a certain critical angle i_c of the initial wave front. Such waves are called head waves and are known to transmit energy back into the upper half space. This phenomenon is illustrated in figure 3.11

TABLE II
Number of Meteoroids Entering Mars' Atmosphere per Terrestrial Year from Eq. (2)

Mass range	Number of meteoroids incident on Mars	Mean mass
30–300 g	165,880	87 g
300–3000 g	33,947	875 g
3–30 kg	6,947	8.750 kg
30–300 kg	1,422	87.45 kg
300–3000 kg	291	874.5 kg
3000–30,000 kg	75	8745 kg

Figure 3.6: List of Mars entering meteoroids [31]

TABLE III
Expected Number of Detected Meteoroid Impacts on Mars per Year by a Single Seismometer

E (Joules)	$N(E_e)$	$N(E_i)$	Detection distance d (km)	N_e/year potentially detected	N_i/year detected
10^6–10^7	147,400	27,750	20	1.2	0.2
10^7–10^8	48,645	6,641	60	3.8	0.5
10^8–10^9	9,955	6,193	200	8.6	5.4
10^9–10^{10}	2,037	1,421	600	15.9	11.0
10^{10}–10^{11}	417	275	2000	36.0	23.8
10^{11}–10^{12}	85	70	6000	66.4	54.8
10^{12}–10^{13}	17	15	All	17.4	15.5
10^{13}–10^{14}	3.6	3.6	All	3.6	3.6
10^{14}–10^{18}	0.9	0.9	All	0.9	0.9
Total	208,560	42,369		154	116

Note. $N(E_e)$ is planetary distribution of entry energies neglecting atmospheric effects. $N(E_i)$ is the distribution of impact energies. N_e is the number potentially detected were there no atmosphere. N_i is the number potentially detected were there no atmosphere. N_f is the number detected when atmospheric effects are included.

Figure 3.7: Martian meteroids, their occurance and impacts [31]

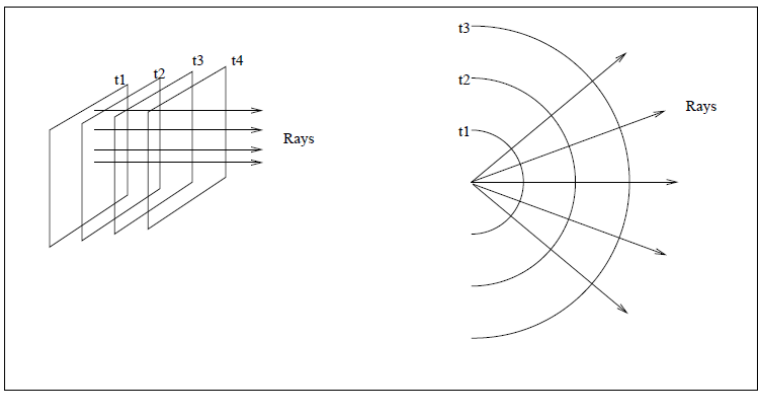

Figure 3.8: Plane waves and spherical waves [84]

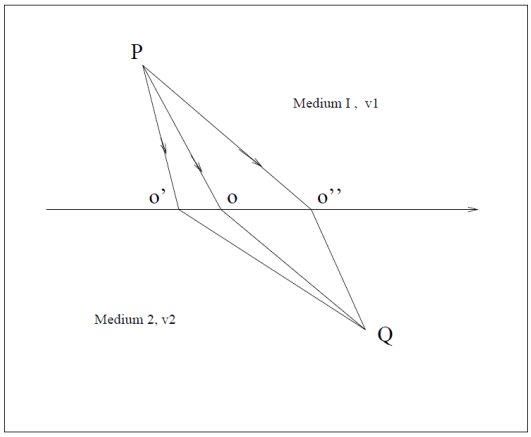

Figure 3.9: Changes due to refraction of a wave front [84]

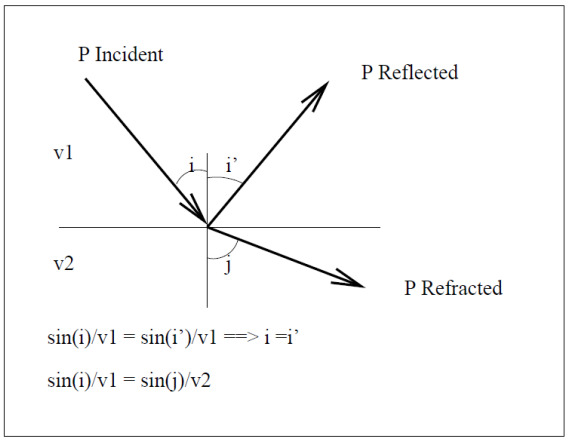

Figure 3.10: Wavefront reaching a material boundary [84]

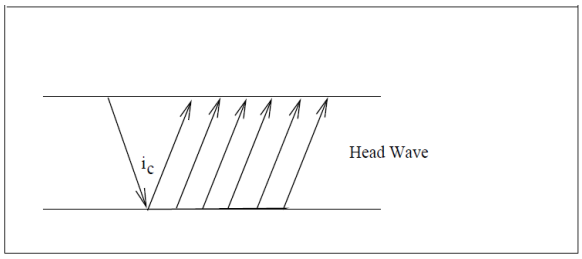

Figure 3.11: The forming of headwaves [84]

From wave propagation, and their behavior on boundaries between different modes or half spaces, the deeper subsurface can be analyzed. This principle is used to analyze seismic data on Earth.

3.1.4 Conclusion

From the subsection *Natural impacts* it can be seen that there are impacts present on Mars that should be detectable. From table 3.7 it can be seen, that there are approximately 15.5 meteoroid impacts that are detectable over the whole planet, per year. These estimations are made for a single seismometer only. Taking into account that on this mission 16 seismometers are taken and spread

over a wide area around Valles Marineres, there is a good chance that also smaller impacts will be detectable. Thus using natural impacts as a source to investigate the soil of Mars is expected to be feasible.

3.2 Scenario analysis for the required amount of landers

The amount of landers needed to fulfill the primary mission requirements, is a key parameter for the further design, planning and budgeting of the mission. This number directly follows from the scientific goal, the measurement technique and its accuracy. This section will describe all steps that were taken towards finding the final number.

3.2.1 Minimum amount of landers needed for measurements

For the primary mission the minimum requirement is to measure any form of plate tectonics. The mission will focus on the area around Valles Marineris, for it is assumed to be a fault line on Mars. The minimum amount of active probes required to measure any kind of movement is two; one on each side of the fault line. However, Valles Marineris could be a transform fault, which implies that the plates do not move away from each other but rather slip along each other in a shearing motion. This would mean that 1 mm of relative plate movement would create a much smaller change in the baseline between the two measurement positions. Using Pythagoras' theorem, it can be calculated that if two probes were aligned perfectly on a line perpendicular to the fault line, a lateral displacement of 1 mm would generate a change in length of the baseline in the order of picometers. Displacements this small can not be measured.

Two additional landers are needed, at least several hundred kilometres away from the other probes along the fault line. Using geometry, it can be determined that a perfect square pattern would be optimal. A movement of 1 mm in any direction will mean a minimum change of 0.7 mm in length of at least one of the baselines. Assuming a "perfect" transform fault line, the pairs of landers, that are on the same side of the fault (thus on the same tectonic plate), should not move relative to each other. The length of the two diagonal baselines should then change by the same, but opposite amount, as shown in figure 3.12. This fact can be used to validate the measurements. Furthermore, due to the multiple baselines present, the direction of all movements can be determined. Thus, at least two landers on each side of Valles Marineris should survive the entire 5-year mission.

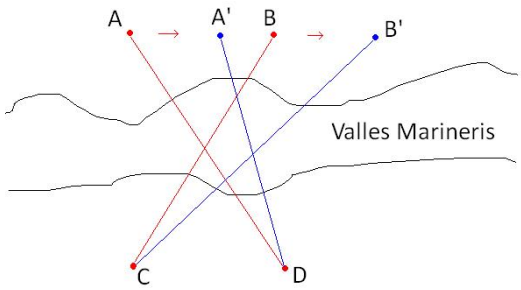

Figure 3.12: Baselines

3.2.2 Mission duration

Surviving for five years in the harsh Martian environment is a hard feat to accomplish. There have not been any missions to Mars with such a long primary design life and only few that lasted more than 5 years on the Martian surface. The history of missions to Mars shows that reaching Mars and take measurements over such a long time is challenging. Not only is there a slight possibility that one of the landers' systems fails during the 5 years of operation, environmental factors could also compromise the accuracy of the probes. High-velocity winds could potentially displace one of the

landers from it's initial landing position. If this happens, it can be wrongly interpreted as tectonic movement.
An extra lander on each side of the fault line will provide the necessary redundancy to guarantee the minimum amount of landers will stay functional for the entire mission. This sets the required amount of landers to 6, three on either side of Valles Marineris.

3.2.3 Landing procedure

As described in section 5.4.1, when the landers are released from the space bus, they are dispersed in a circular fashion, which in turn will lead to an elliptical landing pattern. This ellipse, with it's major axis aligned with Valles Marineris, will ensure an even spread along both rims of the valley. However, probes that land in the peri- and apocentre of the landing zone will land inside the valley. This is not favorable for the primary mission objective seeing the uncertainty of the location w.r.t the fault line. It will be advantageous for the secondary objectives, for it will land closer to the assumed fault zone and thus closer to possible marsquakes. The chances of this happening are very high. Thus two extra landers will need to be included for each ring of probes that is released from the transfer vehicle.

3.2.4 Probability of landing failure

Finally there is the landing itself. Due to the large landing footprint the terrain on which the probe will impact is hard to predict. The place of impact should be on a horizontal plane, with less than 10° inclination. The landing is assumed to have failed if the lander impacts in a terrain with slopes steeper than 10° . Since the mission design uses an passive landing, the exact landing locations cannot be predicted. The terrain in this region is very rough, which means that their is a probability of failure. This is, however, hard to quantify, but due to the high budget of this mission more probes can be landed to account for this uncertainty. Thus, a landing redundancy factor of 2 is chosen.

3.2.5 Total amount of landers required

If all landers would be spread in one big ellipse, a minimum of 12 landers would need to be taken: Four from section 3.2.1, plus two from 3.2.1 results in 6 landers; Multiplied by the redundancy factor 2, from 3.2.4 a total of 12 landers would be needed. The probes are attached to two circular clamping mechanisms, that will spin up and release the probes. The release is done in two phases resulting in two equally elliptical landing patterns next to each other. In order to assure a footprint range of $2900km$ to $3100km$, taking adequate measures, two more probes are taken per probe release. Thus, the total amount of landers will be 16.

3.3 Accuracy

Accuracy of the measurements is most important in this mission, since it defines whether or not this mission will be a succes. In this section the accuracy of both the primary and the secondary measurements of the Ancile mission will be discussed. First the accuracy of the primary objectives will be attended to, after which a short explanation of the accuracy of the secondary objectives is provided.

3.3.1 Primary objectives

For the primary mission, the accuracy of the measurements is the single most important design parameter. The goal is to give conclusive evidence that shows weather or not plate tectonics exist on mars. To do this, the system must be able to pick up even the smallest movements in the crust of the planet. On Earth, relative movements along major plate boundaries have been measured in the range of 1 to almost 20 mm per year. On other locations, movements as small as 0.1 mm/yr have even been measured using VLBI [50] [85]. However, VLBI stations on Earth will always have a higher accuracy than any system that can be deployed on Mars, due to the fact that larger antennae, bigger frequency standards and better reference data can be used.

To be able to compare designs, a minimum resolution of 1 mm/year has ben set by the design team. This was assumed to be a sufficiently high, but still achievable accuracy.

Clock accuracy

The most important aspect in the accuracy of a VLBI system, is the short-term phase stability of the frequency standards used. As described in section 3.1.1, each probe will have it's own atomic clock to control the local oscillators (LO). These LO's produce a reference signal for the down-mixing of the measurement signal. In an ideal world this reference signal would be a pure sine wave. However, as accurate as an atomic clock would seem, the output frequency will still suffer a bit of wobble and drift. This drift creates phase offsets in the reference signal, meaning that the phase offset measured does not completely correspond with the phase offset of the geometric system any more. When this drift becomes to big, the correlator will assume a wrong $\Delta\varphi$ and give a bad estimate for the baseline parameter. A slight wobble around the base frequency is less problematic, this can be filtered out by time-averaging the signal over short timeframes. However, this implies further restrictions on the short-term drift, since the frequency may not drift during the time period that is taken for averaging. The long-term stability of an atomic clock is less important, but needs to be taken into account. The drift, or *clock error* of such a clock is only in the order of a few nanoseconds per year, but a few nanoseconds offset might mean several wavelengths difference at these high frequencies. Therefore, the accuracy of τ_g measured will degrade over time. This can be solved by keeping track of the development of this clock error, modelling and compensating for it, since the drift of these kind of clocks generally follows a known pattern [32].
Thus a frequency standard needs to be chosen, that not only has a high short-term stability, it must also comply with stringent requirements to survive launch, landing and five years on Mars. It must es small enough to fit in a probe, and it must be tough enough to withstand landing impact, all without missing a beat. An explanation of the chosen atomic clock can be found in 4.3.1. An extensive explanation of frequency standards, their drift and phase stability and their application to VLBI can be found in section 9.5 of Thompson, Moran & Swenson [93].

Bandwidth

A way to increase the accuracy of the phase measurements, is by selecting a large bandwith for the source and deviding this in a discrete number of small bandwiths to be sampled at the lander. Using multiple LO's running at a slightly different frequency for each bandwidth, the phase offsets for each of these small bandwiths can be measured [28]. Using only one frequency, φ can be established plus or minus an integer number of complete revolutions ($\pm n2\pi$). Combining all results will greatly reduce the number of possible solutions for the entire system, thus increasing the accuracy of the solution.
The main working frequency of the phased array antenna is 7.51 GHz, when all patches are used (section 4.2.3). However, by only activating a few selective patches, different spacings can be used, thus resulting in different frequencies that can be sampled. Using fewer patches will reduce the antenna gain, as per equation 4.1, so not all combinations will be usefull.
In the landers, the signal from each antenna patch will be amplified separately and the software in the Payload data processing unit will combine these signals in the different "patterns" simultaneously. The resulting signal from each of these combinations will be mixed-down with a signal from a LO of the corresponding frequency and stored. All these narrow bandwiths together will form a broad –albeit non-continuous– baseband, resulting in a high accuracy.
Figure 3.13 shows the chosen sampling patterns and the corresponding frequencies. The chosen frequencies are 7.51 GHz, 5.31 GHz and 3.755 GHz.

Data sampling

The down-mixed signals from each LO are 2-bit digitised and sampled. The sampling rate will be 2 MHz, two times the bandwith to avoid signal aliasing [28]. This will create a data rate of roughly $2 \cdot 2 = 4$ Mbit/s per measured frequency. Using three frequencies, this will generate $4 * 3 = 12$ Mbit/s of data on each lander.
For each measurement set, the DSN will transmit a continuous signal on all three frequencies for 10 minutes. This will generate 7.2 Gbit of data at each lander which will be stored locally untill it can

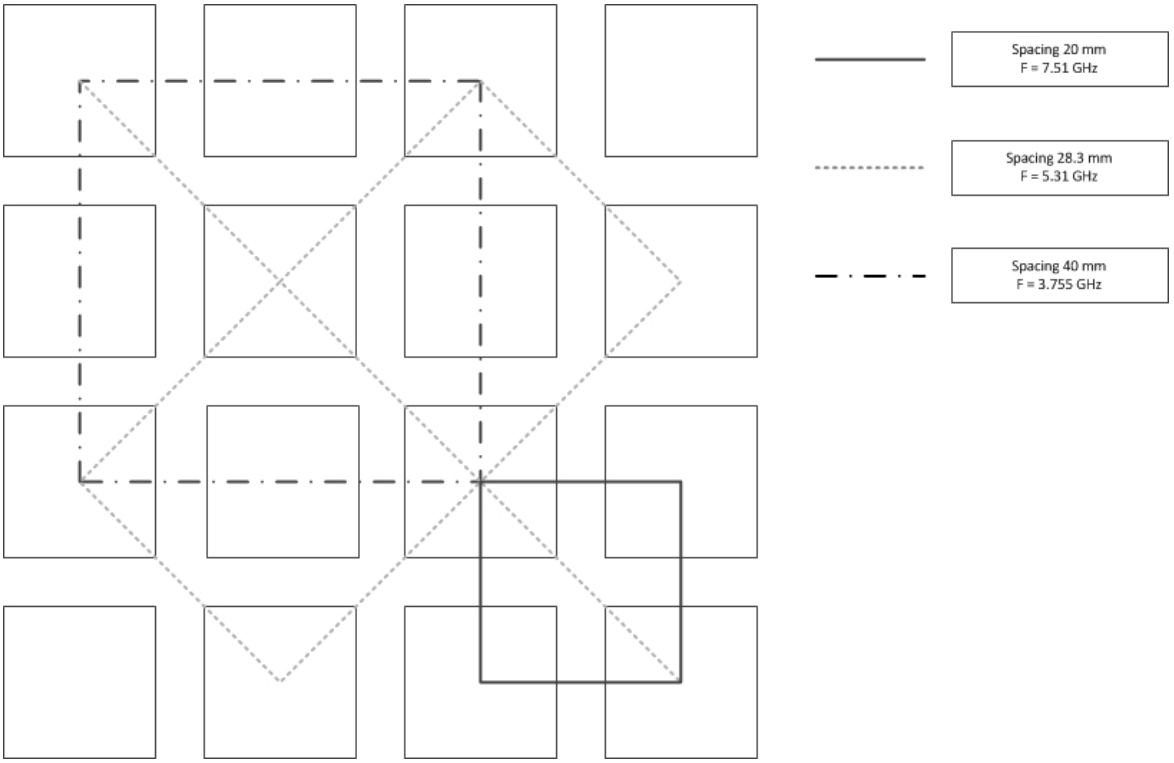

Figure 3.13: Sampling pattern phased array antenna and the resulting frequencies

be sent to the relay satellite. The maximum datarate available for uplink to the MRO is 1 Mbit/s, thus the data from one measurement alone (without the seismometer data) will take two hours to be transmitted. Assuming 12 landers will survive impact, 24 hours are needed to send all data from the Martian surface to the MRO (or any other Mars-orbiting relay satellite).
The measurements will take place on average once a week, thus the transmission of data from the probes to the MRO can be reduced to about 3.5 hours per day. One measurement per week will result in 260 measurement sets over the course of five years. These values were chosen since time on the DSN is very expensive and the MRO is only available for limited time.

Total accuracy

VLBI measurements on Earth generally have measurements spanning multiple hours, since the data tranmission is much less of a problem, but Earth-based VLBI stations suffer from other inefficiencies. A general set of measurements used for geodetic measurements on Earth spans only ten to at most a hundred sessions, where not all stations are available for each session, thus creating a lot of gaps. Another problem is the inconsistency of hardware, every VLBI station on Earth is different, which introduces inconsistend instrument errors. Taking all of these factors into account, These systems are still able to produce measurements with an accuracy of up to 0.1 mm per year over 20 years [85]. All landers in this mission will be identical and designed specifically for maximum accuracy in the VLBI measurements. The required accuracy, as mentioned above is 1 mm/yr. The measurements described in Sarti et al. [85] (mentioned above) are 2.5 times more accurate, thus the required accuracy is theoretically acheivable. Further testing and modelling will however be required to verify this.

Accuracy improvements

If it is found after landing that the accuracy is not sufficient or even better accuracy of certain baselines is wanted, several changes to the schedule can be made. The length of the DSN transmission can be increased, while reducing the number of landers actively participating in the session, such that the total amount of data that needs to be returned does not significantly increase. If an extra or a new

relay satellite would become available, the measurements can also be increased in size and frequency to further increase the accuracy. Finally, since all of the landers are designed to survive *at least* the design life of five years, it is likely that some will survive much longer. Every year that the mission is extended will mean an increase in accuracy.

3.3.2 Secondary objectives

In this design the *VBB* seismometer, designed for the *ExoMars* mission, is the instrument of choice. This seismometer is an instrument designed especially for space applications and is the latest update of *space seismometers*. This seismometer is designed to survive high impacts and the harsh environment on Mars, which is further elaborated on in 4.6 and 4.3.2. Dependent on the sensitivity of the seismometer, a higher accuracy can be reached. Two principles, *seismic interferometry* and *Ray principle* are applied to investigate the crust. *Seismic interferometry* is a principle that uses wind noise as a source whereas *Rays Principle* uses natural impacts. The higher the sensitivity of the seismometer, the more data will be available. Dependent on the amounts of impacts and the sensitivity more impacts might be recognized. As mentioned from the expert *Guy Drijkoningen*, the seismometers, that were used on the Apollo mission, are already sensitive enough to determine seismic activity as well as noise. Thus it is assumed, taking the latest update of *space seismometers*, that the accuracy will be high enough to investigate the crust.

Chapter 4

Probe

This chapter explains the design of the probe. The first section, 4.1, describes the probe, i.e. the functions it needs to fulfil and the requirements that follow from it. The next two sections, 4.2 and 4.3, contain the design of the main payload of the mission. Followed by two sections which describe the components that lands this payload safely during the impact landing, sections 4.4 and 4.6. Other supporting subsystems are the *Power* and *Thermal Control*, which are discussed in sections 4.5 and 4.7 respectively. After all these subsystems are designed and specified, the layout and the structure of the instrument box are finalized in sections, 4.9 and 4.10.

4.1 Probe Design Description

This section describes the functions the probe needs to fulfill and by which subsystems they are performed. The main objective is to measure the relative movements between the multitude of probes triggered by moving plates. As discussed in chapter 3: *Mission Operations*, the principle is based on radio interferometry to determine the relative distance between the probes. Signals send from the Deep Space Network, are captured by the antennas on the probes and in combination with the data from atomic clocks, these can be send back via a Martian satellite to be analyzed.
Apart from the primary objectives, the secondary objectives are to improve the measurements of the internal composition of Mars. A high velocity landing will deliver a seismometer deep into the crust of Mars. The instrument box of the probe is first of all damped by the pin penetrating the surface of Mars, then the crushable aluminum honeycomb structure hits the surface to provide additional damping. The penetrator, with seismometer, then separates from the instrument box going deeper into the Martian surface. The seismometer will have its own crushable structure within the penetrator to damp the loads. A structural analysis will be performed to calculate the needed parameters to design the most efficient and safe system. Figure 4.1 shows all these and more components of the probe, the parachute and the heat shield are discussed in section 5.5: *Entry, Descent and Landing*.
The final dimensions and the masses of the components are listed in table 4.1, these are justified in their respective sections in this chapter.

Table 4.1: Dimensions and masses of the components installed on the probe

Component	Mass [kg]	Dimensions [cm]
Solar Panel	1.1	⊘ 10.40 x 32.4
Battery	2.5	12 x 12 x 6.67
Antenna	0.4	14 x 22 x 0.5
Computer System	4	12 x 30 x 11.11
Thermal	1.03	-
Clock	0.1	2 x 10 x 0.25
Box Structure	1.39	35 x 35 x 15
Gas Tank	2.5	⊘ 13.5
Seismometer	0.57	⊘ 10 x 15
Penetrator	77	⊘ 15 x 45
Despining mechanisms	0.3	⊘ 2.8 x 35
OCHS	3.1	35 x 35 x 30
SCHS	0.1	⊘ 10 x 15

4.2 Communications

This section will describe the communication system on the landers. Since the lander will experience a load of about 1300 g during landing, the antenna on the lander has to be able to withstand these large forces. Because of this, a rigid parabolic reflector (dish-antenna) would break during landing.
Two kinds of antennas, both having advantages and disadvantages, will be discussed. Then the design

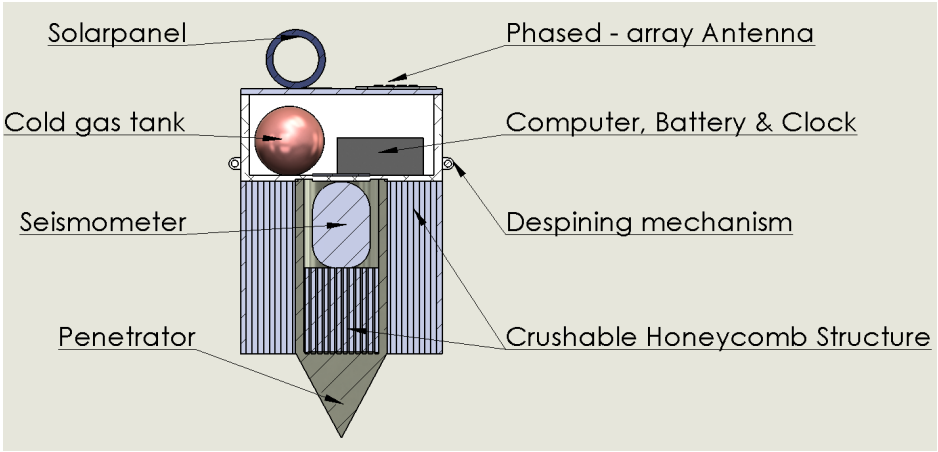

Figure 4.1: Cross-section of the probe, showing all of its components

of the antenna used on the probes will be described, and this section will end with the link budget of this mission.

4.2.1 Options

After consulting literature [94] [42] [96] and talking to Chris Verhoeven (Delft University of Technology, Electrical Engineering), two feasible options were found. The first option is an inflatable parabolic reflector and the second is a phased array antenna.
An inflatable parabolic reflector functions just like a common parabolic reflector except that the structure is not rigid. When inflated it also looks like a 'common' parabolic reflector.
A phased array antenna uses an array of small antennas, or patches, spaced in such a way that the signals amplify each other, to send and receive data. A general picture can be found in figure 4.2.1. Because it has no moving parts or hinges it can be designed to withstand large forces.

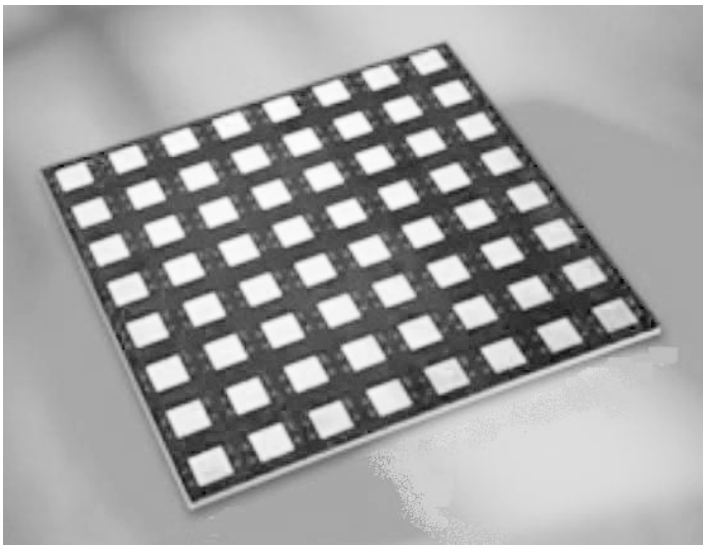

Figure 4.2: A general (8 by 8) phased array antenna

4.2.2 Trade-off

The two antennas will be evaluated on reliability, complexity and data rate.

1. *Reliability:*
   For this criteria the phased array antenna comes out best since it can still function if one of

the patches fails. For the inflatable parabolic reflector a single failure will imply that the whole antenna will fail. Furthermore phased array antennas are widely used while inflatable antennas are still not optimally developed.

2. *Complexity:*
   Combining signals from multiple patches is inherently more complex than evaluating the single signal from a inflatable parabolic reflector. However since the amount of patches used on a phased array antenna for a lander will not be that high (9 will be an initial value), this will be relatively easy.
   A phased array antenna (that is, a dynamic one) can be pointed without any physical movement since this is done electronically. An inflatable parabolic reflector has to be pointed mechanically, which increases the complexity, or it requires a large beam width, which influences the next criteria, data rate.

3. *Data rate:*
   The data rate an antenna can transmit is mainly dependent on the gain of the receiving and the transmitting antenna. This will be explained later in more detail. Since the receiving antenna is fixed (an existing orbiter will be used) the transmitting antenna is the only influence on this. The gain of a phased array antenna can be computed using equation 4.1 [42] and the gain of a parabolic reflector can be computed using equation 4.2 [94].

$$G_{t2} = \pi \cdot N \cdot \eta \cdot cos(\theta_s) \tag{4.1}$$

$$G_{t1} = 44.3 - 10 \cdot log(\alpha^2) \tag{4.2}$$

   In both equations G equals the gain in dB. For equation 4.1 N equals the amount of patches, η equals the efficiency and θ equals the scanning angle in degrees, both for receiving signals from Earth and sending data to the MRO (θ equals zero when scanning perpendicular to the Martian surface). In equation 4.2 α equals the antenna beam width.
   The gain of the inflatable parabolic reflector, using 90° beam width, will be about 5 dB. The gain of the phased array antenna will be between 11 dB (for 9 patches) and 19.5 dB(for 16 patches). This includes a (low) efficiency of 0.55. The conclusion of these numbers is that the phased array antenna can transmit more data than the inflatable parabolic reflector.

As a conclusion, the phased array antenna has better reliability and higher data rate. Thus, the phased array antenna is chosen as the antenna that will be on the lander.

4.2.3 Antenna Design

The size of the phased array antenna will be dependent on three factors, namely the transmitting beam width, the amount of patches (and their lay-out) and the size of a single patch. The transmitting beam width has a large influence on the spacing of the probes. This minimum spacing between the center of each probe can be computed using equation 4.3.

$$spacing = \lambda/2 = \frac{c}{f \cdot 2} \tag{4.3}$$

Here λ is the wave length in meter, c is the speed of light (m/s) and f equals the frequency (Hz). For a transmission frequency of 7.51 GHz (equal to the frequency the DSN uses for X-band transmissions) λ equals 0.040 m, leading to a minimum spacing of 0.020 m, or 2.0 cm. It is important to use this distance to avoid the generation of multiple beams, and to ensure the signals from the separate nodes will amplify each other.
From literature [55] it can seen that additional space has to be reserved for electronic circuits. Therefore a minimum size for an antenna consisting of 16 patches will be 22 by 14 cm. The thickness will be 3.2 mm when used in an array, and weigh 0.4 kg.
The total area of the antenna for a 4 by 4 configuration will now equal 308 cm^2. The thickness will be 5 mm since a small margin will be added to account for the changes in design required to withstand the impact loads. The antenna will use 1.6 watt of power and will be able to transmit a maximum of 1000 kbit/s. This will be explained to more detail in the next section. Why this data rate is required can be found in section 3.3.1

Figure 4.3: The phased array antenna mounted on the instrument box

The antenna will require software to compute the position of the satellite orbiting Mars since the beam has to be pointed. The half power beam width (θ_b) of this antenna can be computed using equation 4.4.

$$\theta_b = \frac{100}{\sqrt{N}} \tag{4.4}$$

This leads to a θ_b of 25°. This implies that if the antenna is pointed with at least this accuracy, a minimum of 500 kbit/s can be sent. This will also be discussed in more detail in the next part.
The antenna will be positioned in such a way that the large loads generated during landing will not critically deform it. A render of the designed antenna mounted on top of the instrument box can be found in figure 4.2.3.

4.2.4 Link Budget

This part will describe how the link budget used in this mission is determined. Firstly it should noted that creating a link budget is an iterative process. There are a lot of parameters that have to be determined, and when a first estimate of the link budget is complete, these parameters should be changed until a satisfactory outcome is produced. The most important information the link budget will provide is the size of all the antennas required, the amount of power they will use and the data rate they can achieve. The link budget will be calculated using literature [94] [42].

In order to transfer data, the received energy-per-bit to noise-density ratio (E_b/N_0) should be 'sufficient'. What is sufficient depends on factors which will be explained later on. The equation to determine the E_b/N_0 is

$$E_b/N_0 = P_{dBW} + L_l + G_t + L_{pr} + L_s + L_a + G_r + 228.6 - 10log(T_s) - 10log(R) \tag{4.5}$$

Here P_{dBW} is the transmitter power in decibel watt, L_l is the transmitter line loss, G_t is the transmit antenna gain, L_{pr} is the receive antenna pointing loss, L_s is the space loss, L_a is the propagation and polarization loss, G_r is the receive antenna gain, T_s is the system noise temperature and R is the data rate.

Transmitter

In order to solve equation 4.5 first some parameters need to be determined. The first one is the frequency (f) used for the transmission. The choice is arbitrary (between 0.2 and 60 GHz), but it will have an effect on the calculations. Also some frequency's might be unavailable because they are used by the military, for example. For this mission a value of 7.51 GHz was picked. This is the X-band frequency used by the DSN. The phased array antenna will also use this frequency to

send data because this kind of antenna can only handle one frequency. The second parameter is the transmitter power in watts (P_W) which will then be converted into decibel watts using

$$P_{dBW} = 10log(P_W) \tag{4.6}$$

Here, P_{dBW} is the power in decibel watts. The transmitter power again is an arbitrary choice, but it has to be taken in account that a high transmitter power might be impossible for an antenna that is not Earth-based. For the transmission from the DNS a value of 400 kW (56 dBW) was picked after some iterations, while for the transmission from the probe a power of 0.2 W (-7.0 dBW) was found to be sufficient.
The third parameter is the transmitter line loss (L_l), which is usually between -1 and -3 dB. This value should be estimated. A value of -1 was picked for both transmissions.

Now, since the transmitting antenna on the DSN differs from the antenna on the probes, the next few equations will differ. First the process for transmitting data using the DSN will be discussed, then the process of transmitting using the phased array antenna on the probe will be shown.

1. **DSN Antenna**
   The first DSN specific parameter is the transmit antenna beam width (θ_t). As will be shown later, a low value will decrease the amount of power required, while a high value will decrease the pointing accuracy required on the receiver. For this transmission, a beam width of 0,082 degrees was picked because this results into an antenna diameter of approximately 34 meter. This will be shown later on. This beam width corresponds to the beam width commonly used by the DSN network for X-Band transmissions [48].
   The final parameter for this transmitter is the transmit antenna pointing offset (e_t). For the antenna used by the DSN, this pointing offset is really low [86]. Values op to 10 millidegrees are achieved. To account for some margins, an offset of 20 millidegrees was chosen.

   When these values are determined, the peak transmit antenna gain (G_{pt1}) can be calculated using

   $$G_{pt1} \approx 44.3 - 10log(\theta_t) \tag{4.7}$$

   the transmit antenna diameter (D_t) using

   $$D_t = \frac{21}{f \cdot \theta_t} \tag{4.8}$$

   and the transmit antenna pointing loss using

   $$L_{pt} = -12(e_t/\theta_t)^2 \tag{4.9}$$

   Finally the transmit antenna gain (G_{t1}) can be computed by adding the peak transmit antenna gain and the transmit antenna pointing loss. This is the most important value for the transmitter. The higher this value gets the better. Also the Equivalent Isotropic Radiated Power ($EIRP$) can be computed by adding the transmitter power in decibel watt, the transmitter line loss and the transmit antenna gain. The calculated values for these equations are in table 1.

Table 4.2: Calculated values regarding the DSN transmissions

	Unit	Value
Peak transmit antenna gain	dBi	66.0
Transmit antenna diameter	m	34
transmit antenna pointing loss	dB	-0.7
transmit antenna gain	dB	65.3
EIRP	dBW	120.3

2. **Phased Array Antenna** To calculate the gain of the antenna on the probe, the same approach as described before in the section about the trade-off and the design should be used. The first parameter to be defined is the amount of elements the antenna consists of (N). 16 was picked as a final value for this (after a few design iterations). Also an efficiency (η) had to be estimated. A

value of 0.55 was estimated [94]. Now the peak transmit antenna gain (G_{pt2}) can be computed using equation 4.10.

$$G_{pt2} = \pi \cdot N \cdot \eta \tag{4.10}$$

When scanning to an angle θ_s, a phased array antenna will lose some of its gain. This loss is equal to the cosine of the scanning angle. A maximum scanning angle of 45° was picked as the design limit. Now equation 4.10 can be used to calculate the phased array antenna gain. Also EIRP can be computed. The calculated values can be found in table 4.3.

Table 4.3: Calculated values regarding probe transmissions

	Unit	Value
Peak transmit antenna gain	dBi	27.6
Transmit antenna gain	dB	19.5
EIRP	dBW	11.5

Additional Losses

While traveling from transmitter to receiver, a signal will lose power. Only one additional input parameter is required, which is the propagation path length (S). This simply is the distance between the transmitter and the receiver. The maximum distance used for transmissions should be picked, and not the average, since this will most likely imply that the signals can not be sent at maximum distance. For the transmission from the DSN to the probes, S equals $3.75 \cdot 10^8$ km. For the transmission between the probes and the orbiter, S equals 750 km. With the propagation path length the space loss (L_s) can be computed using

$$L_s = 147.55 - 20log(S \cdot 1 \cdot 10^3 - 20log(f \cdot 1 \cdot 10^9) \tag{4.11}$$

For the transmission from the DSN this loss equals -281 dB. For the transmission between the probe and the lander it equals -167 dB. Also the propagation and polarization loss have to be determined. This should be done using literature [94]. The loss depends on the frequency used. It also depends on the atmosphere the signal travels through. Common values are between 0 and 0.5 decibel. For the transmission from the DSN 0.3 was picked. For the transmission from the probes 0 was picked.

Receiver

Since two kinds of antennas are used this part will also be split into two parts.

1. **Orbiter Antenna** For the receiving parabolic antenna two parameters have to be determined. The first one is the receive antenna diameter (D_r). The choice is arbitrary, although a diameter of 50 meters will not come in handy for an antenna on a satellite. Therefore the diameter was set to 0.5 m. The second parameter that has to be chosen is the receive antenna pointing error (e_r). A high value decreases the complexity of the receiver. This value should always be lower then the receive antenna beam width (θ_r), because else the antenna might 'miss' the signal completely. Therefore a value of 15° was picked.

   With these parameters determined the peak receive antenna gain (G_{rp}) can be calculated using

   $$G_{rp} = 159.59 + 20log(D_r) + 20log(f) + 10log(\eta) \tag{4.12}$$

   In this equation η is the efficiency of the antenna. 0.55 is a common value. Furthermore the receive antenna beam width (θ_r) can be computed using

   $$\theta_r = \frac{21}{f \cdot D_r} \tag{4.13}$$

   the receive antenna pointing loss (L_{pr}) using

   $$L_{pr} = -12(e_r/\theta_r)^2 \tag{4.14}$$

   And the receive antenna gain (G_r) by adding the peak receive antenna gain and the receive antenna pointing loss. This also is the most important value for the receiver. The higher this value gets, the better. The calculated values are shown in table 1.

Table 4.4: Calculated values for the receiving antenna on the orbiter

	Unit	Value
Peak receive antenna gain	dBi	29.3
Receive antenna beam width	deg	30.0
Receive antenna pointing loss	dB	-3.0
Receive antenna gain	dBi	26.3

2. **Phased Array Antenna** For the receiving phased array antenna most values are already known. They are equal to the transmission values from table 4.3.

Final Calculations

To complete the link budget, a few more parameters have to be determined. The system noise temperature (T_s) will be the first one. It should be determined using literature [94]. Values usually are between 135 and 763 Kelvin. For the transmission from Earth the value equals 614 K. For the transmission from the probes this value equals 400 K. Now, in order to use equation 4.5 the data rate has to be determined. This depends on the system used. The minimum amount (to send simple commands to an orbiting satellite) is in the order of 100 bps. However, for the system designed and to measure small displacements, a higher data rate is required. A data rate of 5 kb/s was determined for the transmission. A data rate of 1 mb/s was determined for the transmission from the probes to the orbiter.

Finally the received energy-per-bit to noise-density can be computed using equation 4.5. This value equals 16.7 dB for the transmission from Earth, and 14.0 dB for the transmission from the probes. The higher this value is the better. With this value the carrier-to-noise density ratio (C/N_0) can be computed using

$$C/N_0 = E_b/N_0 + 10log(R) \tag{4.15}$$

This is the ratio of signal power to white-noise spectral density. It is equal to 53.7 dB-Hz for transmission from Earth and 74.0 dB-Hz for the transmission from Mars.

In order to check whether the calculated E_b/N_0 is sufficient, the bit error rate (BER) should be determined. Typical values are between 10^{-5} and 10^{-7}. The first value was picked for the transmission from Mars while the second was picked for the transmission from Earth.
Then the coding scheme should be determined (using literature). For both transmissions BPSK and QPSK Plus R-1/2 Viterbi Decoding was chosen, because of the excellent BER performance. The value for this $ReqE_b/N_0$ equals 5 dB for both transmitter-receiver systems.
The last input parameter that has to be defined is the implementation loss. Values are between 1 and 2 decibel. Because top of the notch technology will be used, a value of 1 was picked for both transmissions.
Now by subtracting the implementation loss and the required E_b/N_0 from the calculated E_b/N_0 the margin can be computed. If this value is higher than 0 the transmission of data will succeed. The Margin for the transmission from Earth equals 10.7 dB. The margin for the transmission to the orbiter equals 4.7 dB. One final note, if transmitting happens during rainy conditions the losses will be higher. Therefore a sufficient margin (to be determined from literature) should be available. The margin should be higher for the Earth-based transmission since atmospheric disturbances (like rain) are more severe.

4.3 Payload

This section will elaborate on the payload of the probes. The payload on the probes has to fulfill two functions. The first function is keeping track of time so the primary mission objective can be fulfilled. This will be done by a number of clocks, who will be described in the following part. The second function of the payload is measuring seismic activity. This will be performed by the seismometer that is placed in the soil-penetrated pin. The seismometer will described in detail in the second part of this section.

4.3.1 Atomic Frequency Standard

This part will describe the frequency standard used on the probe. There are a few challenges for the timekeeping device on the probe. The first challenge is the high accuracy that has to be achieved in order to make detailed measurements. The second challenge is the low power consumption that the device should have. The final challenge is the large impact load the clock has to withstand during landing.
The accuracy of a clock is generally measured with the Allan Deviation. The lower this value is, the more accurate a clock will be. Most important is the short term phase stability of the clock. More information about accuracy, and how it has influence on the provided measurements will be in chapter 3.3.1. The clock should run on a very low amount of power since it should always function, even when a dust-storm is present. This is critical because the clock can not be synchronized after measurements have started as this would create larger errors in the time-offset. This will require more work to be done by the correlator. Taking this into account, a maximum power usage of 0.5 W was determined, although a lower value is preferred.

Generally spoken, a lower power consumption implies a lower accuracy. The solution that was found is the usage of a chip-scaled atomic clock [32]. These clocks were tested and developed in 2008. A picture of the clock can be see in figure 4.3.1. Money from the mission budget might be spent

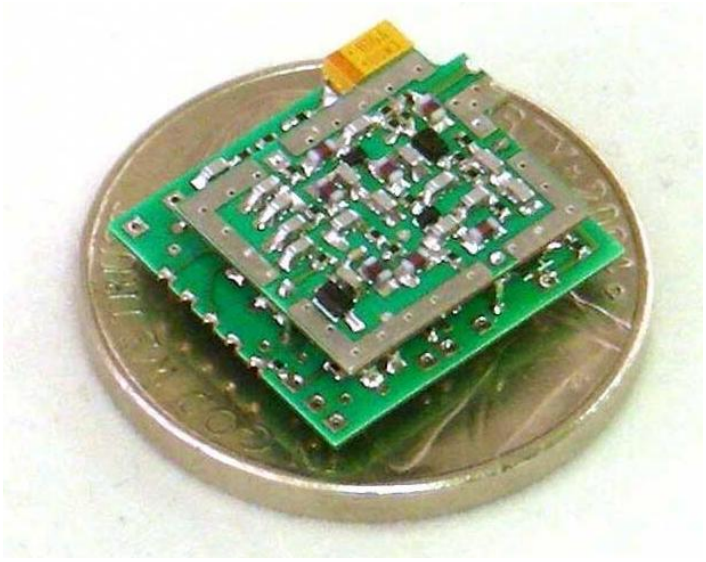

Figure 4.4: A Chip-Sized Atomic Clock

to further develop and improve this kind of atomic frequency standards. Specifics of this clock can be found in table 4.3.1. To further increase the accuracy of the system, 5 clocks will be taken on

Table 4.5: Chip-Scaled Atomic Clock specifications

Accuracy	$1 \cdot 10^{-11}$ per hour
Power Consumption	30 mW
Volume	1 cm^3

one lander. The method of using multiple clocks to end up with one more accurate time signal is also used by the Bureau International des Poids et Measures to determine the Coordinated Universal Time [59].
The clocks that are on the probes have to be protected against the large g-forces that exist during the landing. The clock's durability will have to be improved, and a casing and or layer to protect against large forces has to be developed. This will be possible since there are over 5 year left until the system will be launched. The advantage of this clock is the small size and the low weight, because this implies that few forces will be exerted on the clock (during landing) if the instrument box is designed correctly.

4.3.2 Seismometer

The secondary objective of this mission is to investigate the internal structure of Mars. Thus a seismometer is implemented in each probe. In general seismometers are very sensitive devices that are not designed to withstand the challenges faced on a planet like Mars. Advanced seismometers were designed in the past for interplanetary missions. The first time a seismometer was used in space was in 1993, when a seimometer, called *optimism* was designed for a mission to Mars. After the initial design, the seismometer was enhanced two times. In 2003 a project called *NetLander* was introduced and a new seismometer, called *VBB EMs*, was built. This seismometer was, then again, improved for the project *Exo Mars*, running from 2006 to 2009 [91].

The latest design of a seimometer, for space applications, is the one designed for the *ExoMars* project, by *SODERN*. This seimometer is a very broad band seismometer (VBB) and is in principle the device that is used on this mission. The seismometer will be implemented into the penetrator, to reduce external disturbances. All information presented on the design of the seimometer was found from literature [75]

Principle

In order to assure detection of movement, over all three axes, an inverted pendulum with an angle of 35.25 deg is used. This offset from the vertical axis is advantageous when a low mass of the pendulum and a high sensitivity needs to be achieved. The pendulum, that vibrates and oscillates around the axis, is in an equilibrium. A leaf spring is attached to the pendulum which ,if there are no disturbances, will hold the pendulum in equilibrium. A counter balance mechanism is installed in the seismometer, to assure the equilibrium of the mobile part. If disturbances occur, the leaf spring will transmit this to the pendulum, that then will react. These movements will be detected by two sensors. All devices, included in the seismometer, are sorounded by a sphere which is then set in vacuum. A technical drawing of the seismometer can be found in figure 4.5 and 4.6 .

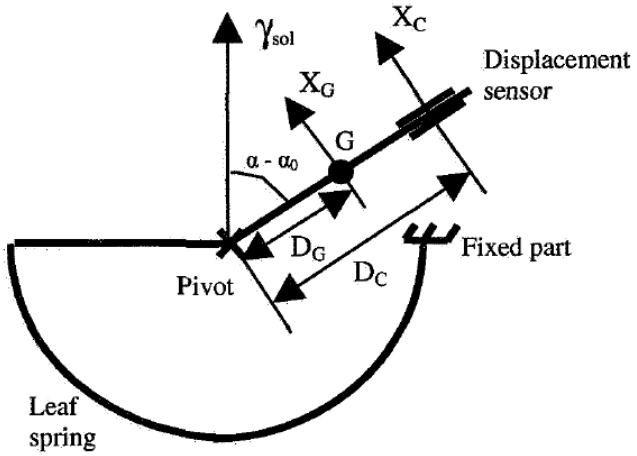

Figure 4.5: The principle of the VBB seismometer [75]

Performance

The VBB seismometer designed by *SODERN* is designed to withstand the harsh environment of Mars. A design criteria for every system in space applications is low weight. This seismometer weighs approximately 570 g. Its dimensions are 15 cm in diameter and 15 cm in height. All performance details, both from the model and the testing, can be found in table 4.7 and table 4.8 respectively.

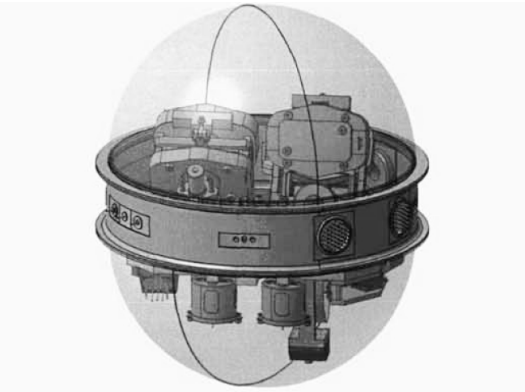

Figure 4.6: The VBB seismometer [75]

Modal analysis	Earth config.	Mars config.
Pendulum	0.35 Hz	0.70 Hz
Spring	81 Hz	81 Hz
Pivot	90 Hz	96 Hz
Fixed part	137 Hz	
Mechanical sensitivity (m/k)	Earth config.	Mars config.
Vertical sensitivity	$1.39\ 10^{-2}\ s^2$	$2.38\ 10^{-2}\ s^2$
Horizontal sensitivity	$1.99\ 10^{-2}\ s^2$	$3.38\ 10^{-2}\ s^2$
Thermal sensitivity		
Leaf spring	7.3 µm/°K $\beta = -16 \cdot 10^{-6}\ K^{-1}$	0.9 µm/°K $\beta = +16 \cdot 10^{-6}\ K^{-1}$

Figure 4.7: Model based performances [75]

Modal analysis	Modeling	Testing
Pendulum	0.35 Hz	0.50 Hz
Mechanical sensitivity	Modeling	Testing
Vertical sensitivity	$1.39\ 10^{-2}\ s^2$	$1.73\ 10^{-2}\ s^2$
Horizontal Sensitivity	$1.99\ 10^{-2}\ s^2$	$2.45\ 10^{-2}\ s^2$
Thermal sensitivity	Modeling	Testing
Leaf spring	4.1 µm/°K $\beta = +1 \cdot 10^{-6}\ K^{-1}$	4.8 µm/°K $\beta = +1 \cdot 10^{-6}\ K^{-1}$

Figure 4.8: Results of the performance tests [75]

For this mission, adjustments will need to be made before implementation. The dimensions of the seismometer are too big. The diameter will need to be adjusted to 10 cm. During testing, the seismometer had to withstand a shock loading of $200g$ over a half sin of 20 ms. This shock loading is not enough for this mission. Here a shock loading of 400 g, over a half sin of 15 ms, needs to be accounted for. Since the mission is only launched in 2018, five years of development time is available. Within this time it is expected that adjustments are realizable. The damping system should be further enhanced to absorb more energy and the seismometer should be enhanced to fit within the dimensions.

4.4 Penetration Depth and Pin Design

This section will show the calculations of the penetration depth of the pin. These calculations are closely related to the design of the pin, since most parameters used in the calculations have an impact on the properties of the pin.
First the general equation for penetration depth will be discussed. A program was made to allow for quick iterations of the design process, since changes in penetration depth can be made dependent on one parameter. First initial values are assumed and an initial calculation is made. Then changes to the nose are implemented. This is followed by changes to the area, the impact velocity and finally to the weight.
This section is ended with a small conclusion containing the final design.

4.4.1 Equations for penetration depth

In order to calculate the depth the pin will reach equations 4.16 and 4.17 are used. These equations were obtained from literature [20].

$$Z = 0.607 \cdot K \cdot S \cdot N \cdot \sqrt{W/A} \cdot ln(1 + \frac{V^2}{4650}) \qquad V < 61m/s \tag{4.16}$$

$$Z = 0,00117 \cdot K \cdot S \cdot N \cdot \sqrt{W/A} \cdot (V - 30.5) \qquad V \geq 61m/s \tag{4.17}$$

In these equations, Z equals the final penetration depth (m). K stands for the mass scaling factor $(-)$, S equals the soil penetrability index $(-)$, N is the projectile nose performance coefficient $(-)$ (K,S and N will be discussed below), W regards the pin mass (kg), A is the cross-sectional area of the pin (cm^2) and V stands for the impact velocity (m/s).
The mass scaling factor is a dimensionless number that is taken from literature [20]. The value depends on the weight of the pin. For a mass of 15 kg, the value equals 0.8. For a value of 20 kg, the value equals 0.9. For values above 27 kg, K equals unity. Since the weight of the pin is always assumed to be higher then 27 kilogram, this factor will always equal unity and will therefore not be further discussed.
The soil penetrability index in a dimensionless number that defines the penetrability of the soil that will be penetrated. To determine this number, properties of the Martian surface were investigated. It was found that the yield-strength of the Martian surface is between 4.5 and 12 MPa [90]. This value will be in the upper regions of these values (± 9-12 MPa) while landing in the lowlands, and in the lower regions of these values while landing into the highlands.
A table with values for S was found in literature [20]. This parameter has a value of 1 for a surface with a yield strength of 13.8 MPa. A value of 2 equals fractured low strength rock. Therefore a value between 1.2 and 2 was chosen for the final design, and a value of 1.5 was picked for initial calculations. S is the only parameter that will remain a variable (between 1.2 and 2) for this design.
The nose performance coefficient is a dimensionless number that was obtained from literature [20]. For a flat surface this value equals 0.56, for a cone with a length-to-diameter ratio (L/D) of 1 this equals 0.82, for an L/D of 2 this equals 1.08 and for an L/D of 3 this equals 1.33.

4.4.2 Initial Values

To design the pin a first set of parameters had to be estimated. These first estimations can be found in table 4.6.

Table 4.6: Initial values to calculate Penetration Depth

Parameter	Initial Value
K	1
S	1.2-2
N	0.82
W	25.6
A	176.7
V	60

K is equal to 1 since V is higher then 27. S is picked as 1.2-2 since those values cover the different strengths of the Martian surface. N is picked as 0.82 since a cone with an L/D of 1 is assumed.
The first design of the pin is a 30 cm long steel (7860 kg/m^3) cylinder with a diameter of 15 cm, with a cone at the bottom for a total length of 45 cm since L/D equals 1. This pin is solid, except for a hollow space where the seismometer is placed. This space is a cylinder with a diameter of 10 cm and a height of 30 centimeter. The volume of this object can be computed from equation 4.18.

$$Volume = (\frac{1}{3} \cdot \pi \cdot r_1^2 \cdot l_1) + (\pi \cdot r_1^2 \cdot l_2) - (\pi \cdot r_2^2 \cdot l_3) \tag{4.18}$$

Here r_1 is the radius of the pin in cm, l_1 is the length of the cone in cm, l_2 is the length of the pin without the cone in cm, r_2 is the diameter of the seismometer area and l_3 is the height of the seismometer area. This leads to a total volume of 3.83 dm^3. Therefore the weight equals 30.1 kg. When a seismometer is included this leads to a total weight of 32.5 kg. A was calculated to be 176.7 cm^2 since the diameter of the pin equals 15 cm. V was assumed to be 60 m/s, the minimum velocity that could be used using parachutes only as a way of slowing down during descent.
The calculated values for penetration depth using these initial values and equation 4.16 can be found in figure 4.4.2. For these values the penetration depth will be between 14 and 24 centimeter. This

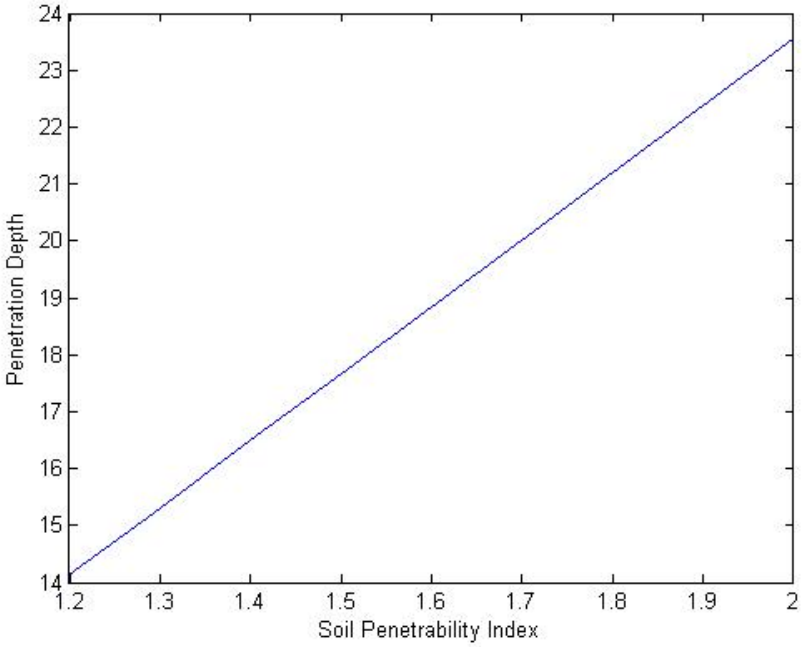

Figure 4.9: Penetration Depth as a function of Soil Penetrability

will not be sufficient since the pin has a height of 45 centimeters and this pin has to be completely submerged. Therefore parameters will be changed.

4.4.3 Optimizing the design

The first change that is considered is a change into the nose performance coefficient. S will be chosen as 1.5 for these computations, and the other parameters will remain constant. The penetration depth for other cone shapes is shown in table 4.4.3. These changes will not cause the pin to penetrate deep

Table 4.7: Penetration Depth for various Cone Shapes

Cone Shape (L/D)	Nose Performance coefficient	Penetration Depth
1	0.82	17.6
2	1.08	23.3
3	1.33	28.7

enough into the surface. Even worse, because the cone gets longer (15 cm for $L/D = 2$ and 30 cm for $L/D = 3$) the back end of the pin will actually be higher above the surface. Therefore the initial value will be kept and other parameters have to be changed.

The next step is the change of the weight. This will be done by changing the material of the pin, because this will not affect the dimensions. Tungsten (wolfram) was chosen as a replacement of steel, since it has a very high density of 19600 kg/m^3. It also has a very high ultimate strength of 1510 MPa. Since the volume of the cylinder equals 3.83 dm^3 the new weight will be 77.5 kg (including seismometer). Keeping the other values equal to the initial values and taking a value of 1.5 for S, using equation 4.16 a penetration depth of 29.4 cm was calculated. This is still not sufficient, but since this change will not negatively influence the design this change will be adopted.
The next parameter that can be changed is the cross-sectional area. If this area is made smaller the penetration depth will increase. However, a smaller diameter implies fewer space for the seismometer, which is not possible. Therefore no changes to this parameter will be made.
The final parameter that can be changed is the impact speed. A plot with a variable impact speed, S at 1.2 (assuming worst case), W at 77.5 kg and all other parameters at initial values in shown in figure 4.4.3. This plot was computed using equation 4.16 and 4.17. For a value of 90 m/s, the

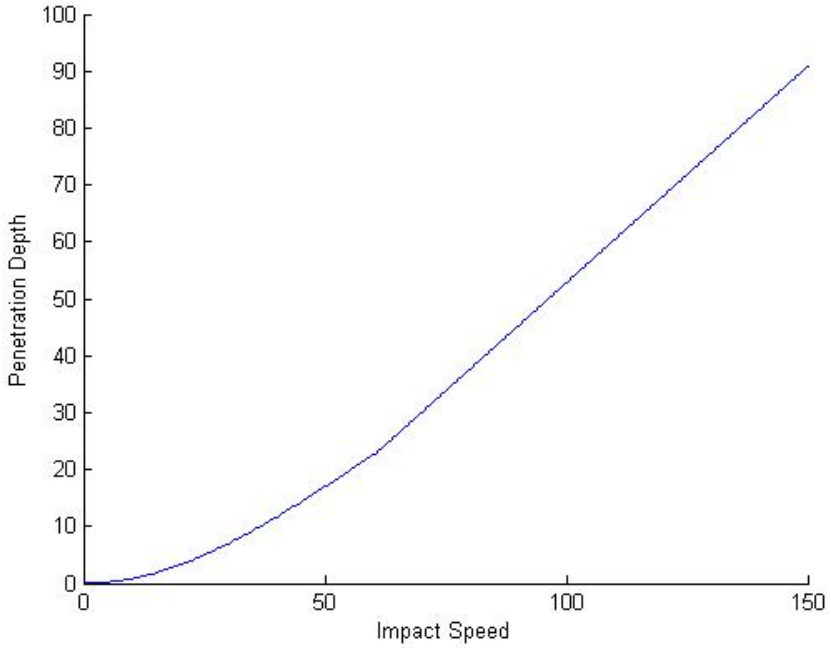

Figure 4.10: Penetration Depth as a function of Velocity

penetration depth will be 45.2 cm. This value was picked since it will completely submerge the pin assuming a worst-case scenario regarding the soil penetrability.

4.4.4 Final Design

The final design parameters for the pin can be found in table 4.8. A plot using this values can be found in figure 4.11.
This leads to a minimum penetration depth of 45.2 cm and a maximum penetration depth of 75.4 cm. This implies that the seismometer and the pin will always be below the surface. Since the surface strength will probably be on the lower side of the range [90], S will be on the higher side. Therefore the penetration depth for the seismometer will be higher, which increases their accuracy.
Another design parameter that can be determined from this design is the length of the connection between the pin and the structure. Subtracting the length of the pin from the penetration depth shows a value between 0.2 and 30.4 cm. The connection should therefore be a little longer then 30.4 cm.

Table 4.8: Final values to calculate Penetration Depth

Parameter	Initial Value
K	1
S	1.2-2
N	0.82
W	77.5
A	176.7
V	90

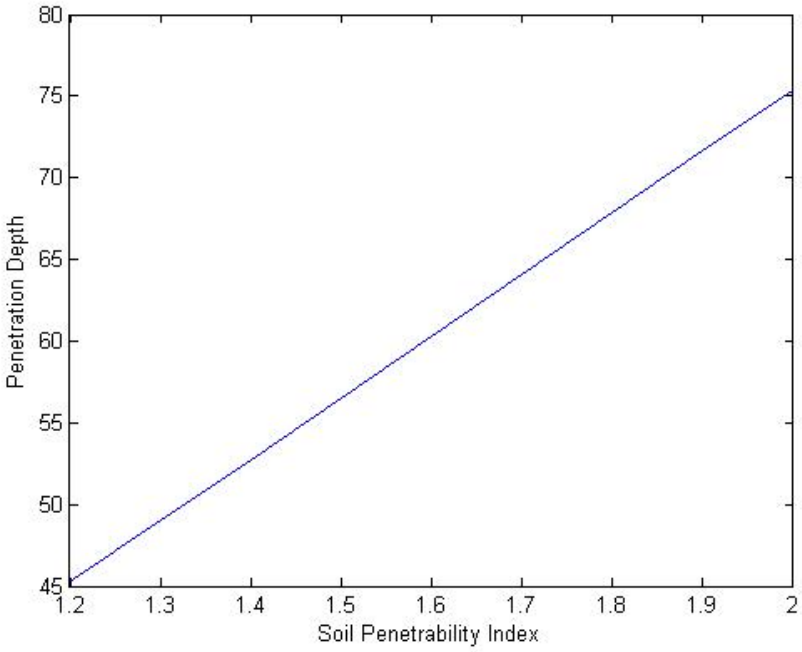

Figure 4.11: Penetration Depth as a function of Soil Penetrability

4.5 Power

This section describes the design of the probe's power subsystem. First the power requirements are described, then the selection of the type of solar panel is explained, after which the effects of wind on the solar panel are elaborated on. The possibility of using a dust shield is evaluated, and finally the energy storage and power regulation are discussed.

4.5.1 Requirements

The requirements that are important for the solar panel design are listed below. Average power consumption by the probe is shown in table 4.9. These power requirements were obtained from the subsystem designs, as described in their respective sections.

- Provide the average power required throughout the 5 years lifetime of the mission
- Store enough energy to last through the night

4.5.2 Solar Panel Design

The design of the solar panel involves the following steps: First the solar irradiance is found, then the solar panel is sized based on the irradiance, solar cell efficiency, average power required and degradation effects. These will lead to a required solar panel area, depending on the type of solar

Table 4.9: Probe power distribution. This table shows the average power used by the probes subsystems during nominal operation

Subsystem	Average Power [W]
Payload	1.0
Communication	1.6
Command & Data handling	10.0
Thermal Control	5.0
Losses	5.0
Total	**22.6**

panel chosen, to which a safety factor is added. Additionally, a mechanism to deploy the solar panels is described.

Solar Irradiance

The solar irradiance can be found in table 4.10. The lowest value, 3938 W-hrs/m^2 (or 164 W/m^2), is used for the solar panel design, in order to assure each probe will have enough power, independent of its location.

Table 4.10: Daily solar irradiance on Mars (W-hrs/m^2), for latitude and longitude around Valles Marineris [80]

	Latitude (°)			
L_s (°)	-30	-15	0	15
270	6381	5865	5033	3938
292.5	6066	5660	4937	3943
315.0	5466	5319	4844	4074

Degradation

The efficiency of the solar panel reduces due to degradation effects. First of all there is a difference between the best efficiency for a cell, and the efficiency after assembling them into an array. This difference is typically about 15% [94]. Temperature has an influence as well, higher temperatures usually lowers efficiency. Finally there is degradation over the lifetime of the probe. Life degradation mainly occurs due to radiation. Another cause is thermal cycling due to temperature differences between day and night. The degradation is assumed to be 3.75% per year for silicon solar cells and 2.75% per year for gallium-arsenide cells. These are typical values for cells in LEO orbits [94].
For the probe, which will operate on the surface of Mars, degradation effects are assumed to be similar. In reality, the radiation and thermal cycling will be less. This is because Mars is further away from the sun than Earth, so the solar radiation is less intense. Thermal cycling is also reduced, since the temperature differences are smaller and there is only 1 cycle per day. LEO orbits, on the other hand, have multiple cycles per day since they typically have orbital periods of up to a few hours. Still the same degradation value is assumed due to uncertainty of how large the difference would be.

Type of Solar Cell

Two different types of solar cells were considered for the design. The first possibility is using conventional crystalline triple junction solar cells, for which the highest achieved test efficiency is 37.5% [46], and the second is thin film amorphous solar cells (highest efficiency 28.8% [46].
The advantage of crystalline solar cells is that the highest possible efficiency can be acquired, meaning a smaller solar panel area is needed. A disadvantage is that crystalline cells are also relatively heavy and rigid, as opposed to thin film cells, which are light and flexible. Using crystalline cells would mean several panels are required, including a complex deployment system. For a spacecraft in orbit, deploying an array of panels is relatively simple due to weightlessness, which means very small forces are required to move the panels. For the probe, this will be more complicated. Forces required to move the panels will be larger due to gravity, and the panels and deployment mechanism need to be

able to withstand the high impact landing.
Thin film solar cells have the advantage of being lightweight and flexible. Even though the efficiency is lower, the total weight can be less for the same amount of power as crystalline cells. Additionally, due to being flexible, the solar panel could be rolled up on top of the probe during the travel to Mars. After landing the panel can be deployed by unrolling.

For this design, thin film solar cells are chosen due to their flexibility. This makes them more likely to survive the landing impact, a much simpler deployment mechanism can be used.

Solar Panel Sizing

The average power consumption of the probe is 22.6 W, as shown in section 4.5.1. A safety factor of 10% is added, which brings the power, for which the solar panel is sized, up to 25 W. The highest efficiency thin film solar cells are gallium-arsenide cells made by the company *Alta Devices*. They have achieved a 28.8% cell and 24.1% module efficiency [12]. The cells have a temperature coefficient for power of -0.095 %/°C. Temperatures on Mars can rise up to 297 K, or 24 °C [14]. Since testing conditions are at 25 °C, the efficiency is not reduced due to temperature. The efficiency component due to degradation at end of life, η_{deg}, is calculated using equation 4.19. For a probe life of 5 years and degradation rate of 2.75%, the η_{deg} is 0.87. Efficiency is also affected by dust. The system will have a dust shield, as described in section 4.5.4. This will be used to limit dust accumulation so that it will at most reduce efficiency by 10%. Therefore η_{dust} is 0.9. The total efficiency is then found through equation 4.20 and is equal to 18.9

$$\eta_{deg} = (1 - degradation/yr)^{probe\ life} \tag{4.19}$$

$$\eta_{solar\ panel} = \eta_{module} \cdot \eta_{deg} \cdot \eta_{dust} \tag{4.20}$$

Knowing the total efficiency of the solar panel, it is possible to compute the required solar panel area by equation 4.21. In this equation P_{req} is the required power of 25 W and I the solar irradiance of 164 W. The required solar panel area equals 0.81 m^2.

$$A = \frac{P_{req}}{I \cdot \eta_{solar\ panel}} \tag{4.21}$$

Deployment

The solar panel area is larger than is possible to fit on the outer surface of the probe. Therefore it has to be folded or rolled up and deployed after landing. Having folded up solar panels requires complex mechanisms to deploy the panels. Therefore it was chosen to have one large rolled up solar panel. This has not been done before in space applications, because usually more efficient multijunction crystalline solar cells are used, which are rigid.
However, thin film solar cells are used for other applications on Earth. Possibilities are using them as a portable power source in remote locations for hiking or military applications. Some parameters for existing thin film rolled solar panels are shown in table 4.11. An example picture of one of these rollable solar panels is shown in figure 4.12.
In order to make these solar panels suitable for use on Mars, some adjustments will likely have to be made. Solar cells for Earth orbiting spacecraft are typically protected by coverslides to reduce radiation damage. This radiation is mainly in the form of electrons and protons from solar flares. For Earth orbits, most of the radiation damage is caused by electrons and protons that are trapped in the Earth's magnetic field [94]. For the Ancile mission, it should be investigated how much the radiation at Mars would degrade solar cells, and whether radiation protection is necessary. Additionally, the panel on which the solar cells are attached needs to be flexible in the cold Mars environment. Either a material should be found that is still flexible in the possible temperature range, or the solar panel needs to be kept warm enough until the deployment.
The width of the solar panel is limited by the probe's dimensions. It is taken at 30 cm, slightly smaller than the probe width of 35 cm, to make sure it will fit on top of the probe. Using this width, a length of 2.7 m is required to have an area of 0.81 m^2. The mass of the panel is assumed to be at most 1.1 kg/m^2, equal to the largest solar panel in table 4.11, which has similar dimensions. An extra 10% is added to allow for possible additional mass of the dust shield, which is being incorporated into the

Table 4.11: Parameters for existing rolled solar panels produced by PowerFilm Solar [13]

Rolled dimensions [mm]	Unrolled dimensions [mm]	mass [kg]	Area [m^2]	mass/Area [kg/m^2]
101 x 101 x 368	368 x 1067	0.45	0.39	1.15
101 x 101 x 368	368 x 1543	0.64	0.57	1.13
101 x 101 x 368	368 x 2025	0.82	0.75	1.10

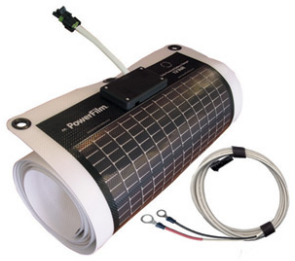

Figure 4.12: Example of a rollable solar panel [13]

solar panel. This brings the mass up to 1.21 kg/m^2, or a total mass of 0.98 kg.

Knowing the solar panel length, a calculation for the diameter of the rolled up panel can be made, as a function of inner diameter of the roll. This calculation is described below.

First, an equation for the solar panel length as a function of time was found. This was done by first finding the equation for an infinitesimal length of the panel, as illustrated by figure 4.13. This results in equation 4.22. In this equation, r refers to the radius, θ the angle, and ds the length of the panel part. The radius of the roll increases by the panel thickness for every revolution, as shown in equation 4.23, where r_0 is the inner radius. The 10.4 cm diameter that was found seems realistic in comparison to the existing solar panels shown in table 4.11.

$$ds = r \cdot d\theta \tag{4.22}$$

$$r(\theta) = r_0 + t\frac{\theta}{2\pi} \tag{4.23}$$

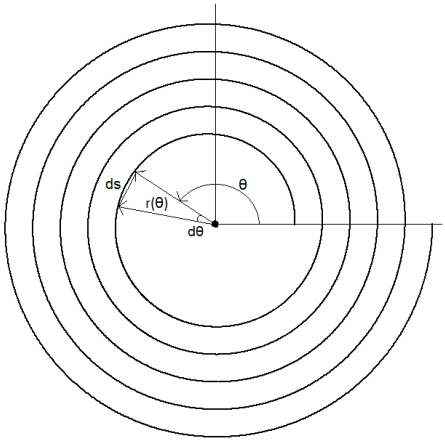

Figure 4.13: Schematic drawing of solar roll

Now, the total length of the panel is found by integrating ds, which results in equation 4.24, where θ_1 is the angle for the end of the panel. This integration leads to equation 4.25 for the panel length as function of θ_1. Rewriting this to find θ_1 as function of total length s results in equation 4.26.

$$s = \int ds = \int_0^{\theta_1} r \cdot d\theta \tag{4.24}$$

$$s = r_0\theta_1 + \frac{t\theta_1^2}{4\pi} \tag{4.25}$$

$$\theta_1 = \frac{-r_0 + \sqrt{{r_0}^2 + \frac{ts}{\pi}}}{\frac{t}{2\pi}} \tag{4.26}$$

Finally, the outer radius of the roll can be found by substituting the value found for θ_1 in equation 4.23. Multiplying this by 2 results in the diameter.
All values related to the calculation of the roll diameter are found in table 4.12. D_{inner} is the inner diameter of the roll, D_{outer} the outer diameter, and $D_{outer,sf}$ the outer diameter when including a 10% safety factor on the inner diameter. The thickness was assumed at 1 mm. The cells themselves are only 0.11 mm thick [12], so this allows for extra thickness of the panel on which they are attached. An additional 0.1 mm was added to the panel to account for possible thickness increase due to the dust shield. This brings the total panel thickness up to 0.11 cm.

Table 4.12: Solar roll dimensions

r_0 [cm]	3.81
t [cm]	0.11
s [cm]	270
D_{inner} [cm]	7.62
D_{outer} [cm]	9.79
$D_{outer,sf}$ [cm]	10.4

To deploy the panel, there will be inflatable tubes on the sides of the panel. Inflating the tubes will then cause the panel to unroll. Since the tubes are on the sides, they are assumed to not add thickness to the panel. The gas, required for inflation of the tubes, can come from the same tank that is used for the inflatable heat shield. Figure 4.14 illustrates how the solar panel would unroll.

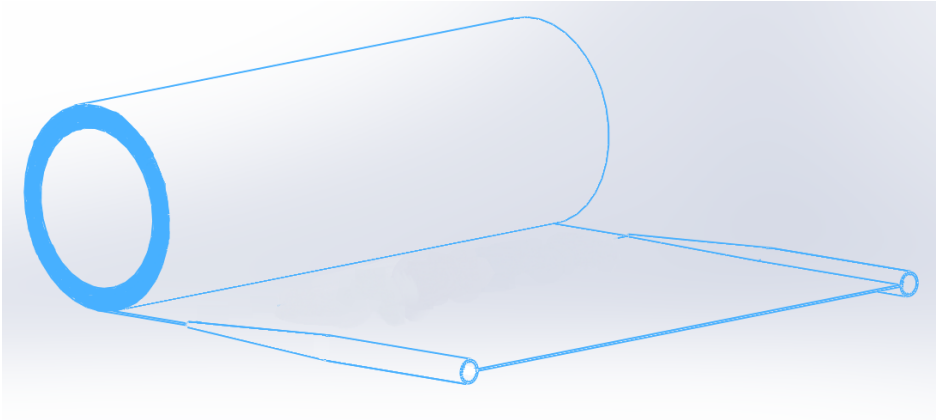

Figure 4.14: Unrolling solar panel

One last issue that needs to be solved is that the rolled up panel needs to be held still during the descent and landing. Especially during the last phase after the parachute and cover are ejected. The panel should be prevented from unrolling during the fall. Since the roll is very light, no large forces will be needed to hold it. This could be done by attaching two elastic bands, placed over the roll and attached to the top of the probe. The attachment could be made so that it breaks from the landing impact, leaving the panel free to unroll when necessary.

4.5.3 Effects of wind

This section elaborates on the effects of wind on the probe. These need to be taken into account as they could disturb the seismic measurements for the secondary objectives. First the different possible effects are identified, then one of these (flapping of the solar panel) is further analysed, after which possible scenarios for the other effects are described.

Possible Movement

The various movements that could be caused by wind are described below.

- **Flapping**
  At high wind speeds, winds may be able to lift the flexible solar panel off the ground, causing it to flap in the wind. This is the strongest motion out of the three considered, and would likely cause the largest perturbations for the measurements.
- **Bending**
  If winds are not strong enough to lift the solar panel, they may still be able to locally bend the panel. If this motion is oscillatory, it may also cause large vibrations in the ground.
- **Vibrations** Besides the two types of movement described above, all winds could cause continuous small vibrations on the solar panel, probe, and heat shield. These could then be transmitted through the ground to the seismometer.

Wind speeds on Mars were measured by the Viking to be about 2 m/s at night and 6-8 m/s during the day. However, during dust storms winds can reach speeds of about 17 m/s. In areas with strong topographic slopes wind is expected to be even higher [14]. However, since the probe is not designed to be able to land on highly sloped surfaces, these higher wind speeds are not taken into account.
For the seismic measurements, it is preferred that the solar panel does not move due to wind and interfere with the measurements. Therefore the effect of wind on the solar panels has to be considered.

Flapping

The aerodynamic forces, which act on the panel due to wind, were analyzed to determine whether they are strong enough to lift the solar panel off the ground. This was done by making an estimation for the lift force, to see if it is higher than the weight of the panel. The aerodynamic forces on the solar panel are very dependent on the shape of the panel. Since the panel is rolled out over the surface, it will be relatively flat, but there can be openings where wind can blow through. This is especially the case at the edge of the probe, but it can also happen because of uneven surfaces. In order to calculate the lift forces, a simplification was made as described below.
The panel is assumed to be like a thin airfoil, and lift forces per area are calculated for a maximum angle of attack of 12 degrees. The angle of the wind cannot be very high, considering the panel is close to the ground. According to thin airfoil theory [17], the lift slope is equal to 2π. The lift per area is calculated by equation 4.27. ρ is the air density on the surface which is equal to 0.016 kg/m^2 [14]. This gives a lift per area of 3.04 N/m^2, or 0.82 kg/m^2 with the Mars gravitational acceleration of 3.7 m/s^2. This value is lower than the estimated solar panel mass of 1.21 kg/m^2, therefore the panel will not be lifted up by the wind.
However, the wind could also have a downwards angle relative to the solar panel. In this case the aerodynamic force would be aimed downwards, and not be counteracted by weight. It could then bend the solar panel. In this case, the flexibility of the solar panel would limit movement. Exact parameters for this are not known as the solar panel is not designed to such a level of detail. Therefore it is uncertain whether the solar panel would move due to wind. For a complete design, a better verification could be done by placing the deployed probe in a simulated Mars environment, and testing it in a wind tunnel.

$$\frac{L}{A} = \frac{1}{2}\rho V^2 2\pi\alpha \tag{4.27}$$

Scenario Analysis

Assuming that there definitely will be noise due to wind, which is very likely as it was also a problem with the Viking lander's seismometer, some measures can be taken to deal with this. First of all, more extensive research is required to determine what kind of noise exactly will be produced by the wind. Since the mission will launch in 2018, there is plenty of time for this. Once this has been figured out, some possible scenarios are:

- **Noise can be completely filtered**
  As described in chapter 3.1.2, two possible sources of seismic waves are considered: wind and natural impacts. Note that by wind, seismic waves caused directly by wind on the surface are meant, not waves generated through vibrations of the probe. If the noise due to wind on the probe could be distinguished from both of these sources, for example due to having a different frequency, then there is no problem and the secondary objectives can be fulfilled as planned.
- **Noise can be partially filtered**
  Another possibility is that the probe noise cannot be distinguished from wind, but can only be distinguished from natural impacts. In this case it will not be possible to investigate the subsurface of the crust, but from impacts the internal structure can still be investigated.
- **Noise can only be filtered at low wind speeds**
  In the worst case scenario, the probe noise is only low enough at low wind speeds. This was the case with the Viking 2, which could only do measurements at winds <2 m/s [56]. In this case, chances are some natural impacts are missed, but some knowledge of the internal structure of Mars could still be gained. This scenario is considered very unlikely, since wind speeds under regular circumstances (i.e. no dust storms) only reach up to 6-8 m/s. This is higher than the 2 m/s limit for the Viking, but the probe noise for the Ancile seismometer is expected to be less, as the seismometer is placed in the ground by the penetrator, and the seismometer itself is also more advanced.

4.5.4 Electrodynamic Dust Shield

From experiments on the Mars Pathfinder mission estimations have been made that dust may reduce solar panel efficiency by 22% to 89%, over a duration of 2 years [27]. Since the mission duration is going to be at least 5 years, this significant decrease in solar panel performance is not acceptable. The possibility of using a transparent electrodynamic dust shield to periodically remove the dust was researched to solve this problem.
These dust shields generally consist of parallel electrodes on the surface of the solar panel, which are connected to an AC (alternating current) source to create an electromagnetic wave. This method is called the *electric curtain*. Dust particles will move with or against the wave, depending on their polarity [26]. NASA is currently developing the Electrodynamic Dust Shield technology for application to future Mars and Moon missions. Besides solar panels, the shield could also be used for spacesuits, thermal radiators and optical instruments [1]. An example of a transparent dust shield is shown in figures 4.15 and 4.16.

Since the electrodynamic dust shield technology is still under development, it is difficult to estimate parameters. However, from experiments that have already been done, some predictions for the effectiveness and the power usage can be made. From tests with a 5 x 5 cm screen, using a Mars dust simulant and testing at Mars atmospheric pressure, results were obtained for solar panel performance before and after dust removal. When the performance was reduced to about 20%, 2 minutes of dust shield activation brought it back up to over 98%. Better performances are expected for later designs [25].
From a different dust shield prototype, a power consumption of 0.02 W/cm^2 was found [27]. Applying this to the probe design, the power consumption for the 0.81 m^2 solar panel would be 162 W. The energy required for a 2 minute activation is 19440 J, or 5.4 Wh. This is very small compared to the daily required energy of 600 Wh. Additionally the dust shield is only used once efficiency of the solar panel is reduced by 10%. Since at most 89% efficiency reduction is expected over 2 years, assuming a linear reduction of efficiency over time, the dust shield needs to be activated less than once per

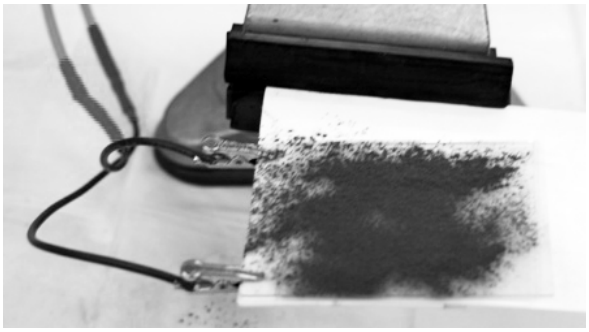

Figure 4.15: Dust shield with dust [1]

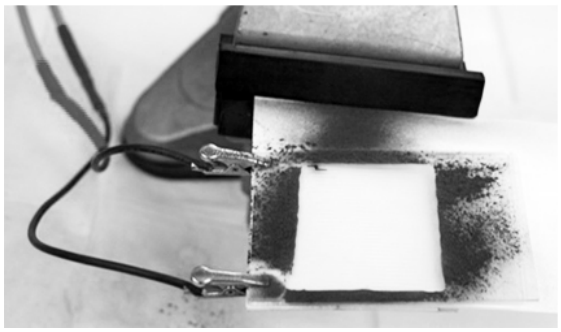

Figure 4.16: Dust shield after dust removal [1]

month. Therefore the energy consumption is neglected in the energy storage sizing.

The dust shield will need to be incorporated into the solar panel design. To account for this, an extra 10% is added to solar panel thickness and mass. Additionally, a converter is required to provide AC power to the dust shield.

4.5.5 Energy Storage

Since the probes require continuous power, and since solar power is only available during the Martian day, energy storage is required. Batteries will be used to store this energy. To design the energy storage subsystem, three steps will be taken. First the energy storage requirements will be determined. Then the type of batteries will be selected. Finally the size and weight of the batteries will be determined.

1. **Storage Requirements**
   To determine the required storage the time the solar panels will not provide power has to be determined. For a latitude of 15° there will be daylight during 46% of the time, which implies the batteries will need to provide power for 54% of a Martian day which equals 13.5 (Earth) hours. During this time the batteries have to provide a power output of 25 W. Therefore the battery capacity has to be 337.5 Wh, if emptied completely during a cycle. Since the batteries will have 1 charge/discharge cycle every day, they will have to go through 1780 of these cycles to remain functioning for 5 years, they can not use a depth of discharge (the percentage of total battery energy used per cycle) of 100%. From literature [61] was found that for a depth of discharge of 80%, lithium-ion batteries will survive at least 2000 cycles. Therefore 80% was chosen as a depth of discharge value.
   This implies that the total battery capacity required (C_r) will be 442 Wh.

2. **Type of Batteries**
   To determine the type of batteries one has to look at two things: energy density and availability. Lithium-ion batteries have a high energy density of about 180 Wh/kg, which equals 410 Wh/l for this type of battery. Nickel based batteries can have almost the same energy per liter (up to 400), but per kg they perform way lower, having only a maximum energy density of 90 Wh/kg [74]. Both are readily available. Sodium-sulfur batteries have a higher energy density then lithium-ion batteries, but since the cells are highly corrosive of nature, they can not be used, taking the landing loads and the long mission length into account. Because of the high energy density per kg, and because a higher depth of discharge can be achieved, lithium-ion batteries will be taken.

3. **Size and Weight of the Batteries**
   The size and weight of the batteries can now easily be calculated using equations 4.28 and 4.29

$$size = \frac{C_r}{Wh/l \cdot \eta} \tag{4.28}$$

$$weight = \frac{C_r}{Wh/kg \cdot \eta} \tag{4.29}$$

Here η equals the transmission efficiency. A value of 0.9 was determined from literature [94]. Picking the determined values for C_r, Wh/l and Wh/kg, the final values regarding battery sizing equal 1.20 liter and 2.73 kg.

4.5.6 Power Regulation

The power on the probes has to be regulated in order to prevent battery overcharging and unwanted heating. Two ways to regulate power are most often used, a peak-power-tracker (PPT) and a direct-energy-transfer (DET). A PPT is a dc-dc converter. It is mostly used on short missions that have higher power requirements at the beginning of life, when compared to end of life. Furthermore, a PPT will use about 5% of the total power.
A DET (using a shunt regulator) will have advantages since it will be made of fewer parts, will have a lower mass and will have a better efficiency at end of life.
Since lithium-ion batteries will be used the discharge voltage will be flat [74]. This allows stable power during discharge of the battery. Therefore an unregulated system can be used, which is the most efficient system. Furthermore, the batteries will be charged independently, using a linear, charge-current control (LC^3). This will increase the complexity of the system but it will ensure a longer battery life. A general overview of this system will be shown in figure 4.5.6.

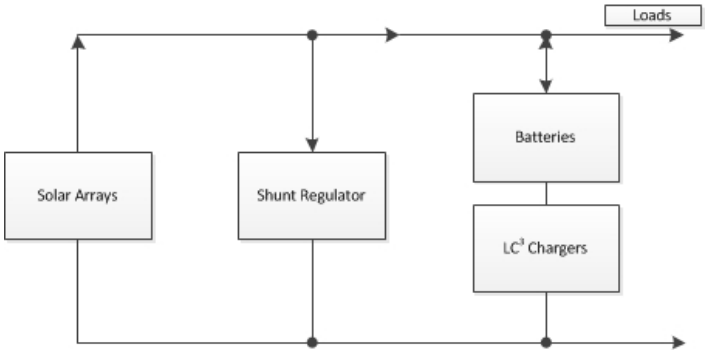

Figure 4.17: Unregulated bus using linear charge, current control and recharge control

Electrical Block Diagram

Figure 4.5.6 shows the electrical block diagram of the probe. It illustrates the power links between the different subsystems. The solar panel provides the power, and the PCDU distributes the power over the different subsystems. The battery both uses power, while charging, and provides power, when discharging.

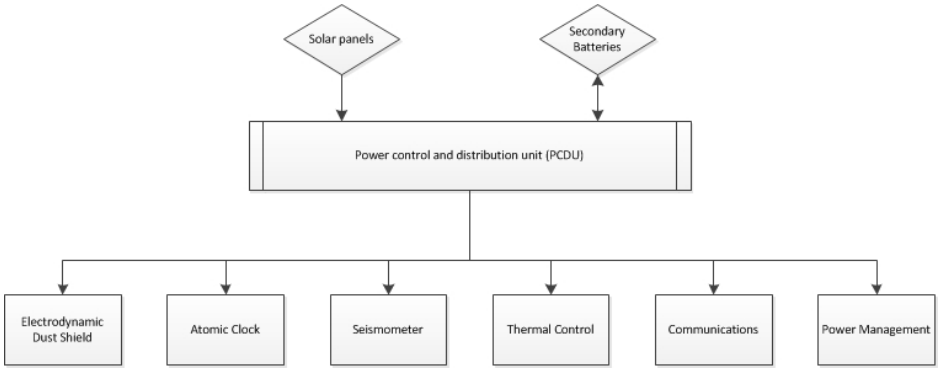

Figure 4.18: Electrical block diagram

4.6 Crushable Honeycomb Structure

During the last part of the landing the lander will penetrate the ground and will experience a heavy deceleration to come to a standstill. In order for each system to withstand the heavy impact loading, a sufficient damping system is designed.

4.6.1 Research

The concept of landers penetrating the ground has been designed for previous missions, although never actually performed, e.g. Mars 95, Mars Penetrator, Lunar A and MetNet. Extensive research was done in order to find suitable damping systems to withstand the high forces at impact. The g-forces experienced during landing can vary between 100 g and 100 000 g. Thus in order to ensure the proper functionality of the sensitive instruments on board, appropriate damping systems needed to be developed.

The MarsNet penetrating lander is designed to penetrate the ground at an impact velocity of 70 m/s and the resulting loads are 5700 g at impact. The sensitive instruments implemented on that lander were only able to withstand a maximum loading of 500 g. Thus the maximum shock loading which the damping structure was designed for, was 500 g over 15 ms modeled as a half sine curve.

There are two shock absorption techniques suited for damping structures which experience such extreme shock loading. Systems based on friction and damping, e.g. *fluid-* and *gas-filled telescopic dampers*; and systems based on the principle of irreversible deformations, e.g. *elastomer shock isolators*, *aluminum honeycombs* and *aluminum foam*. For soft landings, the landing components reflect shock waves by using transmission control damping systems, for example *airbags* and *spring damper shock isolators*. Irreversible deformation has the highest specific energy absorption comparatively and thus is preferably used as a damping system for this mission.

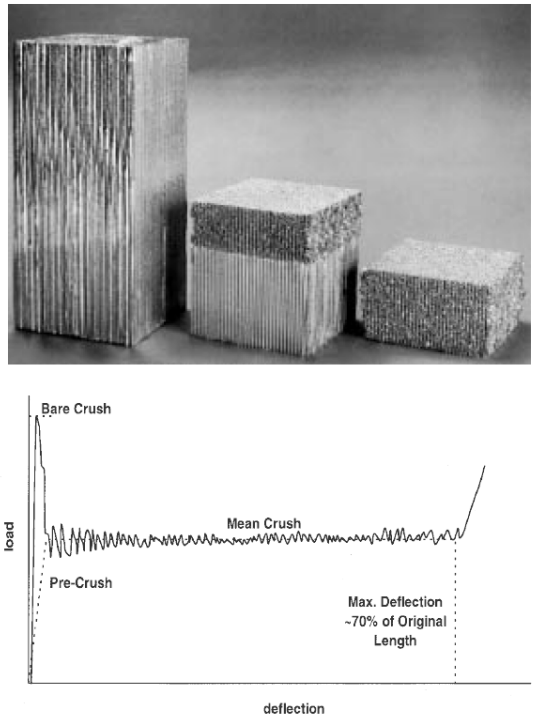

Figure 4.19: Crushable aluminum honeycomb structures and their loading pattern

Aluminum honeycomb structures, with varying densities between 16-150 kg/m^3, can absorb energy up to 30 $[kJ/kg]$ by crushing at a constant deceleration after the initial shock [34]. This phenomenon

lasts till 70% of the original length is crushed, after which the structure starts 'blocking', increasing the loading gradient w.r.t. strain. This crushing process can be seen in figure 4.19. This performance is only valid if crushing appears in the axis of the cell, otherwise the energy absorption will significantly decrease. In the design the walls of the pin will provide vertical guidance for the seisometer onto the honeycomb.

In the past different materials were tested, to validate whether the energy is actually absorbed. Dynamical tests were done with a ballistic air-gun shock test, as can be seen in figure 4.20. With this test the crushables as well as the instruments were tested on their functionality. Although the results differed slightly from the predicted outcome, the test models still demonstrated similar loading patterns compared to analytical models.

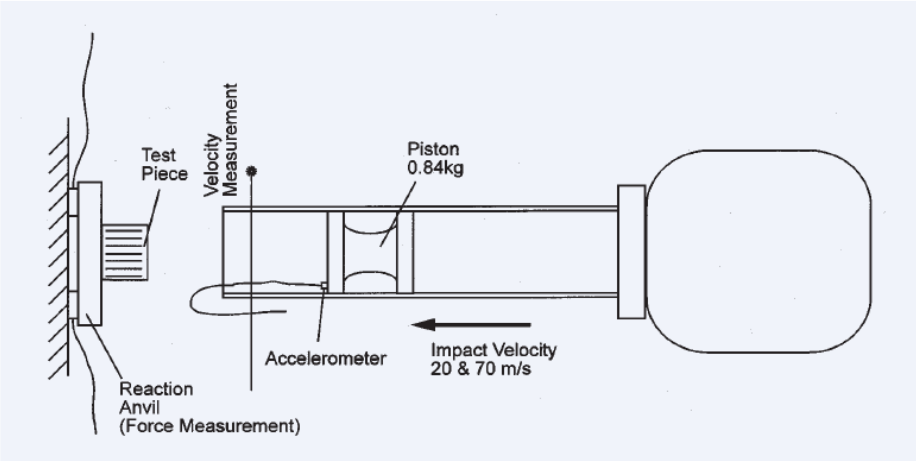

Figure 4.20: Ballistic air-gun shock test for dynamically testing the performance of many kinds of crushable honeycomb structures [34].

4.6.2 Application

For this landing design the probe can be split into two separate parts; the penetrator pin and the instrument box. The instrument is much lighter in comparison to the pin, which is beneficial when impacting the surface and when looking at the forces acting on the box during landing. The most sensitive instrument of this design is the seismometer which is located in the pin. The instruments in the instrument box, like the antenna, the computer, the battery etc., can withstand substantially higher g forces. In order to design a suitable damping system, the structure with the highest energy per volume is chosen for the first iteration, thus the density of the honeycomb is 150 kg/m^3 and the specific energy absorption is 30 kJ/kg. There will be crushable structure needed, both in the pin and beneath the instrument box.

4.6.3 Deceleration

During the penetration the pin will be the first part that will hit the ground. Within the pin is the seismometer, which is the most sensitive instrument onboard this mission; it can withstand a maximum of 400 g. The pin will enter the soil and at the point when the crushable material hits the ground, the pin will detach and continue to penetrate until fully decelerated. Thus the pin will have a longer distance to decelerate than the instrument box. With the crushable material beneath the seismometer, the meter has an even longer distance to decelerate. The instrument box will decelerate from 90 m/s to zero in two steps, first part is due to the pin, the second part is by the crushable structure. A drawing of the deceleration configuration, including the probe's dimensions and components, can be seen in figures 4.21 and 4.22.

In order to find the energy that needs to be absorbed and how to damp the system a simulation model is made. Hereby the two deceleration phases are looked at separately. The pin will have a

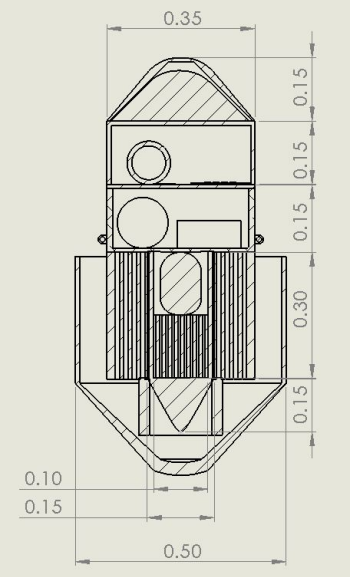

Figure 4.21: Probe dimensions

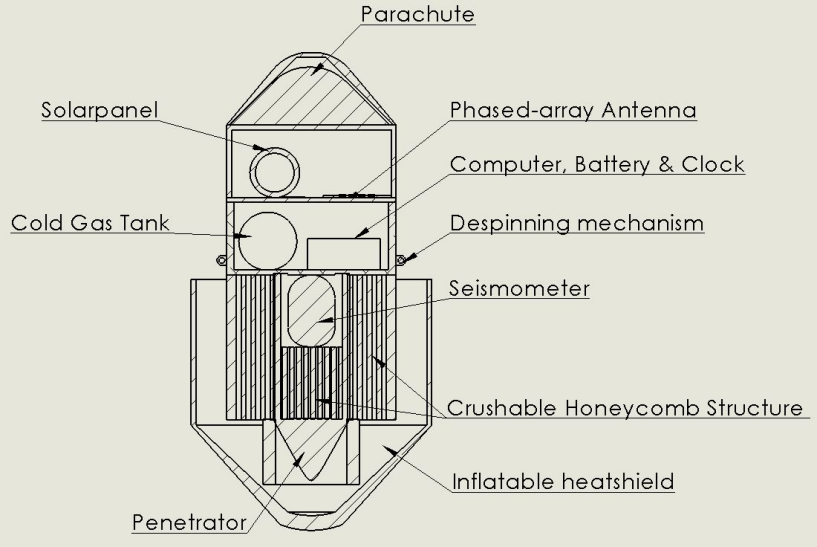

Figure 4.22: Probe components

contribution to the deceleration process of the instrument box. Thus the decelerations will then be combined and iterated in order to find the optimal size and weight of the crushables.

4.6.4 Crushable honeycomb structure inside the pin

The pin will penetrate the ground with an impact velocity of 90 m/s. This velocity was found by iterating the velocity needed to penetrate the ground by a depth of atleast the length of the whole pin, the requirement states that as long as the seismometer is subsurface, the seismometer can fulfill its function. The seismometer crushable honeycomb structure (*schs*) within the pin will need to absorb the kinetic energy exerting forces on the seismometer. The total kinetic energy can be computed from the energy equation 4.30.

$$E_k = \frac{1}{2} m_s V_0^2 \ [J] \tag{4.30}$$

In this equation m_{ib} is the mass of the seismometer and V_0 is the impact velocity.

Knowing the energy that the crushables need to absorb, the height and weight of the crushables can be evaluated from the formulae 4.31 and 4.32.

$$H_{schs} = \frac{E_k}{E_{schs}} \frac{1}{\rho} \frac{1}{A_{schs}} \frac{1}{0.7} \ [m] \tag{4.31}$$

$$W_{schs} = H_{schs} A_{schs} \rho \ [kg] \tag{4.32}$$

Where E_{schs} is the specific energy absorption factor of the aluminum honeycomb structure, ρ is the density of the crushable structure, A_{schs} is the area of the SCHS and the factor 0.7 is to account for the strain before 'blocking'.

4.6.5 Crushables for the instrumentation box

The energy that needs to be absorbed by the crushables attached below the instrumentation box can be computed from equation 4.30, taking the initial weight of the instrument box $W_{ib} = 20\ kg$. The height and weight can be computed from the same equations as used for the pin, equation 4.31 and equation 4.32 respectively, taking the area of the instrument box $A_{ib} = W_{box}^2 - \pi R_{penetrator}^2 [m^2]$. Now the height of the crushables, needed for the weight of the instrument box is computed. The weight of the crushables will be added onto the structure and will contribute in energy absorption needed for deceleration. Thus the same formulae 4.30, 4.31 and 4.32 need to be iterated again to find the actual amount of crushables needed.

4.6.6 Mass of the Penetrator

The pin is made of tungsten. This high density metal allows for a slower impact speed with sufficient depth. The total mass of the penetrator is the sum of all parts, as shown in equation 4.33.

$$m_p = m_{cone} + m_{sc} + m_{seismo} + m_{schs} \ [kg] \tag{4.33}$$

with

$$m_{cone} = \frac{1}{3}\pi R^2_{penetrator} H_{cone} \rho_W \ [kg] \tag{4.34}$$

and the mass of the walls of the seismic cavity

$$W_{sc} = \pi(r^2_{penetrator} - r^2_{seismic}) H_{sc} \rho_W \ [kg] \tag{4.35}$$

4.6.7 Deceleration, Velocity and Depth of the pin

The average acceleration of the pin can be computed using equation 4.36.

$$\underbrace{1/2 \cdot mv^2}_{KineticEnergy} = \underbrace{m \cdot a \cdot s}_{WorkDone} \Rightarrow a_{avg} = \frac{V_0^2}{2s} [m/s^2] \tag{4.36}$$

Where V_0 is the impact velocity and s is the penetration depth. Since the deceleration is described by a half sin, the maximum deceleration can be found with:

$$a_{max} = a\frac{\pi}{2} \ [m/s^2] \tag{4.37}$$

Thus the entire deceleration of the pin can be plotted by evaluating equation 4.38.

$$a_p(t) = a_{max} \sin\left(\frac{\pi t}{T}\right) \ [m/s^2] \tag{4.38}$$

By integrating the deceleration w.r.t. time, the velocity envelop can be evaluated and plotted:

$$v_p(t) = \int_0^t a_{max} \sin\left(\frac{\pi t}{T}\right) dt \tag{4.39}$$

$$= C_1 - \frac{a_{max} T}{\pi} cos\left(\frac{\pi t}{T}\right)\Big|_0^t \tag{4.40}$$

$$= V_0 - \frac{a_{max} T}{\pi}\left[1 - \cos\left(\frac{\pi t}{T}\right)\right] \ [m/s] \tag{4.41}$$

Once again, integrating w.r.t. time yields the penetration depth, 4.42:

$$s_p = \int_0^t \left(V_0 - \frac{a_{max} T}{\pi}\left[1 - \cos\left(\frac{\pi t}{T}\right)\right]\right) dt \tag{4.42}$$

$$= V_0 t - \frac{a_{max} T}{\pi^2}\left[\pi t - T \sin\left(\frac{\pi t}{T}\right)\right] \ [m] \tag{4.43}$$

Figure 4.23 shows the results of these equations. Note that the penetration pin penetrates deep enough even in the hardest soil. However, the probe release does not aim to land on any low lands, the intention is to land on the high lands north and south of the Valles Marineris.

4.7 Thermal Control

In this section the design of the thermal control system of the probe is described. First the thermal requirements of the system are identified, then the thermal environment is defined. Thermal challenges or problem areas are identified, applicable control techniques are described, and finally the mass and power of the system is estimated.

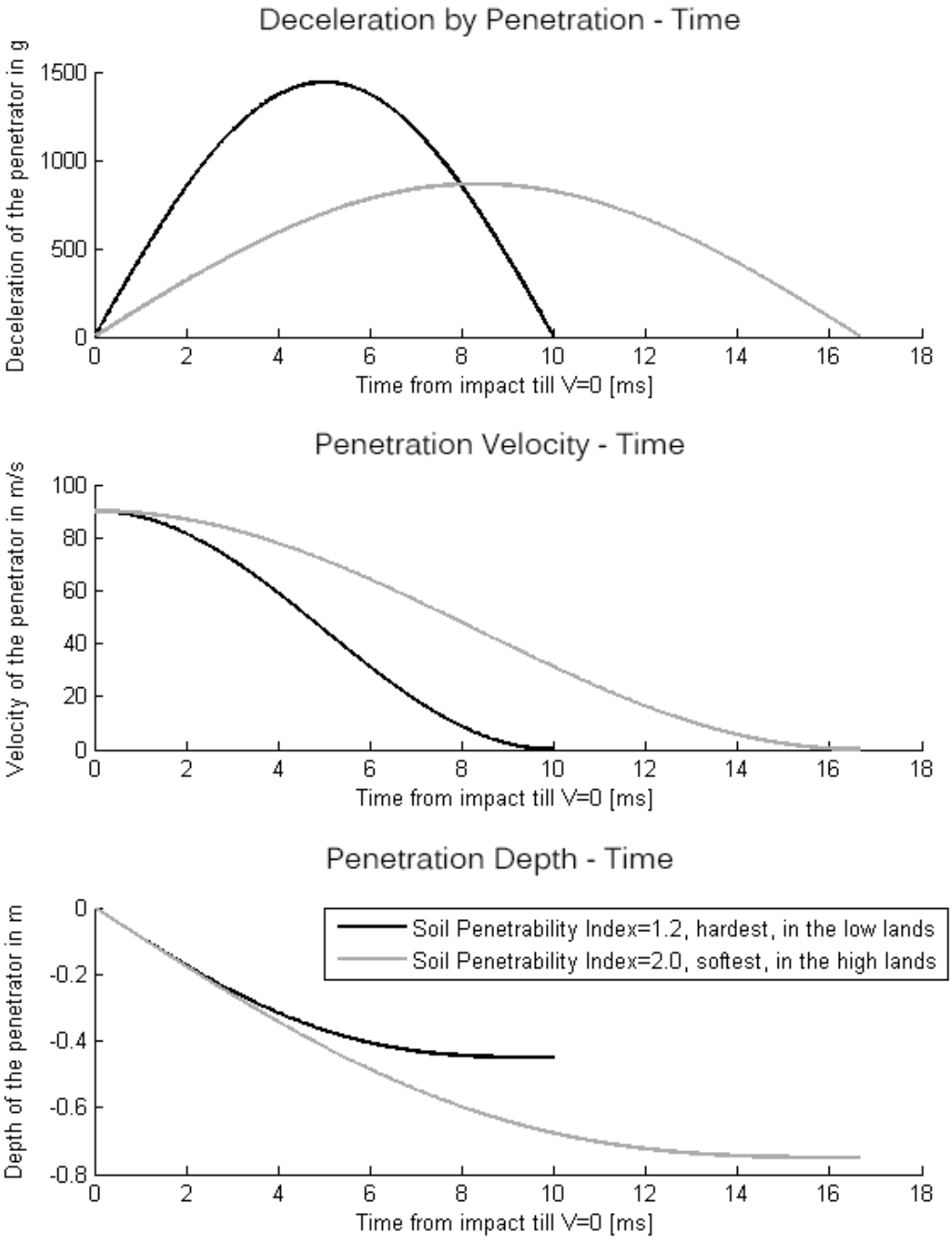

Figure 4.23: G-loads, velocity and depth of penetration

4.7.1 Thermal Requirements and Constraints

The thermal requirements and constraints of all the components on the probe are shown in table 4.13. For most of the components, typical temperature ranges were found from literature. The seismometer temperature range was determined by comparing characteristics of several existing seismometers. The clock temperature range is assumed to be similar to that of C&DH, because it consists of similar chips and electronic circuits [32].

4.7.2 Thermal Environment

Thermal conditions on Mars vary depending on latitude, season and mainly time during the day. Figure 4.24 shows the temperatures during a day on Mars during aphelion for given latitudes (this

Table 4.13: Thermal requirements for probe components.

Component	Temperature ranges °	
	Operational	Survival
Batteries [94]	0 to 15	-10 to 25
Antenna [94]	-100 to 100	-120 to 120
Solar Panels [94]	-150 to 110	-200 to 130
Clock	-20 to 60	-40 to 75
Dust Shield	-150 to 110	-200 to 130
Seismometer [89] [6]	-20 to 65	-60 to 75
C&DH [94]	-20 to 60	-40 to 75

is when it is winter in the south). Since there will be no probes below -30° latitude the minimum temperature will be 156 K which equals -117 °C. The maximum temperature will be 261 K since there will be no probes above 15° latitude. This is because 261 K is the average of the maximum temperatures for the given values for 0° latitude and 30° latitude.
Figure 4.25 shows the temperatures during a day on Mars during perihelion for given latitudes. The minimum temperature will be 165 K which corresponds to -108 °C. The maximum temperature will be 297 K which corresponds to 20°C.

The other thermal environment the probes will experience is space. After probe release from the bus the probes will travel through space for about 36 hours. This implies the probes will be in a very cold environment but will receive unfiltered and unobstructed solar radiation. The solar intensity there will be around 590 W/m^2.

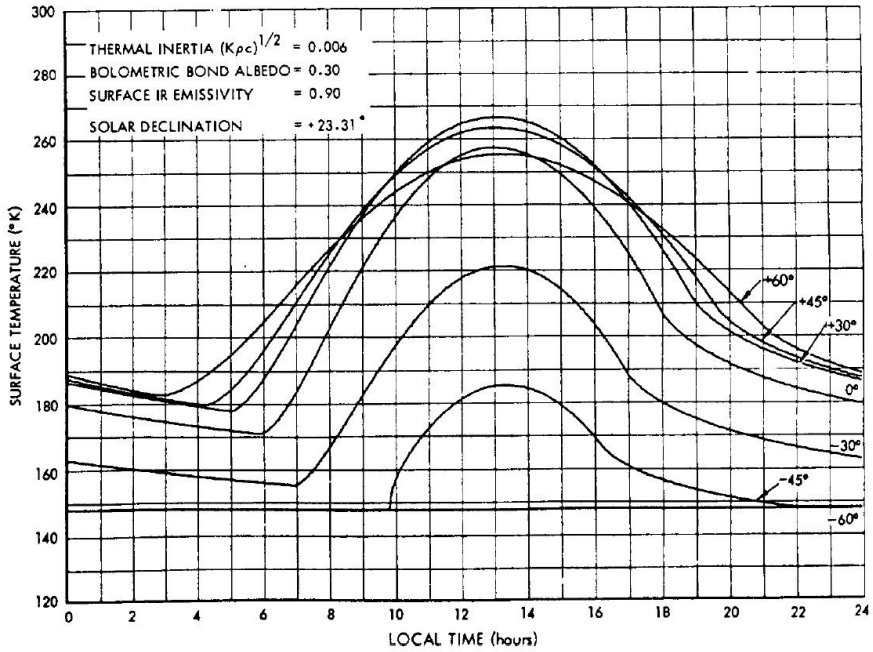

Figure 4.24: Thermal conditions on Mars depending on latitude during aphelion (figure taken from NASA's Mars Transportation Environment Definition Document [14])

4.7.3 Thermal Challenges

The probe has to survive during dust storms where power generation is limited. During dust storms generally only 15% of maximum solar energy output is available [88]. This means the thermal control system has to keep the probe in survival temperature range and batteries in operating temperature range using about 3.75 W of power.

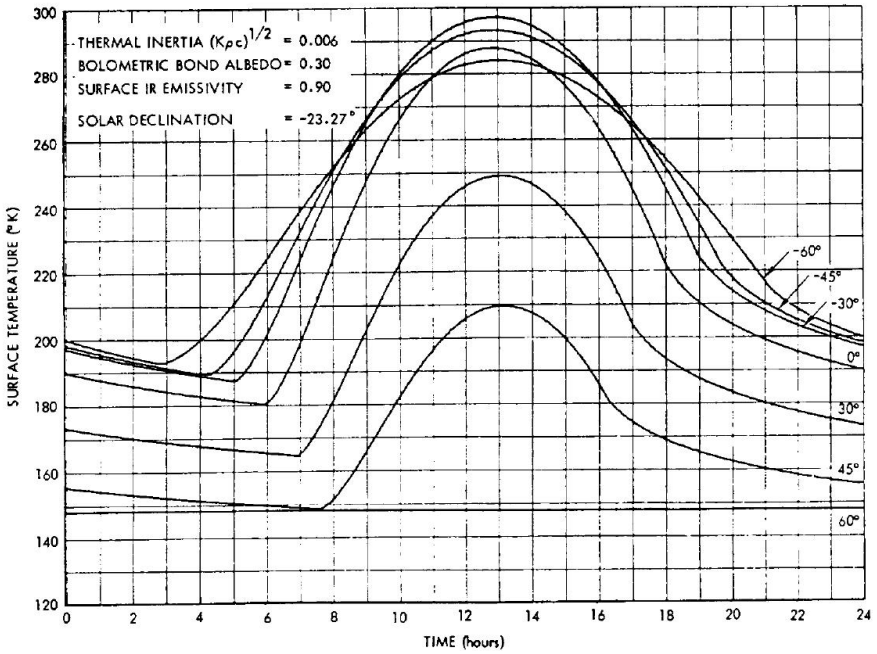

Figure 4.25: Thermal conditions on Mars depending on latitude during perihelion (figure taken from NASA's Mars Transportation Environment Definition Document [14])

4.7.4 Applicable Control Techniques

There are several control techniques available to keep the probe's temperature within limits. They are described below:

- **Surface finishes**
  On spacecraft, surface finishes are generally used as part of a thermal control system. Just like insulation, which is described below, a surface finish is a form of passive thermal control. Black and white paint, surface mirrors, and gold or aluminum layers are the most common. Their thermal properties depend on two parameters, the absorptivity (α), and emissivity (ϵ). Absorptivity is the fraction of radiation absorbed by a surface to the total radiation incident on the surface. Emissivity is the relative ability of a surface to emit energy by radiation. With these parameters known, the average temperature can be calculated by equation 4.44. In this equation, σ is the Stefan Boltzmann constant, S the incoming solar intensity, A the total area and A_p the projected area.
  Vaporized deposited gold is found to be the best surface finish for the probe, since it has a high ratio of α/ϵ. Typical values are between 6 and 10 [94].

$$\sigma \cdot T^4 = \frac{\alpha}{\epsilon} \cdot S \cdot \frac{A_p}{A} \tag{4.44}$$

- **Insulation**
  Insulation is used to keep the temperature steady within the instrument box. This is achieved by reducing the ϵ. A value of ϵ between 0.015 and 0.030 is generally possible on medium sized spacecraft, when using multilayer insulation (MLI). Since the probe in this mission is small, the expected value for ϵ will be between 0.05 and 0.10.
  Since atmospheric pressure reduces the performance of MLI, aerogel is usually added to landers to provide insulation while operating in an atmosphere. MLI might still be required to protect the probe during its travel through space.
  Since the batteries in the instrument box have the smallest operational temperature range, they may require additional insulation.

- **Heaters**
  Since a passive control system will not be sufficient for the temperature variations on the Martian surface, and because surface finishes degrade over time, an active system has to be present.

For the probe, electrical patch heaters or cartridge heaters could be used. Patch heaters are selected since cartridge heaters are used when high temperatures are required. A solid state controller will be added and will be programmed to shut the heaters off when the temperature rises above 15 °C and turn them on when the temperature drops below 0 °C. It could be beneficial to position a heater close to the battery due to its small temperature range. The rest of the instruments only need to be kept within -20 and 60 °C.
If the power required to keep the temperature above the minimum design value will be higher than the power available during a dust storm, radioactive heating units have to be considered. This should be investigated further.

- **Radiators**
  Radiators can be used to get rid of excess heat. The thermal control system will be designed in a way that no radiators are required. This should be possible since temperatures on Mars are generally far below the operational temperatures (see figures 4.24 and 4.25). Furthermore no RTG is used in the concept, therefore there will be little excess heat generated.

4.7.5 Mass and Power Estimation

For the mass and power estimation, the probe is assumed to have MLI over the entire inside box surface area, a controller, and heaters. The aerogel mass is neglected since it has a very low density of 1.9 kg/m^2. Even a volume equal to the entire box would weight only 35 g [79].

Multilayer insulation typically has a mass of 0.73 kg/m^2 [94]. The box has dimensions of 0.35 x 0.35 x 0.15 m. This means the surface area is equal to 0.455 m^2,and the MLI would have a mass of 0.33 kg.
The controller mass is estimated to be 0.2 kg and uses 1-3 W of power [94]. A power consumption of 1 W is assumed since the probe is small.
Since heaters have not been sized, an accurate estimation of mass is not possible. However, if 0.5 kg of mass is assumed, this would lead to a total thermal control mass of 1.03 kg, which is 7.45% of the total mass of the instrument box. This is within range of the typical spacecraft thermal control mass of 2 to 10%. Moreover, it is towards the high end of the range, which is expected as active heating is required and the lander is small.
The power estimation for the heaters is based on the Mars Exploration Rover, as it operates in a similar environment. It required 8 W of heating [4], but the rover has a length of 1.6 m. Since the probe is much smaller, with a box width of 0.35 m, it is assumed that at most 4 W is enough to keep the instruments warm. Since heating is not required all the time, and 4 W is the maximum, it is expected that the average power available during dust storms (3.75 W) is enough to keep the thermal control working.

4.8 Command and Data Handling

In this section the command and data handling (C&DH) is described. First a general description will be given. After that the hardware, software (H/W, S/W) block diagram and data handling block diagram are presented.

4.8.1 Command and Data Handling system

The C&DH system is the last system designed since it depends on the payload and its requirements. In order to estimate the weight, size, and power usage of the system, reference values were found from literature [94]. However, since the literature is from 2003 and systems have developed a lot over the past years, the system is assumed to be smaller and able to handle more data. The system is a combined telemetry and command system, for which typical parameters are shown in table 4.14. Average values were picked because the system only has one task, which is relatively little compared to spacecraft which have multiple measurement instruments, but it has to perform it very accurately with little margin for error.

Table 4.14: Typical command and data handling parameters for combined systems [94]

Parameter	Typical Value	Design Value
Size (cm^3)	2500-6000	4000
Weight (kg)	2.75-5.5	4.0
Power (W)	7-12	10

Since the probability of failure for a single probe is quite high due to the high impact landing, the other systems should have the highest reliability possible. Therefore some critical components in the C&DH system will be made redundant by adding a spare. Furthermore, class S parts will be used to manufacture the C&DH system. This will provide a reliability of 0.9987 [94]. The development time for this system will not be longer than 18 months. This easily fits in the available development time of for the mission.

4.8.2 Hardware - Software Block diagram

The Hardware - Software block diagram for the probe is presented in this part. It shows the relations between all the hardware and the software used on the probes. The diagram can be found in figure 4.8.2

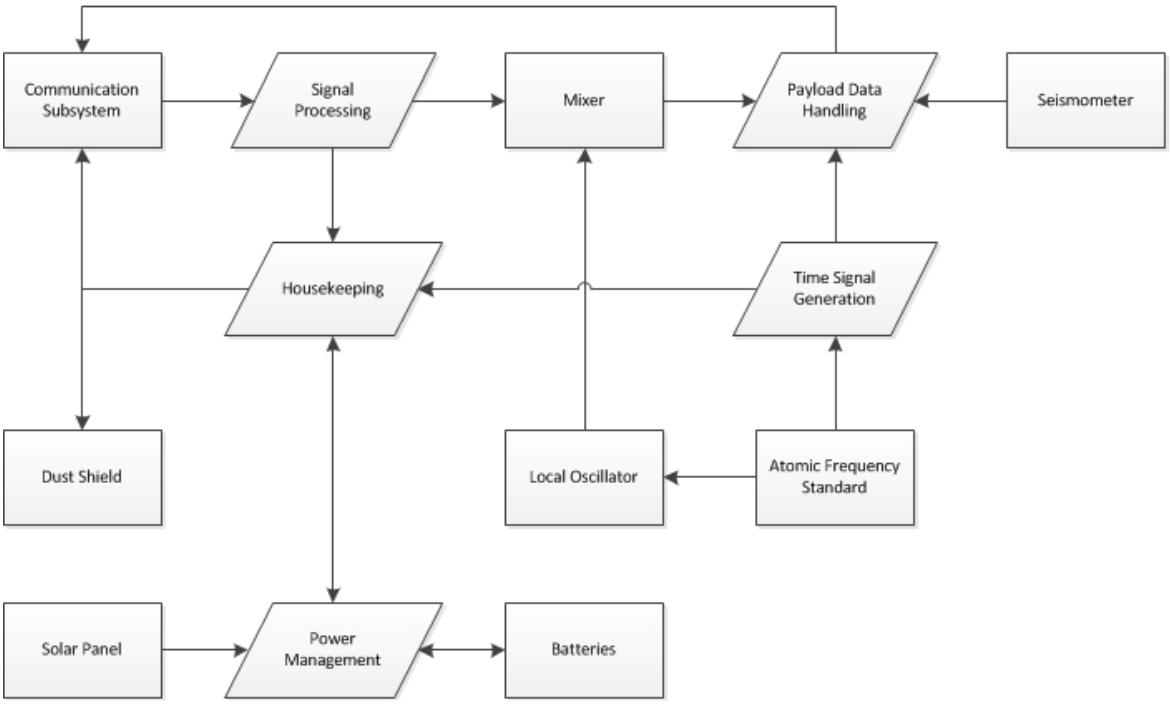

Figure 4.26: The Hardware - Software block diagram

4.8.3 Data Handling Block diagram

The data handeling block diagram is shown in this part. It shows the order in which certain systems handle incoming data. Data can be generated by the DSN, the seismometer and the local frequency standard. The diagram is presented in figure 4.27.

4.9 Layout

In this section the layout of the probe's instrument box is described. The instruments are positioned such that the weight is distributed over the box as evenly as possible, in order to optimally distribute

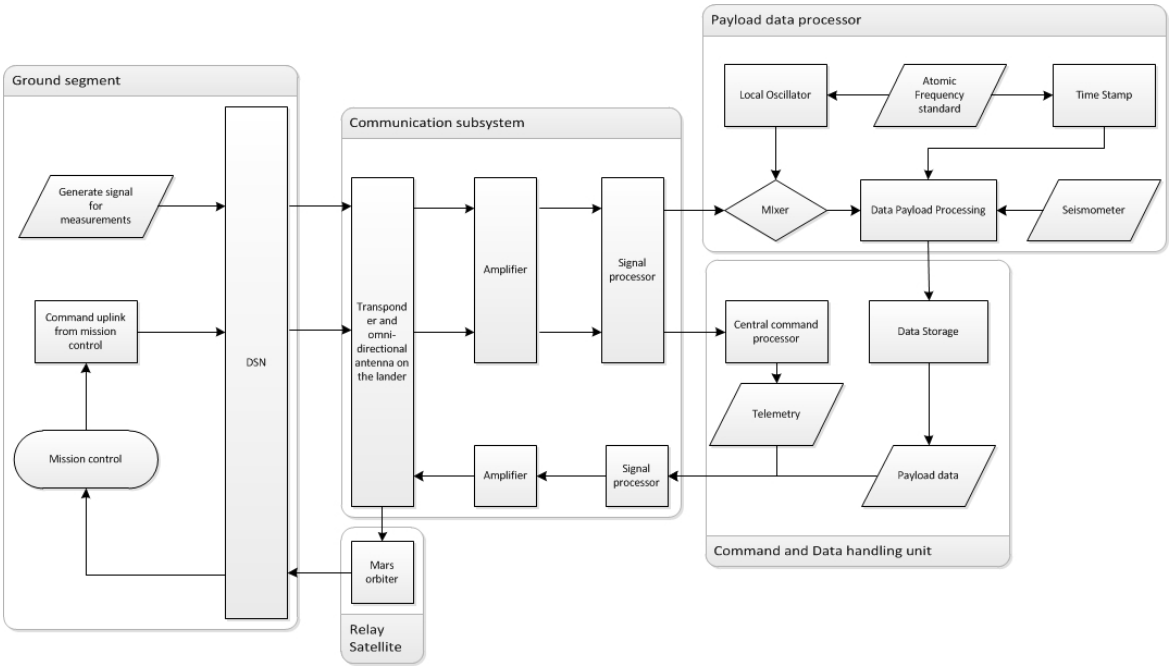

Figure 4.27: The Data Handling block diagram

the forces exerted on the box during the landing.
All of the components of the box, including their dimensions and mass, are listed in table 4.1 on page 26. The thermal control system is assumed to be evenly distributed over the box.

The positions of the components were found by determining the center of gravity (c.g.) of the box for an initial layout and iterating until the c.g. was in the middle of the box. Equations 4.45 and 4.46 are used to find the c.g. position. The final layout is shown in figures 4.28 and 4.29.

$$\bar{x} = \frac{\sum m_{component} \cdot \bar{x}_{component}}{\sum m_{component}} \tag{4.45}$$

$$\bar{y} = \frac{\sum m_{component} \cdot \bar{y}_{component}}{\sum m_{component}} \tag{4.46}$$

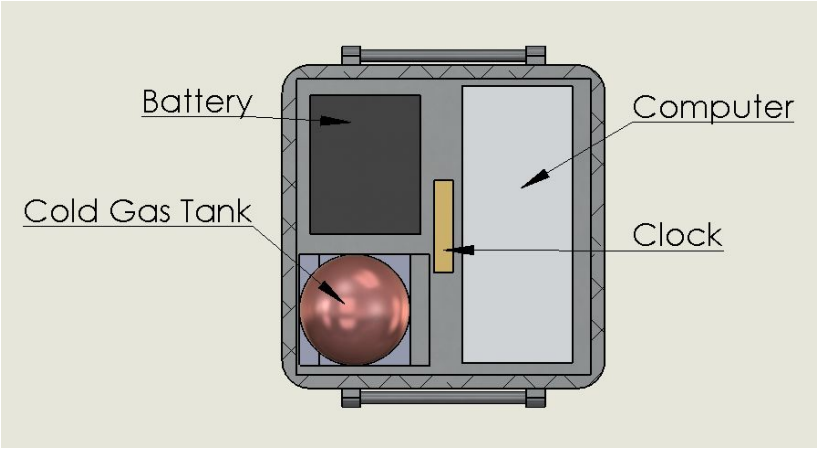

Figure 4.28: Internal layout of the instrument box

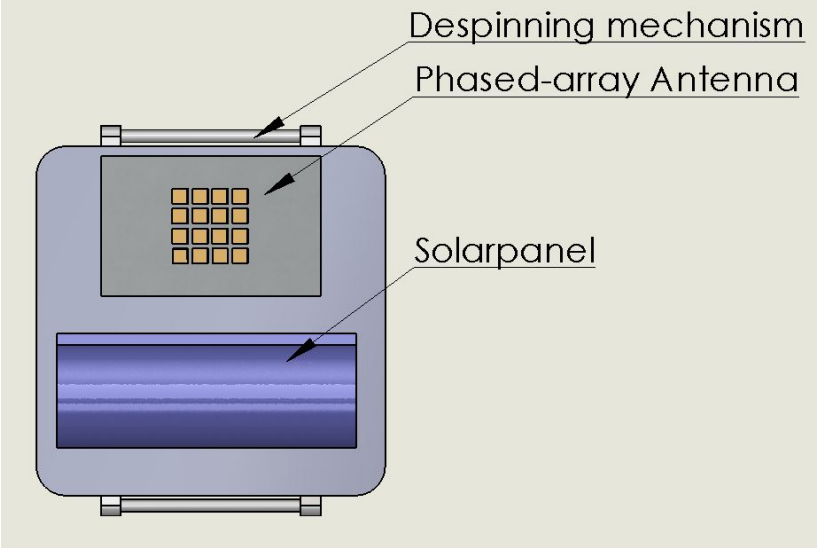

Figure 4.29: Top view of the external layout of the instrument box

4.10 Instrument Box

The instrument box houses the primary payload along with all the supporting subsystems. This structure needs to be designed to fit all the instruments into it, and to cope with the loads induced by the high velocity impact landing. Because of the instruments, the dimensions of the box is specified, i.e. [35x35x15] cm. The instrument box is initially decelerated by the penetrator pin, where the outer crushable honeycomb structure (*OCSH*) starts the pin separates and continues its deceleration into the Martian soil. While the aluminum crushable honeycomb, distributed on the bottom surface of the box, takes over the deceleration till the velocity reaches zero. The analysis is modeled in MATLAB.

With the load case known, the first step is to determine the deceleration of the instrument box. This is split in two parts, the deceleration by the pin and by the honeycomb structure. Recall that figure 4.23 shows this initial deceleration experienced by the penetrator. The loading profile of the box transitions when the OCHS touches the surface, i.e. the OCHS takes over when the penetration depth of 0.15 cm is reached. As can be imagined, this point in time after impact is dependent on the soil in which the lander lands. Furthermore, unlike the deceleration envelop due to the penetrator, which is a half sine curve, the deceleration profile by to the OCHS is close to constant. This was as discussed in the *Crushable Honeycomb Structure* section, section 4.6. Also, be reminded that this constant acceleration is determined by looking at the equation, number 4.47, relating kinetic energy and work. This equation assumes an adiabatic process for damping, i.e. all kinetic energy is absorbed by performing work on the OCHS causing no friction hence heat.

$$\underbrace{1/2 \cdot mv^2}_{KineticEnergy} = \underbrace{m \cdot a \cdot s}_{WorkDone} \Rightarrow a = \frac{v^2}{2s} \tag{4.47}$$

where v is the impact velocity [m/s], a is the acceleration [m/s^2] and s is the penetration depth [m].

Figure 4.30 shows the deceleration for the instrument box. Note the difference between the landing into soft and hard soil, the jump is smaller for the harder soil (red), this is because the hard soil absorbs more kinetic energy during the penetrator phase, thus the OCHS needs to decelerate the box less. The opposite is true for landing into the soft soil, generally in the highlands, where the majority of the probes are expected to land.
This result is then used as input to analyze the normal stresses and shear stresses exerted on the bottom plate of the instrument box by the penetrator and the OCHS. For the first iteration, the material is assumed to be Al7075T6, a high strength aluminum alloy very commonly used in aerospace applications [92]; and the thickness is calculated using the maximum deceleration experienced by the

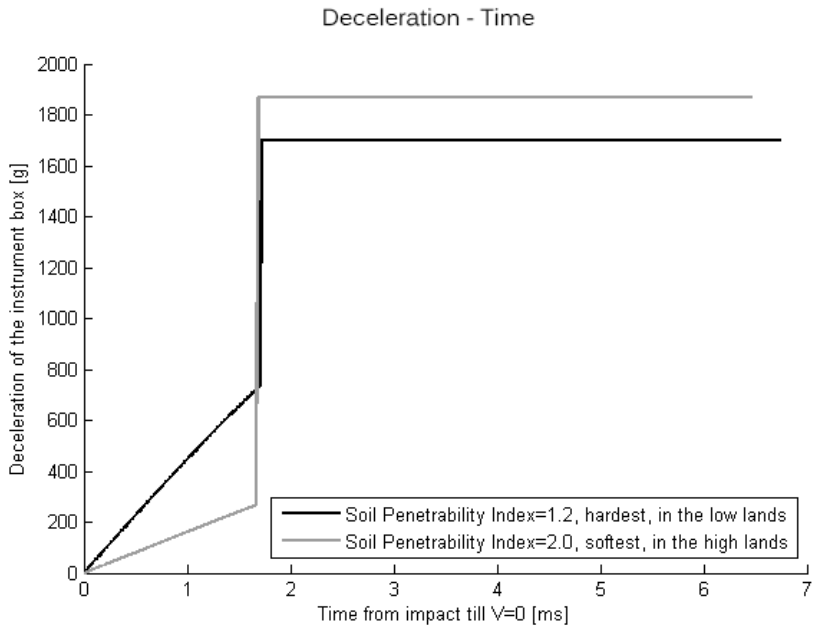

Figure 4.30: The deceleration experienced by the instrument box for landing in soft and hard soil.

penetrator and the shear strength of said material. The equations for the normal stress and shear stress on the bottom plate of the box are:

$$\sigma = \frac{m_{ib}a_{ib}}{A_{penetrator}} = \frac{m_{ib}a_{ib}}{\pi(r^2_{penetrator} - r^2_{seismometer})} \tag{4.48}$$

$$\tau = \frac{m_{ib}a_{ib}}{C_{penetrator}t_{plate}} = \frac{m_{ib}a_{ib}}{2\pi r_{penetrator}t_{plate}} \tag{4.49}$$

Where m_{ib} is the mass of the instrument box with the attached OCHS and a_{ib} is the deceleration previously acquired. Note, these equations are basic knowledge for structural analysis. The set of illustrations are shown in figures 4.31, 4.32 and 4.33.

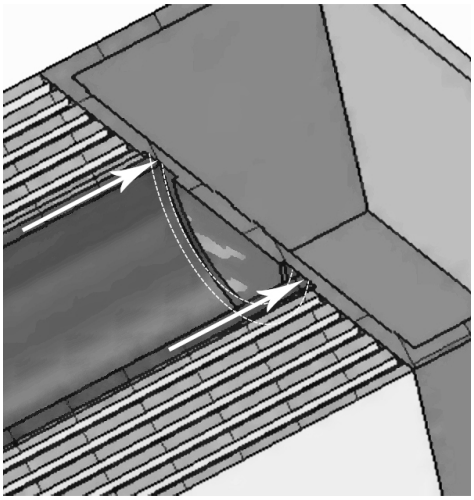

Figure 4.31: An illustration of the normal forces acting on the instrument box during the first phase of the impact

Figure 4.34 shows the maximum normal and shear stresses acting on the bottom plate of the instrument box. Considering the load case, it can be expected that the highest stress will be due to

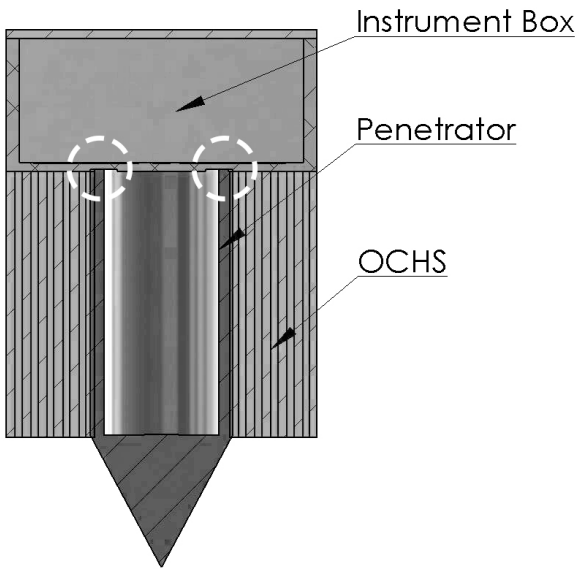

Figure 4.32: An illustration of the area on which the shear stress acts on the instrument box, due to the penetrator in the first phase

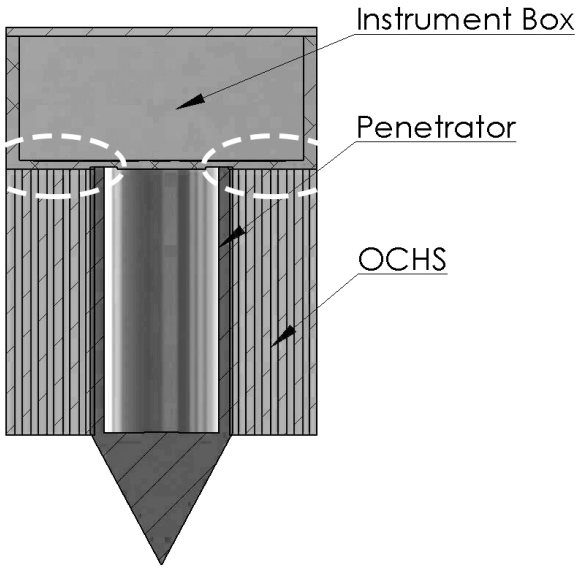

Figure 4.33: An illustration of the area on which the shear stress acts on the instrument box, due to the OCHS in the second phase

the penetrator acting on the plate under shear, i.e. cutting through the plate. As can be seen in figure 4.34, this shear stress is indeed the highest, but significantly lower than the allowable shear strength of the material, which is 331 MPa [92].
The static load cases are of no concern to the design. The only remaining structural requirement is to determine whether dynamic phenomenon might occur. Most likely considering the load case is bending due to inertia caused by the high shock loading. Refer back to figure 4.30, the maximum deceleration is almost 2000 g, but note that this phase is decelerated by the honeycomb structure covering much of the bottom area, which makes bending stresses of no concern in the bottom plate. However, the top plate might experience loads that might cause failure.

The analysis is made with certain assumptions, reducing complexity, although the assumptions assume a case worse than reality, thus the design can bear with loads higher than is required. The loading due to the penetrator is modeled as a point force acting on a circular box with a radius of the

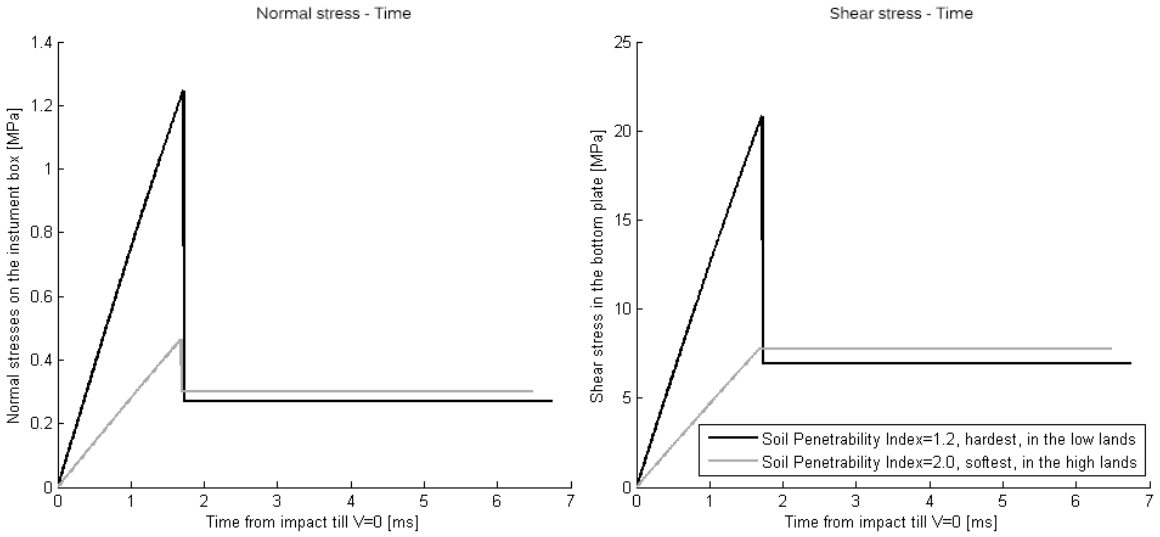

Figure 4.34: The maximum normal and shear stresses experienced by the bottom plate of the instrument box.

diagonal of the original box. This is worse than in reality because the bending moment is increased due to taking the maximum arm in all directions, in reality the wall that are closer are structurally stiffer, hence will carry more loads. By modeling the bending stresses in this way, the instrument box will not fail before other subsystems will.

Only the penetrator deceleration phase will be considered. The equation for bending stress due to pure moment is:

$$\sigma_{bending} = -\frac{M\bar{y}}{I} \tag{4.50}$$

where M is the bending moment [Nm], $\bar{y}$ is the distance to the centroid of the cross-section [m] and I is the moment of inertia of the cross-section [m^4].

Computing these values gives:

$$M = F \cdot R = a_{pmax} m_{ib_{outer}} \frac{\sqrt{(2W_{ib})^2}}{2} \tag{4.51}$$

$$\bar{y} = \frac{H_{ib}}{2} \tag{4.52}$$

$$I = 2 \cdot \frac{1}{12} t_{ib} H_{ib}^3 + 2 \cdot \left[\frac{1}{12} W_{ib} t_{ib} + W_{ib} t_{ib} \frac{H_{ib}^2}{2^2} \right] \tag{4.53}$$

Where a_{pmax} is the maximum deceleration by the penetrator [m/s^2], $m_{ib_{outer}}$ is the mass of the portion of the box which is outside the penetrator radius [kg], W_{ib} and H_{ib} are the width and height of the instrument box [m].

Figure 4.35 shows the highest bending stress in the top side of the box, this side is in tension. The bending stesses reach a maximum of 110 MPa, with the material tensile yield strength at 503 MPa. Hence the instrument box will also not fail in bending, in a case worse than in reality.

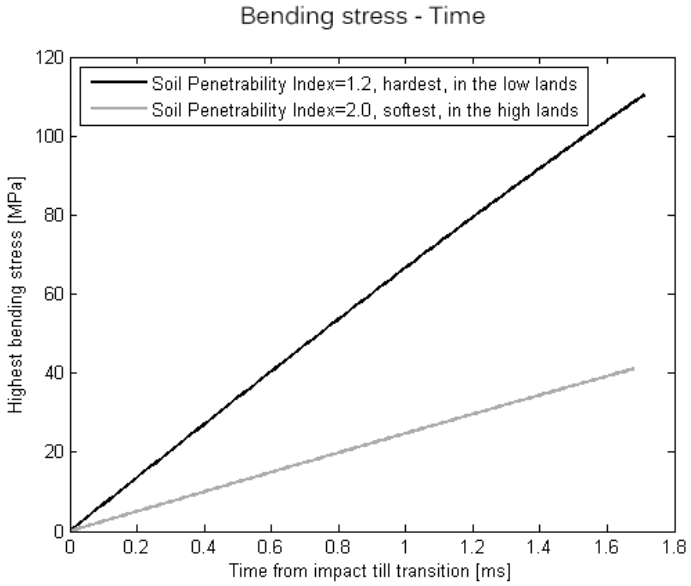

Figure 4.35: The highest bending stress in the cross-section of the instrument box.

Chapter 5

Earth-Mars Transfer

This chapter examines the Earth-Mars transfer sequence. First, a launcher is defined that compiles with the weight and size estimations of the payload design. Then, a detailed analysis is performed to optimize the orbit trajectory by defining a Launch date and estimate all important δV components. Finally, the entry, descend and landing approach on Mars is explained.

5.1 Launch

5.1.1 Launcher selection

Before the actual mission is performed, a suitable rocket launcher needs to be chosen. In general, there are many possible launch systems available. However, the weight and size of the payload constrains the assortment. A summary of the payload dimensions is given in table 5.1.

Table 5.1: Payload dimensions

Diameter [m]	2.2
Height [m]	4.5
Mass [kg]	2867

Due to the relatively large mass of the payload with 3 tons and estimated payload fairing of 3 meters, the range of launchers can be limited to: Ariane 5G(Astrium), Atlas V-401(ULA) and Delta IV 4M(ULA). All rockets are multi-stage systems, designed for heavy missions and have a sufficient diameter for the Ancile-module. It is important to know the amount of mass that the launcher can lift to an heliocentric transfer orbit (HTO) for an interplanetary mission. These values are listed in table 5.2. It can be seen that all chosen launchers have the capability to bring the payload into the mentioned orbit trajectory. The possibility of using two rocket systems was not an option. A two-launchers concept would implement higher costs and an additional negative impact on sustainable development. In order to choose the correct launcher, additional trade-off criteria have to be defined: The specific impulse, cost and the number of successful launches.

The specific impulse implies the efficiency of the propulsion system by comparing the thrust with respect to the amount of fuel used per unit time. The average is between 300 to 400 s. Looking at table 5.2 it can be concluded that the specific impulse does not vary significantly and therefore does not lead to an affirmative result. Looking at the cost perspective, the Delta IV rocket demands the highest cost with 140 to 170 million dollar, followed by the Atlas V with 138 million dollar [2]. The Ariane 5G is the cheapest with 120 dollar [21]. This rocket is also by far the most experienced launcher with 63 successful launches. Whereas the Delta IV and Atlas V only count 20 and 33 respectively [95] [15].

Table 5.2: Launchers [78] [95] [15]

Launcher	Diameter [m]	Payload-mass HTO [kg]	I_{sp} [s]			Cost [M$]
			Booster	First Stage	Second Stage	
Ariane 5G	4.57	4100	275	430	430	120
Atlas V-401	4.72	4000	275	311	451	138
Delta IV-M	4.07	3600	275	410	462	150

To conclude, the Ariane 5G comes out best with respect to cost/performance and is chosen as the launcher system for the Ancile project. Furthermore, this launcher was used already within the Rosetta Mars mission in 2004. The orbiter had a comparable payload weight of 3000 kg. Detailed characteristics of the Ariane 5G and structural integrity are described and analyzed in the following subsection.

5.1.2 Launcher characteristics

The Ariane 5G consists of two boosters (EAP) and a two stage rocket propulsion. Table 5.3 lists all important thruster characteristics. The mass-flow is calculated by dividing the thrust by the exhaust velocity. The exhaust velocity is the product of the specific impulse and the gravitational constant of Earth at sea-level(9.81 m/s^2).

Table 5.3: Thruster characteristics [78]

EAP (2)	
I_{sp} [s]	275
Total Thrust [kN]	12940
$V_{exhaust}$ [m/s]	2697.75
Massflow [kg/s]	4796
First stage	Vulcain
Isp [s]	430
Thrust [kN]	1114
$V_{exhaust}$ [m/s]	4218.3
Massflow	264.1
Second stage	Aestus
Isp [s]	324
Thrust [kN]	27.4
$V_{exhaust}$ [m/s]	3178.44
Massflow [kg/s]	8.62

Furthermore, the mass fractions are stated in table 5.4. The total weight is around 780 tons, whereas only 0.4% is considered to be payload. Most of the amount is fuel weight which takes up to 95%. The rest is structural weight of the two rocket stages and boosters. The weight specifications for the launcher, i.e. mass of boosters and stages is based on assumptions. The dry weight of the Ariane 5 is around 35200 kg [78]. Half of this weight is considered to be the structural weight of both boosters. The other half is split into first and second stage. Since the first stage is the main stage and much bigger than the second, only 25 percent is accounted for the second stage. A chart for mass allocation is given in figure 5.1.

Table 5.4: Launch mass fraction

$M_{payload}$ [kg]	2867
M_{EAP} [kg]	17600
$M_{fuelEAP}$ [kg]	618760
$M_{firststage}$ [kg]	13200
$M_{fuelfirststage}$ [kg]	113557
$M_{secondstage}$ [kg]	5866
$M_{fuelsecondstage}$ [kg]	4399
M_{total} [kg]	780016

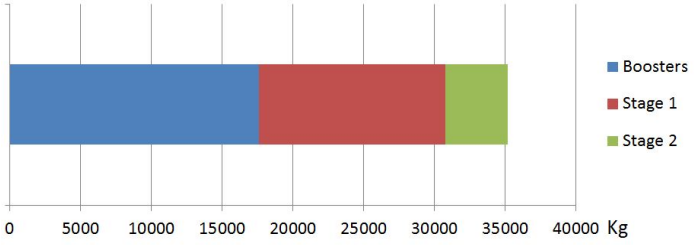

Figure 5.1: Structural mass fraction of Ariane 5. The total dry mass is 35,200 kg

The shape and all dimensions of the fairing for the Ariane launcher is given in figure 5.2. Its height equals to about 15.9 m and it has a diameter of 3.9 m. On the other hand, the Ancile cruise stage only consists of a diameter of 2.20 m and a height of 4.5 m and therefore fits within the fairing (see figure 5.3).

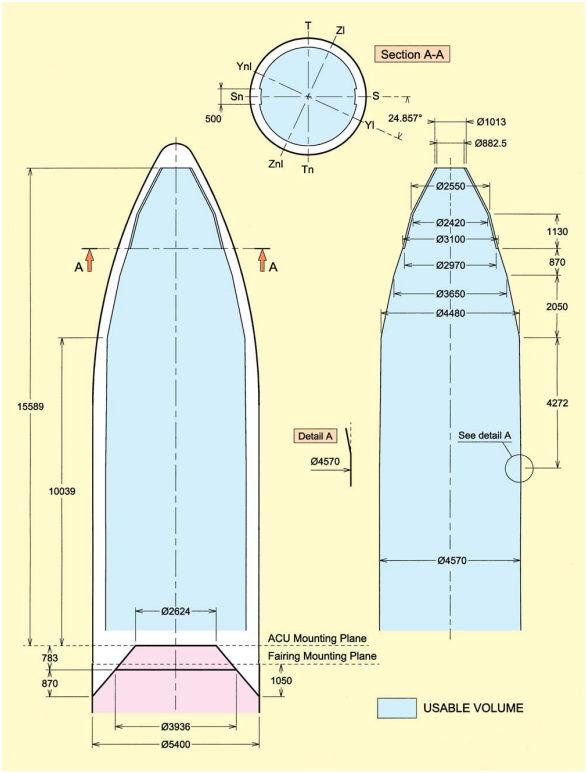

Figure 5.2: Ariane 5 payload capsule [78]

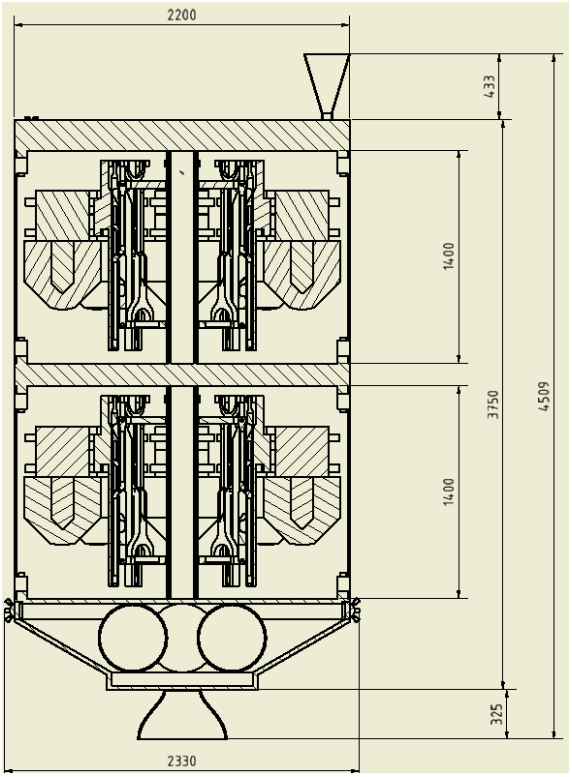

Figure 5.3: Ancile space-bus dimensions

5.1.3 Launch date

The synodic period of Mars with respect to Earth is 26 months. In addition, the lowest transfer energy needed, varies on a 15 and 17 years cycle alternately. That is because the orbit of Mars is not completely circular around the sun and varies in distance from 206 to 249 million km. Furthermore the orbit is inclined 1.8 degrees with respect to the Earth-Sun plane. According to literature, the last optimal opportunity was in 2003 and repeats in 2018 (see figure 5.4 and figure 5.5) [43] [24] [62]. The time intervals for the next launch windows from year 2016 to 2020 are listed in table5.5.

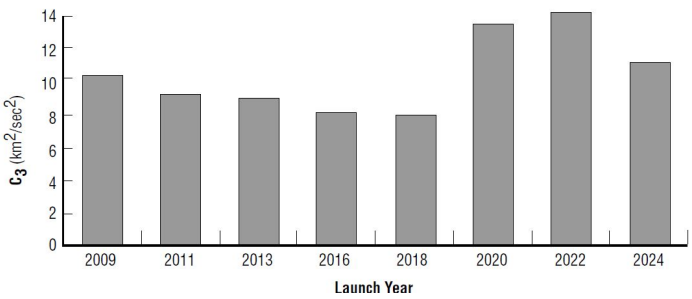

Figure 5.4: Required Escape velocity with respect to launch-year [43]

Since a start in 2018 would mean the least required transfer energy, this time-slot seems to be most reasonable. Furthermore, it provides a sufficient time-span of 5 years for tests, development and construction. The launch window is open from end of the April to end of May. As a preliminary

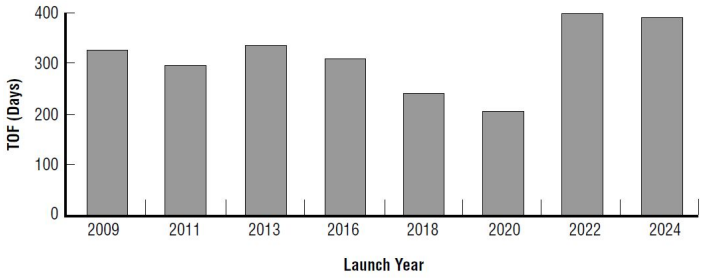

Figure 5.5: Required travel time with respect to launch-year [43]

Table 5.5: Launch Windows [43] [24] [62]

Year	Launch Period
2016	Jan 2016 Apr 2016
2018	Apr 2018 May 2018
2020	Jul 2020 Sep 2020

selection, the Tuesday, first of May 2018 is chosen as launch date. Regarding the transfer time, the Arrival date is therefore the night between the 13th and 14th of January 2019.

5.1.4 Launch Sequence

Given the mass fraction and thruster characteristics (see table 5.3 and 5.4), the launch sequence can be modeled. The process is divided into 4 phases: Lift-off and EAP separation, Fairing jettison, First stage separation, Second stage separation. The calculations are based on the Tsiolkovsky rocket equation (see equation 5.1), launch-vehicle properties (see table 5.3 and 5.4) and the aerodynamic drag is neglected. The general procedure is implemented in figure 5.6 as well.

$$\Delta V = V_e \cdot ln(\frac{M_0}{Me}) \tag{5.1}$$

Lift-off and EAP seperation

Boosters (EAP) and Cryogenic main core stage (EPC) are ignited simultaneously during lift-off. Within 129 seconds, the rocket accelerates to a speed of 4440 m/s. That is mainly due to the two EAPs which provide a ΔV of 4252 m/s, whereas the first stage contribution is calculated to be only 188 m/s. After 2 minutes and 9 seconds, the EAPs will be separated from the rocket and fall back on Earth. Within this phase the acceleration is maximum and corresponding to that the g-loads. In total, 3.5 g are operating on the rocket launcher and payload.

Fairing jettison

Within the next 90 - 120 seconds the fairing will be split off from the main stage in order to prepare the second stage burn. The rocket will start to turn more towards a horizontal trajectory.

First stage separation

The module reaches the LEO parking orbit and ejects the main stage (EPC) from the payload. The second stage (SYLDA 5) start-up is initiated. This might not be introduced immediately after separation in order to adjust for the correct timing.

Second stage separation

During the last 12 minutes, the bus is accelerated to escape velocity in order to leave the Hill radius of Earth and enter the correct trajectory to mars. The second stage is then shut off, isolated from the payload and slowed down with a ΔV boost in the opposite direction such it returns to Earth.

A Launch time-line is given in table 5.6.

Table 5.6: Launch sequence

Lift off	
Time [h:mm:ss]	0:00:00
EAP separation	
Time [h:mm:ss]	0:02:09
Burning time [s]	129
ΔV [m/s]	4440
Velocity [m/s]	4440
Fairing Jettison	
Time [h:mm:ss]	0:03:45
First Stage(EPC) separation	
Time [hh:mm:ss]	0:07:10
Burning time [s]	301
ΔV [m/s]	5451.11
Velocity [m/s]	9892
Second stage(SYLDA5) separation	
Time [hh:mm:ss]	0:19:34
Burning time [s]	744
ΔV [m/s]	1517
Final velocity [m/s]	11409

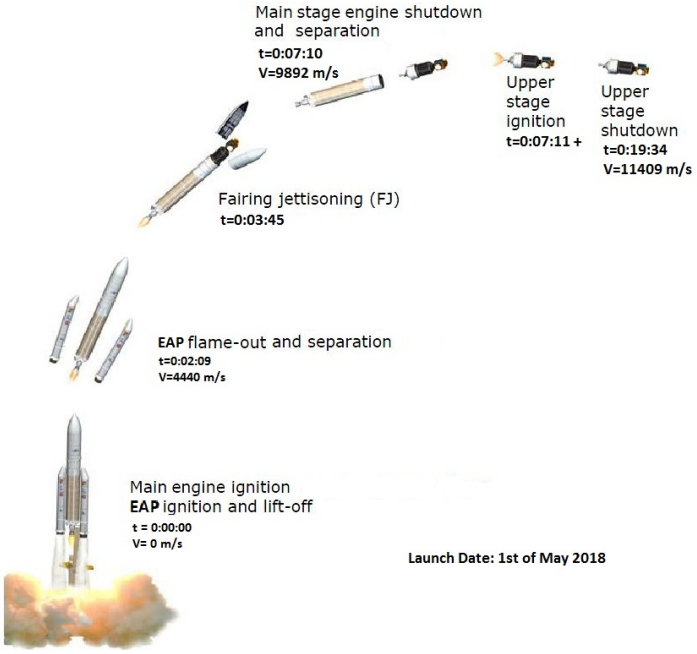

Figure 5.6: Launch sequence of the Ariane 5 [78]

5.2 Transfer Module

In this section the transfer module will be discussed. The transfer module transports the probes to Mars and protects them from the space environment. It will consist of the following subsystems: attitude determination, propulsion, thermal control, communication and power management.

5.2.1 General description

The transfer module transports the probes to Mars. To protect the probes from the space environment a shell is placed around the probes. Within this shell the temperature will be controlled by active

thermal control, louvers to get rid of excess heat and heaters to add heat. The batteries of the probes will be charged, although they are charged at launch, they slowly discharge over time, so they will be charged by the power provided by the solar panels on the back of the transfer module. The solar panels will be pointed towards the sun during the transfer. To control the attitude of the transfer module star and sun sensors are used to determine the attitude, and two sets of four thrusters are used for maneuvering. To communicate with the Earth a horn antenna is used, which is also at the back of the transfer module. The antenna has to be pointed towards the Earth, this means that the solar panels are most of the time under an angle away from the sun. The solar panels are designed to still deliver sufficient power for an offset of 43 degrees from the sun. In figure 5.7 the layout of the transfer module is shown.

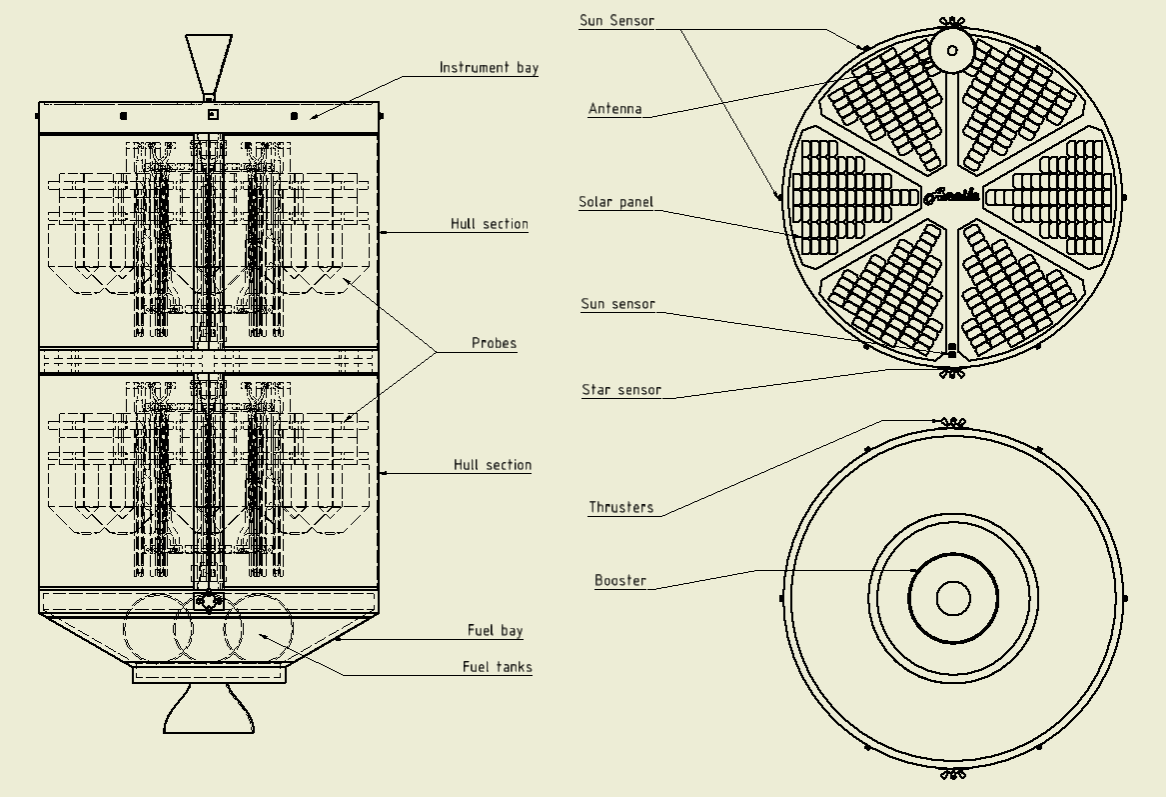

Figure 5.7: Layout of the transfer module

5.2.2 Attitude determination

The transfer module will need to orientate itself. To be able to orientate the module, the attitude of the module needs to be determined by using star en sun sensors. Two star sensors, of which one is for redundancy, are placed on the outer shell of the transfer module, opposite to each other. The star sensor used must always be pointed away from the sun for proper functioning, this is achieved by switching between the two. The sun sensors are also redundant, bringing eight instead of the necessary four. Two are placed in the same plane as the solar panels, pointed towards the sun. The other six will be placed on the outer shell, distributed over the transfer module, so the attitude can be determined accurately. The properties of the selected sensors are listed in table 5.7. These sensors are chosen because of their accuracy and power usage.

5.2.3 Propulsion

The transfer module needs to be able to perform manoeuvres, for this propulsion is needed. To be able to manoeuvre around each axis, two sets of 4 thrusters are used. The amount of propellant needed for the manoeuvres is determined by using the Mars Science Laboratory (MSL) as reference mission. The MSL mission is chosen, because of its comparable weight. The MSL had 139 kg of

Table 5.7: Star and Sun sensors used in the transfer module

	Units	Star sensor [53]	Sun sensor [54]
Model		S3S	SS-411
Accuracy	deg	0.01	0.1
Mass	g	90	34
Dimensions	mm	59 x 56 x 32.5	34 x 32 x 21
Power (max)	W	1	1.35

propellant for manoeuvring [68]. This mission performed six manoeuvres during its transfer, three in the transfer orbit and three near Mars.

In this mission five manoeuvres will be performed during transfer of which 3 in the transfer orbit and 2 near Mars. The first manoeuvre near Mars is to adjust the attitude for the first probe release. After the first release, a second manoeuvre is needed to adjust the attitude and velocity for the second probe release.
The velocity change after the first probe release is 80 m/s. For this velocity change, according to equation 5.2 [94], 109 kg propellant is needed. In this equation is M_{prop} the propellant mass [kg], M_{begin} the mass of the complete transfer module at the beginning of the velocity change [kg], ΔV the change of velocity [m/s], I_{sp} the specific impulse [s] and g_0 the gravity at sea level on Earth [m/s^2]. The mass at the beginning of the velocity change is about 3000 kg. A mono-propellant hydrazine thruster will be used, with a specific impulse of 220 s [94]. For this large velocity change a separate larger thruster is used, which provides 667 N of force. This force is calculated by equation 5.3, where F is the force the thruster needs to provide [N] and Δt is the time in which the velocity change takes place [s]. This time is 360 s.

$$M_{prop} = M_{begin}\left(1 - e^{-\frac{\Delta V}{I_{sp} \cdot g_0}}\right) \tag{5.2}$$

$$F = M_{begin} \cdot \Delta V / \Delta t \tag{5.3}$$

During the trajectory manoeuvres about 70 kg of propellant will be used. This value is derived from the MSL mission, since it is very hard to predict the amount of propellant needed for manoeuvring. Each thruster for manoeuvring can provide 5 N of force. The total propellant mass will be 179 kg. The propellant will be stored in four spherical pressure tanks with a radius of 0.207 m, this is calculated by equation 5.4. Where r_{tank} the radius of one tank is [m] and V_{total} is the volume of the propellant [m^3], which is calculated by equation 5.5. Where ρ is the density of the pressurized mono-propellant hydrazine [kg/m^3], which is 1200 kg/m^3. This value is derived from the MSL.

$$r_{tank} = \left(\frac{1}{4}\frac{V_{total}}{\frac{4}{3}\cdot\pi}\right)^{1/3} \tag{5.4}$$

$$V_{total} = \frac{M_{prop}}{\rho} \tag{5.5}$$

5.2.4 Thermal control

Thermal control is needed to keep the transfer module within a certain temperature range. The operational temperature range of the subsystems are listed in table 5.8.

According to these temperature ranges the temperature the hydrazine tanks and lines should be less than 15 °C, and the rest of the transfer module will be held around 10 °C. To achieve this the transfer module is insulated and has a radiator surface of 0.86 m^2 to radiate the excess heat. This surface is calculated by equation 5.6. Where A_{rad} is the radiator area in [m^2], Q_{in} is the minimum incoming heat plus the heat generated by the subsystems [W], ϵ_w is the emissivity of the white paint which is used on the radiator area [-], σ is the Stefan Boltzmann constant [W/m^{2}K^4] and T is the absolute temperature of the transfer module [K]. The incoming heat is the heat coming into the transfer module from the sun. The heat generated by the subsystems is approximately 20 % of the

Table 5.8: Operational temperature rage of subsystems in the transfer module [53] [54] [94]

Component	Operational temperature range [°C]
Star sensor	0 - 30
Sun sensor	-25 - 50
Batteries	0 - 15
Hydrazine tanks and lines	15 - 40
Antennas	-100 - 100
Solar panels	-150 - 110

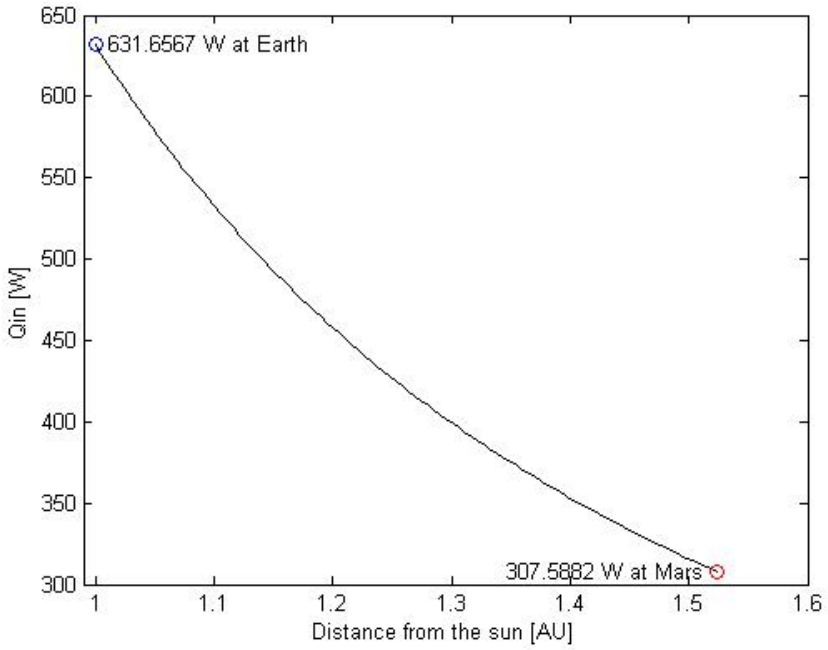

Figure 5.8: Q_{in} of the transfer module from Earth to Mars

power they consume. The Q_{in} from Earth to Mars is shown in figure 5.8. Emissivity of white paint Z93 is 0.92 [94].

$$A_{rad} = Q_{in}/(\epsilon_w \cdot \sigma \cdot T^4) \tag{5.6}$$

With this the temperature in the transfer module will be as shown in figure 5.2.4. To be able to keep the transfer module at 10 °C, near Earth louvers are used to get rid of the excess heat. At a certain moment the louvers will be closed and heaters will be used to keep the transfer module at 10 °C. To keep the hydrazine tanks and lines at least at 15 °C extra insulation and heaters are placed around it.

5.2.5 Communication

Communication with Earth is essential to make sure the transfer module is still on the predetermined transfer orbit and in the preferred attitude. If this is not the case commands need to be send towards the transfer module. As antenna a horn antenna is used which will communicate with the Deep Space Network (DSN) on Earth. To be able to determine the size of the antenna, the power it uses and the data rate it can achieve, a link budget is made.

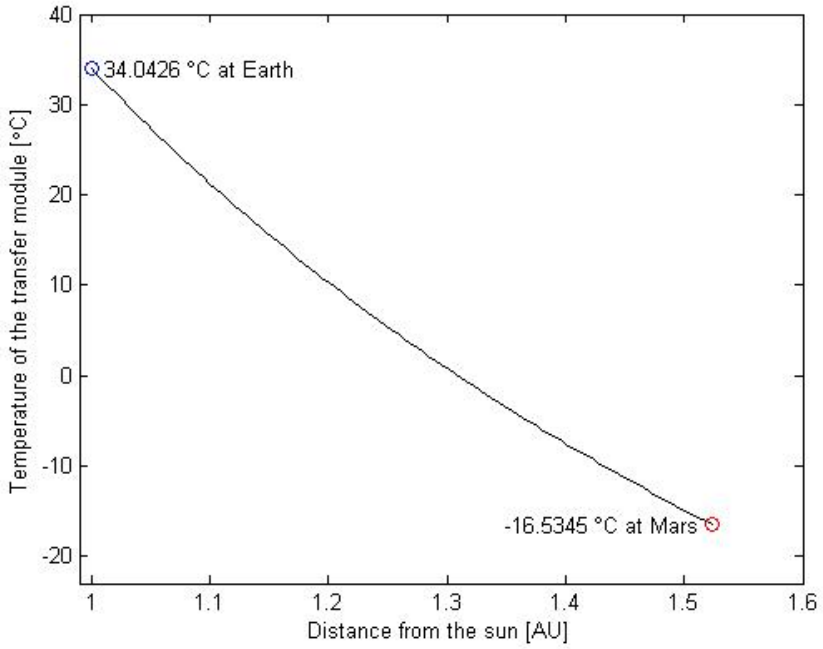

Figure 5.9: Temperature of the transfer module from Earth to Mars with insulation and a radiator area of 0.86 m^2 without louvers and heaters

Link budget

This link budget is partially the same as for the probes, but in this case a horn antenna is used. This means that some other equations are needed, so the complete link budget is explained.

To be able to transfer data, the received energy-per-bit to noise-density ratio ($E_b/N0$) should be sufficient. This depends on factors explained later. Equation 5.7 is the equation used to determine the ($E_b/N0$) [94].

$$E_b/N_0 = P_{dBW} + L_l + G_t + L_{pr} + L_s + L_a + G_r + 228.6 - 10log(T_s) - 10log(R) \tag{5.7}$$

Here P_{dBW} is the transmitter power [dBW], L_l is the transmitter line loss [dB], G_t is the transmit antenna gain [dBi], L_{pr} is the receive antenna pointing loss [dB], L_s is the space loss [dB], L_a is the propagation and polarization loss [dB], G_r is the receive antenna gain [dBi], T_s is the system noise temperature [K] and R is the data rate [bps].

In order to solve equation 5.7, some parameters should to be determined. The first one is the frequency (f) used for transmission. A horn antenna uses most of the time the C-band frequencies, for this mission a frequency of 4 GHz is chosen. The second parameter is the transmitter power in watts (P_W), which will be converted into transmitter power in decibel watts (P_{dBW}) using equation 5.8 [94].

$$P_{dBW} = 10log(P_W) \tag{5.8}$$

For the power some iteration in the link budget were required. A high transmitter power might be impossible, because the power generation method might not be able to deliver the amount of power asked for. A transmitter power of 25 W was found. The third parameter is the transmitter line loss (L_l), which is usually about -1 dB [94].

To determine the peak transmit antenna gain (G_{pt}), the transmit antenna diameter (D_t) and the transmit antenna pointing loss (L_{pt}), equations 5.9, 5.10 and 5.11 are used [94]. For these equations the final parameters for the transmitter are the antenna beam width (θ_t) and the transmit

antenna pointing offset (e_t). The standard value of the antenna beam width for a horn antenna is 18 degrees [94], and the transmit antenna pointing offset is 1 degree.

$$G_{pt} \approx 44.3 - 10log(\theta_t^2) \tag{5.9}$$

$$D_t \approx \frac{225}{\pi \cdot \theta_t \cdot f/c} \tag{5.10}$$

$$L_{pt} = -12 \cdot (e_t/\theta_t)^2 \tag{5.11}$$

Finally the transmitter antenna gain (G_t) and equivalent isotropic radiated power ($EIRP$) can be calculated, this is done in equations 5.12 and 5.13 [94]. All the values regarding to the transfer module antenna transmission are summarized in table 5.9.

$$G_t = G_{pt} + L_{pt} \tag{5.12}$$

$$EIRP = P + L_l + G_t \tag{5.13}$$

Table 5.9: Values regarding the transmitting transfer module antenna

	Symbol	Units	Value
Frequency	f	GHz	4
Transmitter power	P_W	W	25
Transmitter power	P_{dBW}	dBW	13.98
Transmitter line loss	L_l	dB	-1
Transmit antenna beam width	θ_t	deg	18
Peak gain transmit antenna	G_{pt}	dBi	19.2
Transmit antenna diameter	D_t	m	0.30
Transmit antenna pointing offset	e_t	deg	1
Transmit antenna pointing loss	L_{pt}	dB	-0.037
Transmitter antenna gain	G_t	dBi	19.16
Equivalent isotropic radiated power	$EIRP$	dBW	32.137

The signal has to travel a large distance through space, which will cause a loss of power. To calculate this space loss (L_s), with equation 5.14, the maximum distance between the transmitter and the receiver needs to be known. This propagation path length (S) will be at maximum 272,690,000 km. Also the propagation and polarization loss (L_a) has to be determined. This value is chosen to be 0.3, since the signal has to travel through the atmosphere of the Earth. These transmission losses are listed in table 5.10.

$$L_s = 147.55 - 20log(S \cdot 10^3) - 20log(f \cdot 10^9) \tag{5.14}$$

Table 5.10: Transmission losses

	Symbol	Units	Values
Propagation path length	S	km	272,690,000
Space loss	L_s	dB	-273.2
Propagation and polarization loss	L_a	dB	0.3

The receiving antenna on Earth will be an antenna of the DSN. For this antenna the first parameter that has to be determined is the receive antenna diameter (D_r). This will be a diameter of 70 m, which is the diameter of the largest antennas of the DSN. The second parameter is the receive antenna pointing error (e_r), which is for the DSN antennas 0.02 degrees. With these parameters the peak receive antenna gain (G_{rp}), the receive antenna beam width (θ_r) and the receive antenna pointing loss (L_{pr}) can be calculated with equations 5.15, 5.16 and 5.17 [94].

$$G_{rp} = -159.59 + 20log(D_r) + 20log(f) + 10log(\eta) \tag{5.15}$$

$$\theta_r = \frac{21}{f \cdot D_r} \tag{5.16}$$

$$L_{pr} = -12 \cdot (e_r/\theta_r)^2 \tag{5.17}$$

In equation 5.15 is η the efficiency of the antenna, a value of 0.55 is commonly used. Finally the receive antenna gain can be calculated with equation 5.18 [94]. The values for the receive antenna are listed in table 5.11.

$$G_r = G_{rp} + Lpr \tag{5.18}$$

Table 5.11: Values regarding the receiving DSN antenna

	Symbol	Unit	Value
Receive antenna diameter	D_r	m	70
Peak receive antenna gain	G_{rp}	dBi	66.76
Receive antenna beam width	θ_r	deg	0.075
Receive antenna pointing error	e_r	deg	0.02
Receive antenna pointing loss	L_{pr}	dB	-0.85
Receive antenna gain	G_r	dBi	65.90

To complete the link budget, some final parameters have to be determined. The first one is the system noise temperature (T_s). For transmission from space this values is equal to 135 K [94]. To be able to use equation 5.7, the data rate (R) has to be determined. There is not a lot of data that needs to be send, so a data rate of 200 bps is determined.

Now the received energy-per-bit to noise-density ratio can be computed from equation 5.7 for transmission from the transfer module. With these values the carrier-to-noise density ration (C/N_0) can be computed by using equation 5.19 [94].

$$C/N_0 = E_b/N_0 + 10log(R) \tag{5.19}$$

In order to check whether the calculated E_b/N_0 is sufficient, the bit error rate (BER) should be determined. This value is typically between the 10^{-5} and 10^{-7}. A value of 10^{-5} was chosen for the transmission from the transfer module. The required E_b/N_0 ($reqE_b/N_0$) is 5 dB. The last parameter that has to be determined is the implementation loss. Values for this loss are between the 1 and 2 dB, since the best technology will be used, a value of 1 dB is chosen.

Now the margin can be calculated using equation 5.20 [94]. This margin has to be larger than zero, to succeed the transmission of data. The last values of this link budget are listed in table 5.12. The margin is larger than zero, so the horn antenna that will be used is 0.30 m in diameter and will use 25 W of power.

$$Margin = E_b/N_0 - reqE_b/N_0 - implementationloss \tag{5.20}$$

Table 5.12: Final link budget values

	Symbol	Units	Value
System noise temperature	T_s	K	135
Data rate	R	bps	200
Received energy-per-bit to noise-density ratio	E_b/N_0	dB	7.93
Carrier-to-noise density ratio	(C/N_0)	dB-Hz	30.94
Bit error rate	BER	-	10^-5
Required E_b/N_0	$reqE_b/N_0$	dB	5
Implementation loss	-	dB	1
Margin	-	dB	1.93

5.2.6 Power management

In order to provide enough power for the subsystems in the transfer module, solar panels are used to deliver the required power. For this the power consumption of each subsystem has to be known. A list of power consumption per subsystem is provided in table 5.13. Also a battery is used for just after launch, when the solar panels are not delivering power yet. This battery will also be used for spinning up the probes.

Table 5.13: Power consumption of subsystems in the transfer module

Subsystem	Power consumption [W]
Communication	25
Thermal control	100
Attitude determination	12.8
Command and data handling	5
Battery	10
Probes	160
Total	312.8

To be able to calculate the area of solar panels needed, some parameters have to be determined. First the type of solar cells have to be chosen, this will be multi-junction devices InGaP/GaAs/InGaAs, with an efficiency of the solar panels 37.5 % in the laboratory [46]. After production 85.6 % of the efficiency in the laboratory is left [94]. This gives an efficiency of 32.1 %. Solar cells can not be directly next to each other, because of the electronics, so they have a packing factor. This factor is usually 80 %. The degradation of the solar panels is not taken into account, since they are only in space for eight months.

Also to be taken into account is that the solar panels are not always perpendicular to the sun, so an angle needs to be defined, in which the solar panels still deliver enough power. This angle is chosen to be 43 degrees. The amount of power the solar panels can provide also depends on the solar irradiance. This is the power the sun delivers per square meter. This is lowest near Mars, 586 W/m^2. This value will be used, since in the worst case the solar panels still have to be able to deliver the required power.

With these values the area of solar panels can be determined by using equation 5.21. Where A is the area of solar panels [m], P_{cons} is the total power consumption [W], ϵ is the efficiency [-], S_{Mars} is the solar irradiance near Mars [W/m^2], f_p is the packing factor [-] and θ is the angle away from the sun [rad].

$$A = \frac{P_{cons}}{\epsilon \cdot S_{Mars} \cdot f_p \cdot cos(\theta)} \tag{5.21}$$

With the values given above, the area of solar panels needed is 2.84 m^2. This is a circle with a radius of 0.95 m, so it will fit on the back site of the transfer module.

In figure 5.10 the electric block diagram for the transfer module is shown. The solar panels deliver the needed power, this goes via a shunt regulator to be able to let the excess power flow away. The direct current will go through DC-DC converters to deliver the right voltage to the subsystems.

5.3 Transfer Orbit

The choice of the correct orbit and timing is essential for the mission guideline. It defines the ΔV requirements as well affects the transfer time. In this section, an transfer orbit is selected and the timing described in more detail.

5.3.1 Orbit selection

Next to the launch, the transfer orbit has to be set. There are four different trajectories possible to transport the payload to Mars: Spiral Transfer, Gravity Assist, Hohmann Transfer and Direct

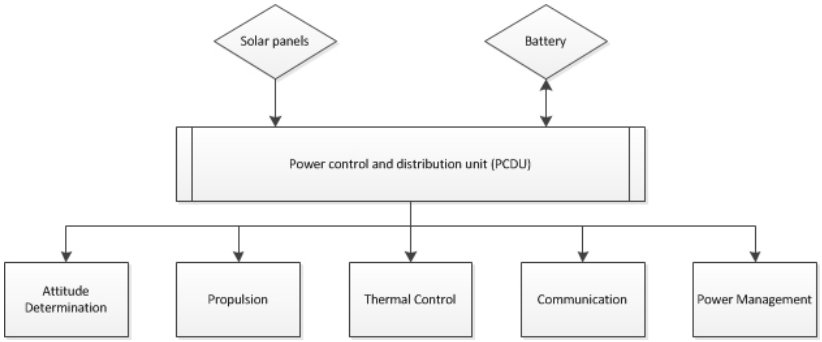

Figure 5.10: Electronic block diagram of the transfer module

Transfer.

Spiral Transfer

The spiral transfer is a low thrust transfer. Mars will be approached after multiple orbits around the Sun. This strategy requires low energy and therefore the thrust can be achieved by electric propulsion. A small chemical rocket will only be used to escape Earths sphere of influence. However, it also takes significantly more time and electric power. One or several years have to be budgeted, depending on the total number of thrusters. For example, with a chemical rocket propulsion serving a ΔV of 450 m/s to introduce the module into Orbit and then activating an electric propulsion with about 600 kW electric power and a specific impulse of 1600 to 5000 s would lead to a transfer time of 1.5 to 2 years [8]. The trajectory can be seen in figure 5.11. Within that transfer, the spacecraft is exposed to the unfavorable space environment with solar radiation, particle radiation (highly energetic particles) and temperature differences of up to 275 degrees [67]. These extremes can damage the systems if not designed for it. The design has to be adjusted to the continuing electromagnetic radiation and thermal affects. That is done by using additional layers of aluminum. In addition the demand in power is significantly higher than in any other transfer due to the electric propulsion.

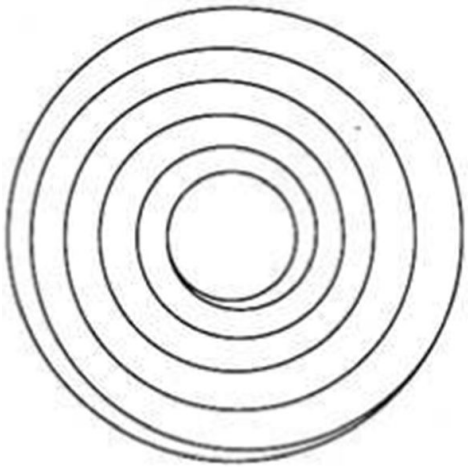

Figure 5.11: A spiral trajectory with electric propulsion [94]

Gravity Assist

Instead of approaching Mars directly, the spacecraft uses other planets to accelerate and adjust its trajectory direction. Until now, two gravity assist trajectories have been researched in literature for an Earth-Mars transfer. The Venus and the lunar gravity assist. These maneuvers however, have not been often be applied in practice yet.

The concept, using the Venus as a gravity assist is depicted in picture 5.12. Recently, this method

gains more attention by scientists for cargo missions to Mars. The cruiser decelerates in order to enter the lower Venus orbit. During this maneuver, the spacecraft gets closer to the sun and is therefore exposed to a higher amount of electromagnetic radiation and thermal constraints. The intensity of solar radiation increases from Earth to Venus with a factor of two from 1366 W/m^2 to 2611 W/m^2 [7]. Therefore, using this transfer concept, all additional loads (i.e temperature extremes and electromagnetic radiation) have to be considered and implemented in the design as it is done for a spiral transfer. When passing Venus, the total velocity vector of the spacecraft is altered by the gravity, leading into a change in path and increase in speed. This maneuver gives sufficient energy to transfer the module into the higher Mars orbit. The advantage of the whole process is the savings in ΔV components. However, since the trajectory depends now on two planet constellation it makes the planning and accomplishment of the mission more complex and risky. The launch window is only open every 6.4 years instead of 26 months (Hohmann transfer) and the transfer time equals roughly one year or more [73].

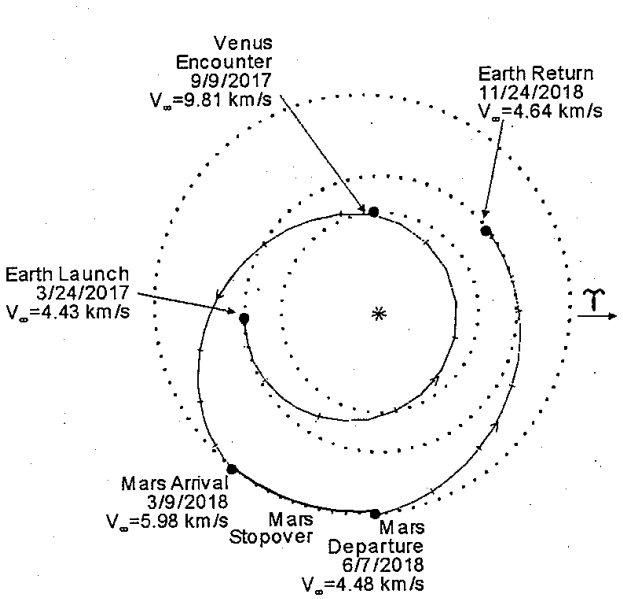

Figure 5.12: Venus gravity assist trajectory [73]

Using a Moon-Earth gravity assist has one advantage over the Venus. The module is not orbiting the sun in a significantly lower orbit. That means that the influences of solar radiation and thermal impact are not increasing. The procedure of this concept is shown in figure 5.13. First, the spacecraft circles Earth with several high ellipse loops to geostationary orbit (GTO) and then boosts to the Moon with a certain ΔV. The planet is then used to accelerate and change the orientation of the transfer module. It surrounds Earth again to increase the speed even more to travel to Mars. Altering the relative movement of the spacecraft by gravity of Moon and Earth saves in fuel (lower ΔV requirement) such that only 1400 m/s is required from GTO to Mars [77]. The launch window repeats every 26 months. However, since the trajectory is dependent on multiple planets again, the launch is only possible for a couple of hours on specific days. Next to that it induces more complexity and risks. Considering the transfer time, the Moon gravity assist has a slightly longer travel period than for instance the Hohmann transfer with about 1 year [77]. An example is the orbiter Nozomi from 1999 which used such an orbit. Nevertheless, due to an engine sub-function it did not enter the trajectory correctly. In addition, instruments got damaged because of solar eruption and the mission failed [65].

Hohmann Transfer

The Hohmann transfer is the most common used maneuver for interplanetary flight. In theory the spacecraft is brought into a parking orbit around Earth and then boosted with an immediate change in the ΔV component to Mars-trajectory. This transfer is the ideal and minimum energy solution type. In practice however, the change in velocity is not instantaneous but requires a certain time

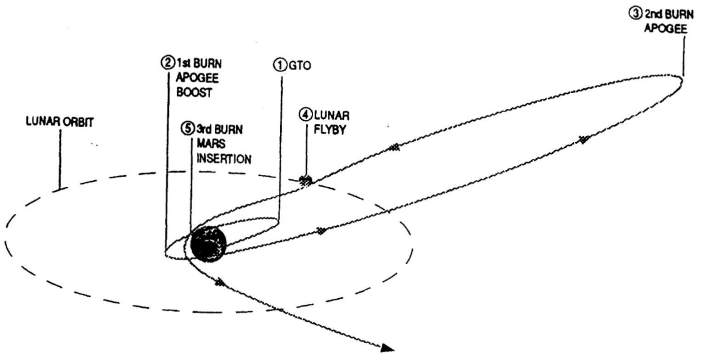

Figure 5.13: Moon gravity assist trajectory [77]

interval to achieve the terminal velocity. Therefore it is more a Hohmann-like transfer. In order to emend for this, several correction maneuvers have to be done during the transfer. An overview of the theory is given in figure 5.14. The transfer time is about 8 Months. With a parking orbit of about 200 km above Earth would require a ΔV of 3.6 km/s (see calculations in subsection 5.3.2). Using a transfer from GTO as it is done for the Moon, the demand of ΔV becomes 2.8 km/s.

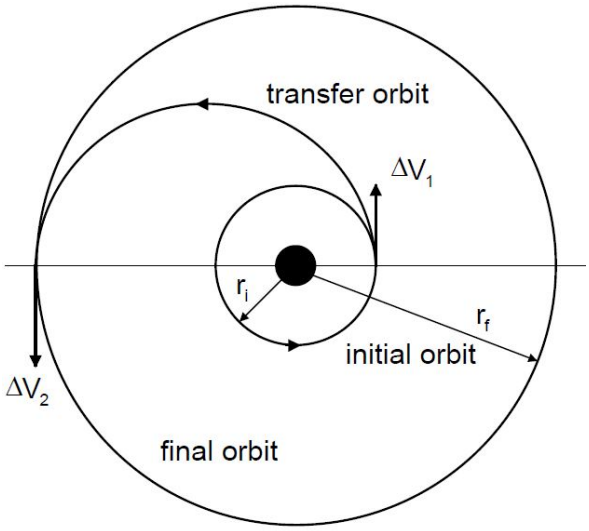

Figure 5.14: Hohmann transfer [36]

Direct Transfer

The Direct transfer is basically a type I Hohmann transfer. That means that the spacecraft will travel from Earth less than 180 degrees around the sun in order to reach Mars. It stands out with its short-transit-time trajectory of 147 - 170 days [73]. Mars is going to be approached directly by a high ΔV boost. This requires high energy supply not only to bring the spacecraft into the correct flight path, but also to decelerate when reaching Mars. An example is given in figure 5.15 .

Conclusion

Regarding energy-level, transfer time and reliability, the Hohmann transfer is the most applicable maneuver. The spiral transfer contains a low thrust approach by using an electric propulsion. However, this system has a much higher demand on electric power. Due to its long transfer the spacecraft is also exposed to the unfavorable space environment for a longer time. Solar eruptions pose a substantial problem. Till now, this transfer method has not been used for any Mars mission. Gravity assist maneuvers are very complex and imply much more risks. They have not been applied yet in extend and contain a high unreliable factor. The trajectory depends on the constellation of 3 planets and

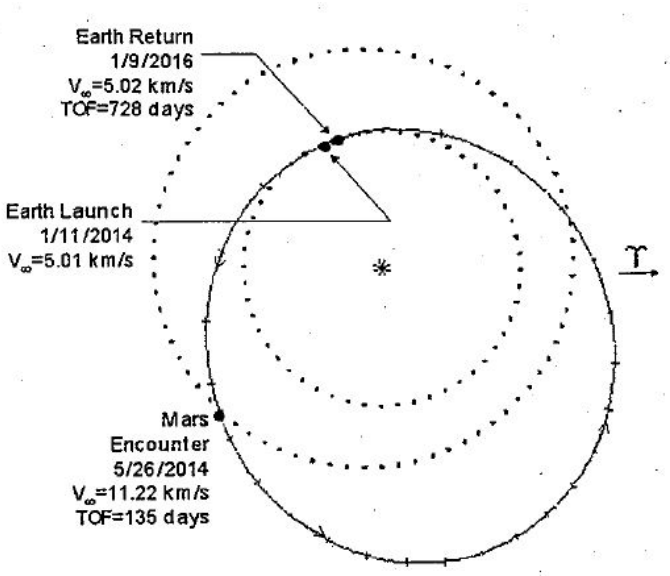

Figure 5.15: Direct transfer [73]

the synodic period only repeats every 6.4 years (Venus). The travel time is slightly longer but the ΔV requirement is less than the Hohmann transfer. However, the driving factor within this trade-off is the reliability. The saving in ΔV is not significant enough to satisfy within this consideration. Looking at the direct transfer, it accomplishes a fast trajectory based on high fuel/energy consumption. This would be more applicable for manned Mars mission, in order to expose the humans to electromagnetic and gamma radiation for the shortest amount of time possible. Nevertheless, within the mission objectives the transfer time does not play that an important role. The Hohmann transfer provides a relatively fast Earth Mars transfer with a limited energy requirement and a predictable risk-level. It is used in most Mars missions so far and proven in practice. A summary is given in table 5.14.

Table 5.14: Summary of Transfer Orbits

Characteristics	Spiral	Gravity Assist Venus	Gravity Assist Moon	Hohmann	Direct
ΔV) [m/s]	450+elec. propulsion	3300	1400 (GTO)	3600 (2800 at GTO)	5000+
Transfer time [years]	1.5 - 2	1 - 1.4	1+	0.8	0.3 - 0.5
Synodic period [years]	2.2	6.4	2.2	2.2	2.2
Reliability	Marginal	Low	Low	High	High

5.3.2 Transfer description

The ΔV requirements and transfer time of the Hohmann transfer is now estimated. All important parameters for calculations are listed in table 5.15. The semi-major axis and eccentricity are calculated, using the average distance of Mars and Earth with respect to the sun which is 1AU and 1.542 AU respectively. The equations are based on the flight and orbital mechanics manual from Ron Noomen [72].
The semi-major axis and eccentricity are:

$$a = \frac{d_{Earth+d_{Mars}}}{2} = 188.8 \cdot 10^6 \ [km] \tag{5.22}$$

$$e = \frac{d_{Earth-d_{Mars}}}{Earth + d_{Mars}} = 0.2076 \ [] \tag{5.23}$$

Table 5.15: Parameters for calculations [72]

Characteristics	Value
μ_{Earth} [km^3/s^2]	398600
μ_{sun} [km^3/s^2]	$1.327 \cdot 10^{11}$
μ_{Mars} [km^3/s^2]	42828
d_{Earth} [AU]	1
d_{Mars} [AU]	1.542
r_{Earth} [km]	6378
r_{Mars} [km]	3397
AU	$149.6 \cdot 10^6$

First, the heliocentric velocities of Earth (V_{dep}) and Mars (V_{tar}) are determined using equations 5.24 and 5.25.

$$V_{dep} = \sqrt{\frac{\mu_{Sun}}{d_{Earth}}} = 29.785\ [km/s] \tag{5.24}$$

$$V_{tar} = \sqrt{\frac{\mu_{Sun}}{d_{Mars}}} = 24.127\ [km/s] \tag{5.25}$$

Earth moves with about 29.785 km/s around the sun, whereas Mars travels slower with 24.127 km/s. The next step is to define the parking orbit around Earth and set the terminal Orbit at Mars. Since most interplanetary missions remain in an low Earth parking orbit for several minutes, the altitude was assumed to be 200 km [95] [78] [15]. After the transfer, the module will not stay in an orbit around Mars but crashes onto the martian surface. Therefore, the terminal orbit was assumed to be at 0 altitude. The required circular velocity at Earth is estimated by using equation 5.26.

$$V_{circ,E} = \sqrt{\frac{\mu_{Earth}}{r_{Earth} + h_{orbit}}} = 7.784\ [km/s] \tag{5.26}$$

In order to stay in an Orbit of 200 km above Earth a velocity input of 7.784 is required. Now, the escape velocities at departure and target position can be determined. These are needed in order to calculate the excess velocity.

$$V_1 = \sqrt{\mu_{Sun} * (\frac{2}{d_{Earth}} - \frac{1}{a})} = 32.731\ [km/s] \tag{5.27}$$

$$V_2 = \sqrt{\mu_{Sun} * (\frac{2}{d_{Mars}} - \frac{1}{a})} = 21.477\ [km/s] \tag{5.28}$$

The excess velocity become:

$$V_{infty,1} = |V_1 - V_{dep}| = 2.946\ [km/s] \tag{5.29}$$

$$V_{infty,2} = |V_2 - V_{tar}| = 2.65\ [km/s] \tag{5.30}$$

Finally, the velocity at pericenter and apocenter of the Hohmann transfer can be estimated. The pericenter is the position closest to Earth, whereas the apocenter describes the location at the target planet Mars.

$$V_{per} = \sqrt{\frac{2 * \mu_{Earth}}{r_{Earth} + h_{orbit}} + V_{infty,1}^2} = 11.396\ [km/s] \tag{5.31}$$

$$V_{apo} = \sqrt{\frac{2 * \mu_{Mars}}{r_{Mars}} + V_{infty,2}^2} = 5.677\ [km/s] \tag{5.32}$$

The velocity at the pericenter (i.e. parking orbit around Earth) is 11.396 km/s. That means that there needs to be a ΔV input of 3.6 km/s in order to leave the parking orbit at 200 km altitude (V_{per} - $V_{circ,E}$). The arrival velocity at Mars is than approximately 5.68 km/s. During the transfer, there are several maneuvers needed in order to correct for the correct trajectory.

The transfer time is about 258 days (0.709 years) and is calculated with equation 5.33.

$$T = \sqrt{\frac{\mu_{Sun}^3}{a}} = 0.709\ [years] \tag{5.33}$$

Since the spacecraft does not brake when reaching Mars, but uses its atmosphere to decelerates, there is no additional ΔV required during arrival.

5.3.3 Timing

In order to reach Mars precisely the timing is very important. For that reason, the orbital motions of Earth and Mars have to be modeled and analyzed. Based on the Hohmann transfer, there is a launch window of only 4 to 6 weeks. Not launching within this time frame results in a delay of the mission for 26 months. This is because the constellation of the planets is only acceptable at every 2.2 years, the so called synodic period [43] [24] [62]. The required constellation is determined and described in this subsection and a possible launch window is set.

Planet constellation

The alignment and orientation of Earth and Mars with respect to each other plays an important role for the timing of the transfer. The ideal Hohmann transfer describes a trajectory of meeting the arrival planet on the exact opposite site of the departure planet on launch date (see figure 5.16). Since the Mars orbit is inclined of about 1.85 degrees with respect to the Earth-Sun plane, there are only two intersecting points each year. Going to Mars, not considering these intersecting points as arrival point would require an additional amount of ΔV to travel along the inclination. It is assumed in this approach, that the intersection or ascending/descending node is exactly opposite Earth on departure date. That means that the spacecraft is meeting Mars right at the apogee of the Hohmann transfer. For this configuration, the transfer time and ΔV components are estimated in the transfer description subsection.

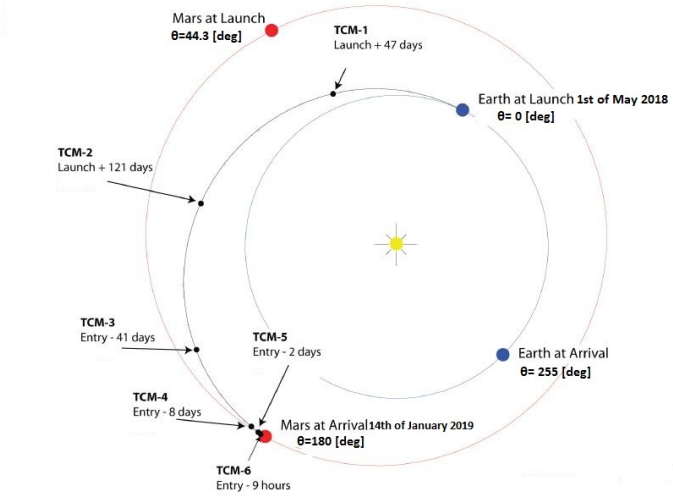

Figure 5.16: Optimal planet constellation during mission time-line

The next step is to define the required Planet constellation. The position of Earth at start date (t_0) is given as reference orientation with zero degrees. The position, i.e. degrees of Mars with respect to Earth can now be determined, knowing the transfer time. At t_1, the end of the transfer sequence it is known that Mars has to have a position of 180 degrees:

$$\theta_{Earth}(t_0) + 180\,\text{deg} = \theta_{Mars}(t1) = 180\,\text{deg} \tag{5.34}$$

The starting point of Mars can be now calculated with respect to the starting orientation of Earth.

$$\theta_{Earth}(t_1) = \theta_{Earth}(t_0) + n_{Earth} \cdot T \tag{5.35}$$

$$\theta_{Mars}(t_0) = \theta_{Mars}(t1) - n_{Mars} \cdot T \tag{5.36}$$

$$\theta_{Mars}(t_0) = 180 - n_{Mars} \cdot T \tag{5.37}$$

Where n_{Earth} and n_{Mars} is the angular velocity of Earth and Mars with 0.9856 rad/s and 0.5241 rad/s respectively. It can be concluded that Mars has to have an angle of 44.3deg with respect to Earth at start date of t_0. Only within this configuration a launch would be most optimal (see figure 5.16).

5.4 Approach

After the multi-probe bus has done its manoeuvring and is close to Mars the probes need to be released, then de-spun and their heat shield inflated.

5.4.1 Probe Release

The probes will be scattered over the area of Valles Marineris by deploying them while still in approach to Mars. The offset in space between each probe will result in two elliptical distributions due to the procedure described below. It uses two separated releases with a period of velocity reduction of the transfer module in between.

The entire phase can be described by two main procedures: *Release Procedure* and *Velocity Reduction*. The release procedure is executed twice, at the first and second probe release. The only difference between these two releases is the use of different parameter values. All steps are simulated to determine the exact parameters required to meet the landing requirements.

The two procedures are discussed below. The simulation of these procedures, including the numerical results, is elaborated upon afterwards.

Release Procedure

The release of eight probes is performed by a delicate procedure, to make sure the required scatter is met. First, the transfer-module spins up to a low rotational speed to be able to release the hull which has been covering the probes in the transfer phase. After separating the hull of the transfer module, the individual sections will slowly move away, perpendicular to the trajectory of the module itself.

To make sure the probes do not hit the parts of the hull released earlier, the hull sections will need to be accelerated parallel to the trajectory of the module as well. This can be accomplished with a two-step release, using a front and rear connection on each hull section. The sections will tilt forwards and outwards by releasing the rear connections while spinning the transfer module. The front connections will release after the section gathered some angular and linear momentum. The hull sections will then travel out of the expected path of the probes.

After the hull has been removed, the probes release mechanism is able to extend to a larger radius (figure 5.17). The mechanical clamps that have been holding the probes during launch and transfer are removed, after the magnetic clamps are activated. The release mechanism is then spun up by an electric motor. This motor will spin up the transfer module in return, as the total angular momentum of the system has to be maintained. The external thrusters will keep the module from spinning. The original spin from the transfer module, which was used to release the hull sections, can be used to spin up the release mechanism using the electric motor, reducing the required thruster fuel. At this point, the probes are spinning at their required angular velocity and still attached by the magnetic forces from the electromagnets.

The release of the probes is accurately timed to meet the requirements. After the release, the probes move perpendicular to the trajectory of the transfer module with respect to the transfer module itself. This is indicated by figure 5.18. On the left, the movement of the system just before release is shown, while the right side details the situation moments after release. The arrows indicate the velocity vectors of each probe and the angular movement of the release mechanism. It can be seen

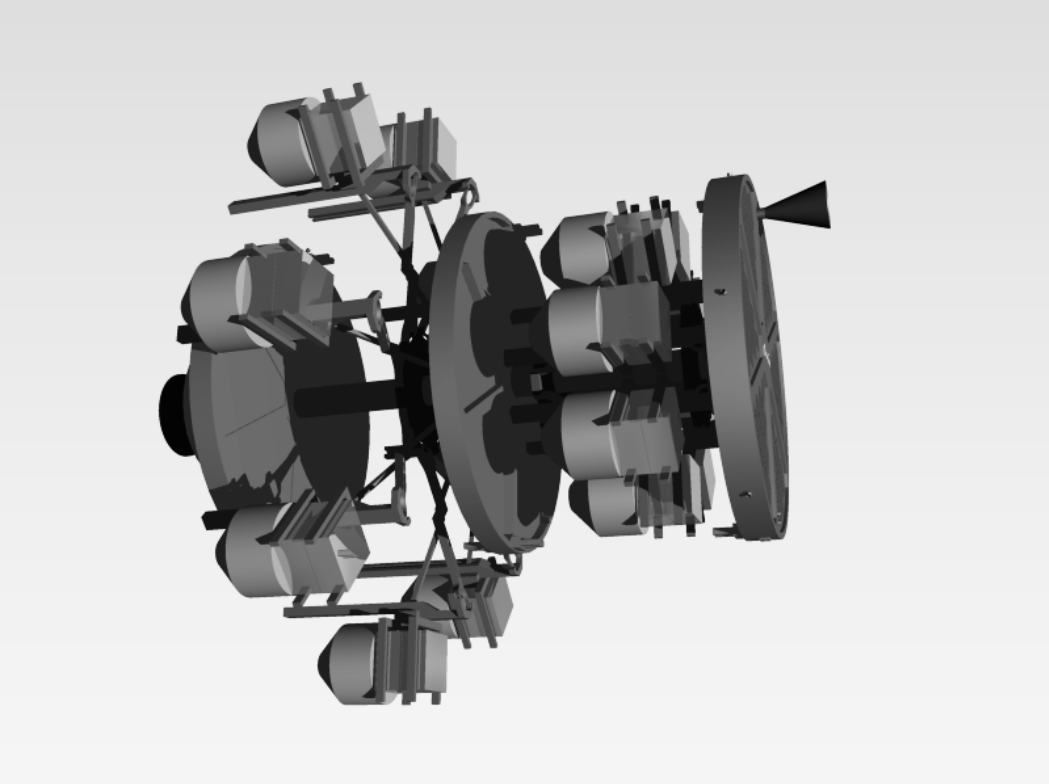

Figure 5.17: The transfer module with both a stowed and extended probe mechanism

that the instantaneous velocity during separating is maintained after release. The movement of a probe with respect to its individual clamp is shown by two lines ending with dots, which represent the moment of release and their locations afterwards. Note that the angular velocity of the probes is equal to the angular velocity of the transfer module during release. The velocity relative to Mars is the addition of the perpendicular velocity explained in figure 5.18 and the velocity of the transfer module.

Finally, the probe release mechanism retracts and the angular velocity can be reduced by regenerative breaking from the electric motor, spinning up the transfer module and charging the batteries in return.

Velocity Reduction

After the release of the first eight probes, the transfer module needs to slow down to release the second batch of probes. When the module has been stabilized, a short burn period will start, followed by stabilization of the module again. During this period the transfer module traveled an insignificant distance, but reduced its velocity enough for the second set of probes to be placed on a different location than the first.

Entry Conditions

The simulation of the two procedures is performed using several initial conditions and evaluated to meet certain requirements. The three parameters that define the starting conditions of the transfer module are its altitude from Mars, the relative velocity with respect to Mars and the angle between the velocity vector and location vector from Mars. These are listed in the first three columns of table 5.16.

The requirements are depending on the descent conditions in the Mars atmosphere and the distribution of the probes around Valles Marineris. The landing area is roughly 3,000 km wide, so the probes need to be spread over this area. The atmospheric entry requires the probes to enter with an angle between 10 to 32 degrees. These requirements are listed in the last three columns of table 5.16.

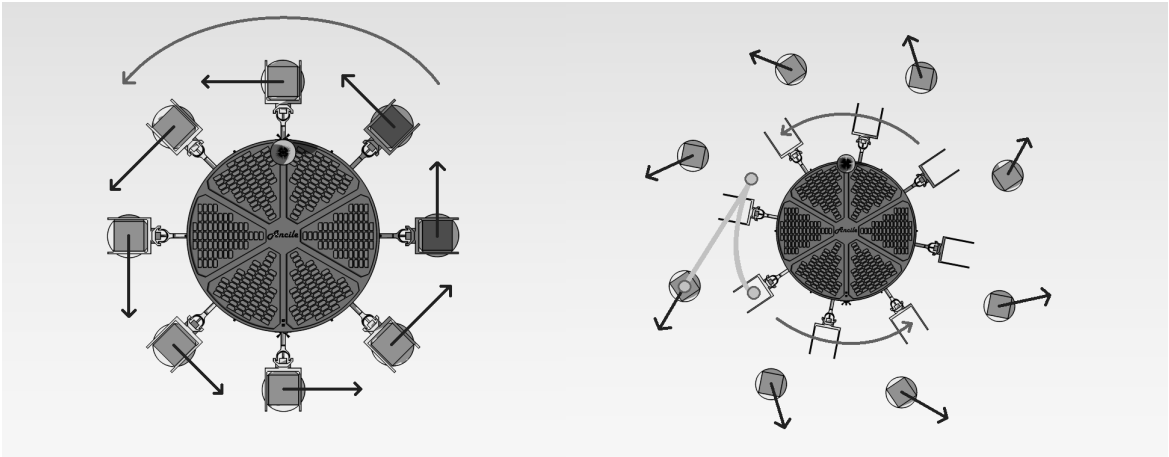

Figure 5.18: Two kinetic diagrams showing the movement of the transfer module and the probes before and after the release procedure, note the change in scale

Table 5.16: Initial conditions and requirements for release procedure

Initial conditions			**Requirements**		
Parameter	Unit	Value	Parameter	Unit	Value
Altitude	km	$5.8 \cdot 10^6$	Landing Area	km	2,900-3,100
Approach velocity	km/s	2.65	Entry Angle	deg	10-32
Approach angle	deg	0.80			

Numerical Simulation Results

The parameters that are required to define the approach and the release procedures are calculated using a simulation. The simulation calculates the trajectory of the transfer module when it enters the sphere of influence of Mars (figure 5.25). The sphere of influence is a virtual sphere around Mars where at the surface the gravitational acceleration of Mars is equal to the Sun's in magnitude. The simulation assumes Mars to be stationary and the transfer module to approach at the end conditions of the Hohmann transfer, see table 5.16. The steps taken in the simulation will be discussed in turn below. The values that are derived from the simulation are summarized in table 5.17.

By spinning up the first set of probes to 10 rotations per minute, the probes travel in circles of 3.5 m diameter, with a velocity of 1.83 m/s. Using a three-dimensional model, the polar moment of inertia is used to calculate the angular kinetic energy of the system. This was found to be equal to 1649 J. The probes are released at a distance of 310,000 km to the center of Mars, to meet the requirements on landing area and entry angles. The simulation shows the probe's extreme cases, where one extreme is the probe that is accelerated away from Mars and the other extreme is the opposite, shot in the direction of Mars. These probes will have the lowest and highest entry angles respectively. The other probes will enter with angles within this range.

The velocity reduction is visible as a continuous deceleration during the burn time of 360 s. It is preceded and succeeded by a short phase of loitering where the transfer module stabilizes and orientates, 60 s each. The reduction in velocity of 80 m/s causes the second set of probes to arrive approximately 90 minutes after the first set, utilizing the rotation of Mars to generate more distance between the first and second set (figure 5.26).

The second release of probes is performed with a higher rotational speed of 15 rotations per minute. Although the second set of probes has more time to generate an offset, they enter at steeper angles. Steeper angles cause the projection of the probes' trajectory to be more circular than elliptical and therefore less wide. Higher rotational speed compensates for these steeper angles, in terms of distance

Table 5.17: Approach parameter summary

Parameter	Unit	Value
First Release		
Center distance	km	310,000
rpm	#/min	10
Radius	m	1.75
Angular kinetic energy	J	1649
Release velocity	m/s	1.83
Velocity Reduction		
Velocity reduction	m/s	80
Burn time	s	360
Pre-burn loiter	s	60
Aft-burn loiter	s	60
Second Release		
Center distance	km	298,940
rpm	#/min	15
Radius	m	1.75
Angular kinetic energy	J	3701
Release velocity	m/s	2.75
Entry		
First probes spread	km	1265
Second probes spread	km	1351
Total spread	km	2989
Entry angle min.	deg	10.8
Entry angle max.	deg	29.0
Probes		
Time in space max.	hr	36
Arrival delay	min	89

on the Martian surface (figure 5.27). The probes are released at a velocity of 2.75 m/s. The system has a total angular kinetic energy of 3701 J.

The entry angles of the four probes modeled range from 10.8 to 29.0 degrees. The first set of probes lands over an area 1265 km wide and the second set distributes over 1351 km (figure 5.28). As these two ellipses are placed next to each other, the total area is covered by two circles, in total 2989 km wide. During the approach, the probes have been in space for 36 hours maximum, arriving in a time window of 89 minutes.

Model Verification

The simulation is performed by a model based on the gravitational acceleration of Mars, backed up by an atmospheric analysis when the probes reach the atmosphere. The calculations performed, involving the equations used, are discussed below.

The main calculation involves a discrete representation of a point object in a gravitational field. The time step is the variable which drives the accuracy of this representation. The results discussed in the previous sections are calculated with a time step of 0.1 seconds. For most of the approach, this is more than accurate, as the entire approach lasts for almost two days. The events in which 0.1 s is a larger fraction of the duration of the event, accuracy could be an issue. However, the results of the simulation stabilized and converged to a result at time steps higher than five seconds. This verifies the use of 0.1 s as the common time step.

The equation used to update a coordinate of the location of the point mass over time is given by equation 5.4.1. The variable x as the coordinate can be interchanged if needed.

$$x_n = x_{n-1} + \left(\frac{dx}{dt}\right)_n \cdot dt + \frac{1}{2}\left(\frac{d^2x}{dt^2}\right)_n \cdot dt^2 \tag{5.38}$$

For the procedure to work, the first and second derivatives of the coordinate need to be evaluated. The second derivative is the component of the gravitational acceleration of Mars to this coordinate. It is calculated using equation 5.4.1. The angle between the position vector from Mars to the point mass and the reference frame is θ. The product of the gravitational constant G and the mass of Mars M_{mars} is a constant. Like equation 5.4.1, the variable x can be interchanged, by implementing *sin* instead of *cos*.

$$\left(\frac{d^2x}{dt^2}\right)_n = cos(\theta_n)\frac{G \cdot M_{mars}}{\sqrt{x_{n-1}^2 + y_{n-1}^2}} \tag{5.39}$$

A method to determine the first derivative of the coordinate is given by equation 5.4.1. As a variable dependent on the previous value of the variable itself, it uses a simple update by adding the acceleration over the time step.

$$\left(\frac{dx}{dt}\right)_n = \left(\frac{dx}{dt}\right)_{n-1} + \left(\frac{d^2x}{dt^2}\right)_n \cdot dt \tag{5.40}$$

The atmospheric analysis of the probes and their final location is performed using a separate model, which is discussed in section 5.5. The verification of the remainder of the approach model is omitted, as it involves no differential analysis but static calculations.

Release Sensitivity

The use of passive probes during release simplifies the design and thereby reduces the risks of failure. However, the release mechanism on the transfer module is solely responsible for the proper spread of the probes on the surface of Mars. The deviation from the planned rotational speeds or release times can be of influence to this spread. This sensitivity to unplanned disturbances is analyzed in this section.

By deviating the conditions of release in the model that is used for the simulation, the resulting disturbances can be found. The change in total landing area due to changes in angular velocity and release timing is given in figures 5.19, 5.20 and 5.21. It shows that the landing area requirement of table 5.16 is met within a wide range of deviations.

The influences on the entry angle due to deviations in angular velocity and release timing are shown in figures 5.22, 5.23 and 5.24. The entry angles are less sensitive to these effects and will remain within the range of the requirements.

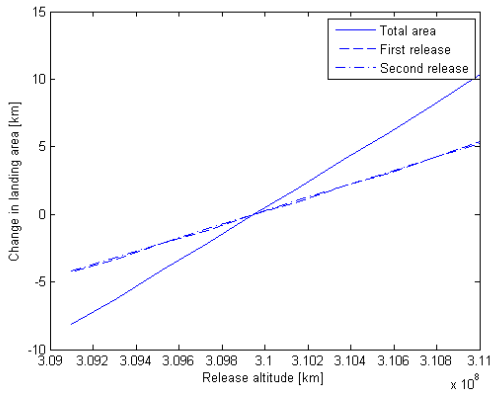

Figure 5.19: Influence of release timing on landing area

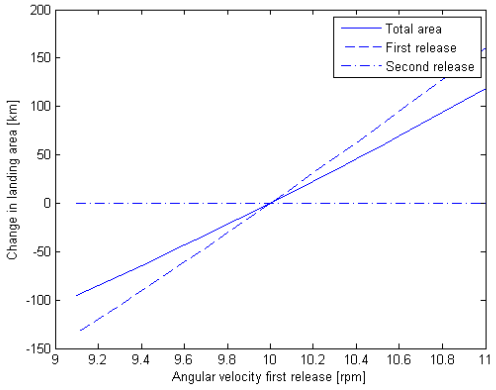

Figure 5.20: Influence of first release angular velocity on landing area

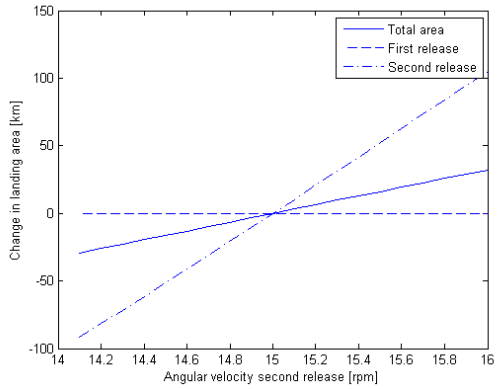

Figure 5.21: Influence of second release angular velocity on landing area

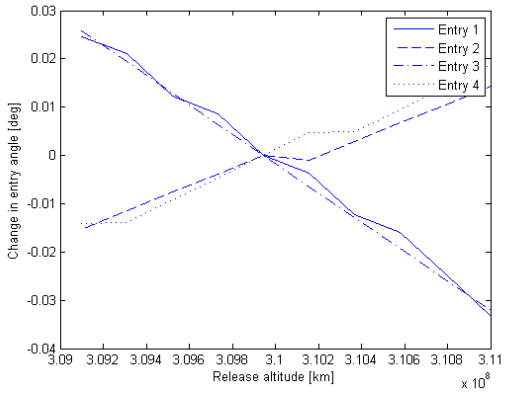

Figure 5.22: Influence of release timing on entry angles

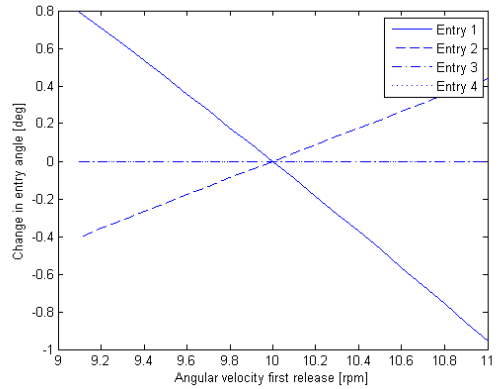

Figure 5.23: Influence of first release angular velocity on entry angles

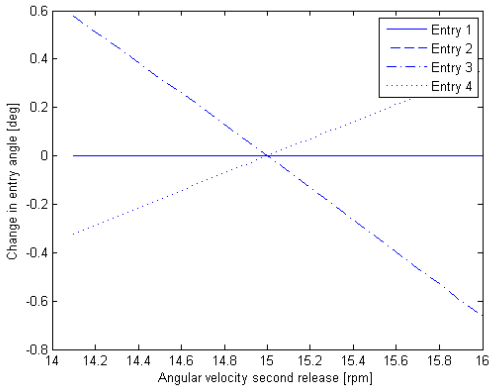

Figure 5.24: Influence of second release angular velocity on entry angles

5.4.2 De-spinning

At this point the probes are individually traveling towards Mars. The first set of probes is spinning at a rate of 10 rpm. The second set of probes are released at a later time and will spin at 15 rpm. The spinning rate needs to be decreased before entering the atmosphere. Spinning at such a high rate will cause problems when releasing the parachute, the wires would entangle. Thus a de-spinning mechanism needs to be developed. In the following the simulation that was constructed, to design this mechanism, is explained and the final outcomes are presented. All information and calculations that were used, were gathered and taken from Nasa's technical notes on the "Analytical theory of the strech YoYo for de-spin of satellites" [51] and [41].

There are different de-spinning mechanisms like *De-spin thrusters* or *YoYos*. A YoYo is a principle using a wire and a mass which will be deployed and due to increasing the polar moment of inertia decreasing the spinning rate. De-spin booster are small boosters slowing the spinning rate by counter-thrust. The disadvantage of such De-spin booster in comparison to a YoYo is that extra propellant will be needed. For this design YoYos were chosen as the de-spinning system for the probes. The structure of a YoYo consists of a wire, a mass and some attaching device.

There are two types of YoYos, *ridged YoYos* and *stretch YoYos*. Solid de-spinning systems were used frequently in the past. After researching how to increase the performance of ridged YoYos it was found that stretch YoYos are having a higher de-spinning performance. Stretch YoYos are YoYos where a spring is added to the structure. The spring adds extra length to the structure when released.

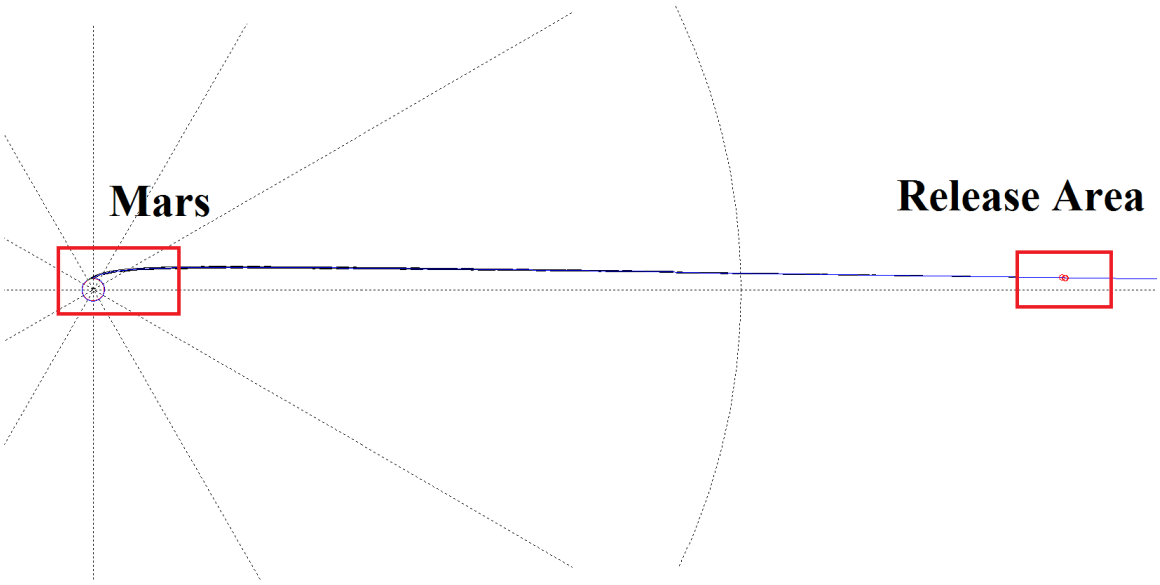

Figure 5.25: An overview of the approach trajectory inside the sphere of influence

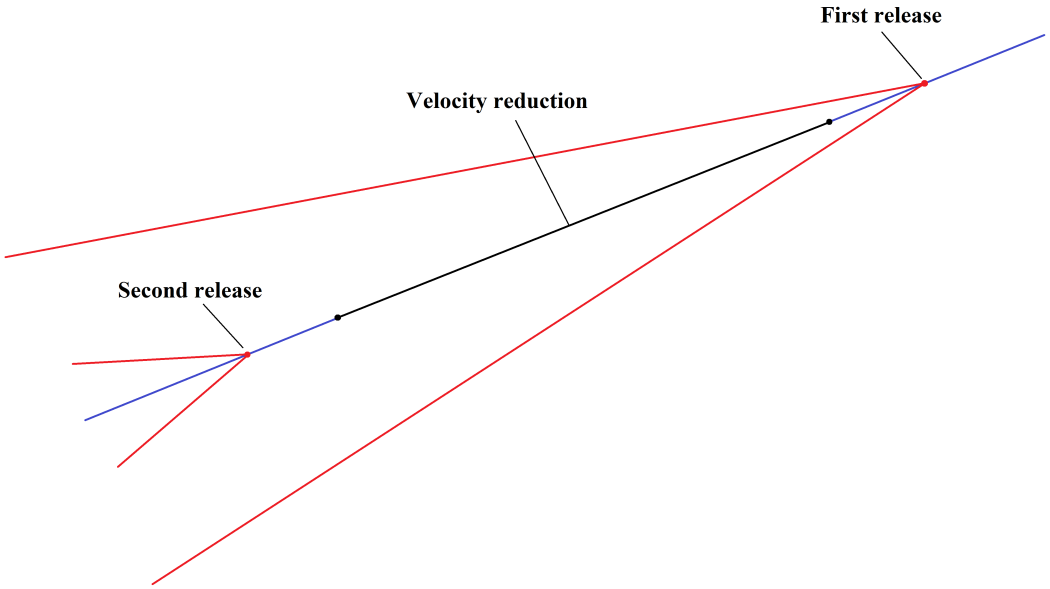

Figure 5.26: The trajectories of the transfer module and probes during the release phase, not to scale

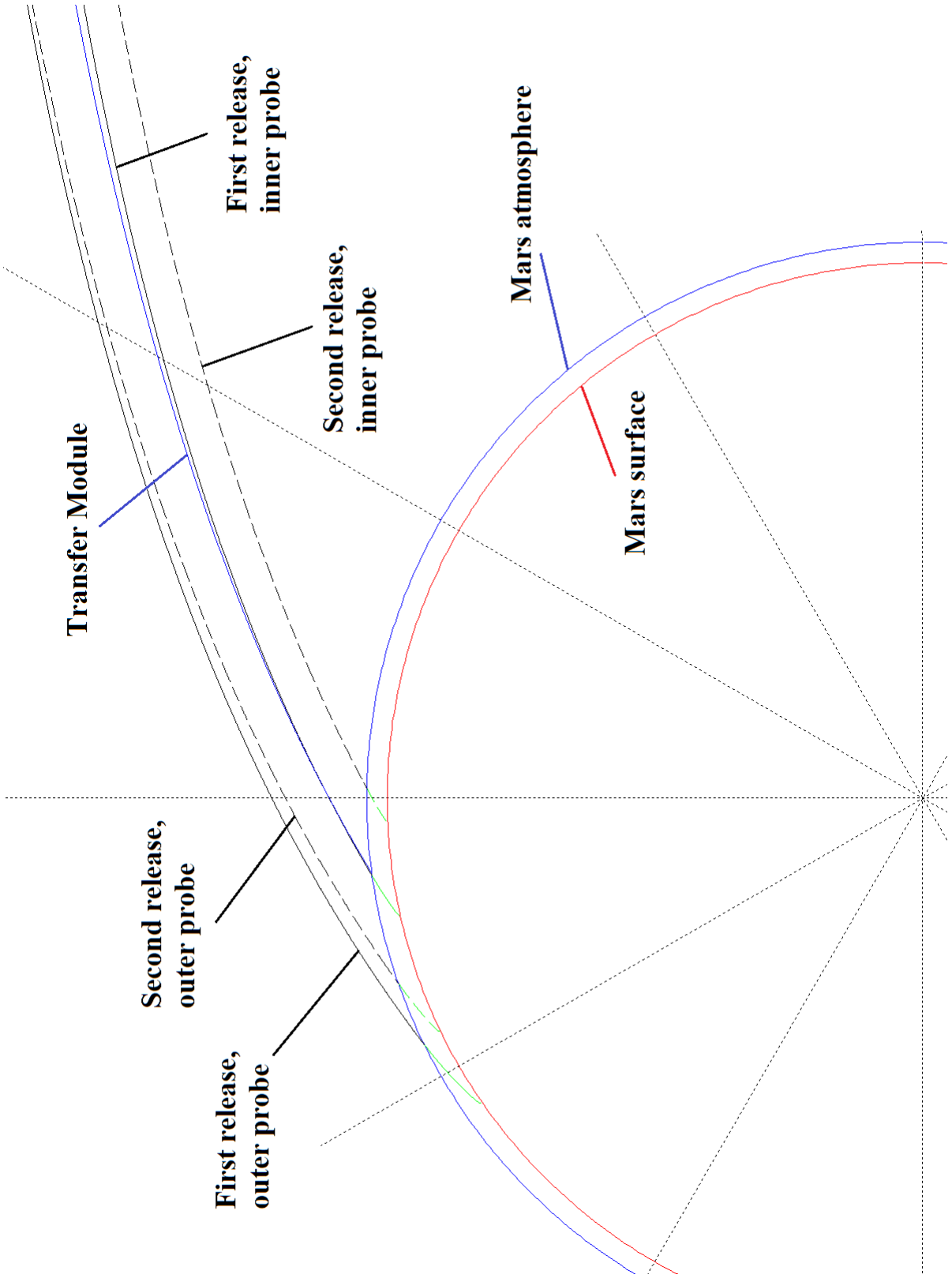

Figure 5.27: The individual probe trajectories during the entry in the atmosphere of Mars

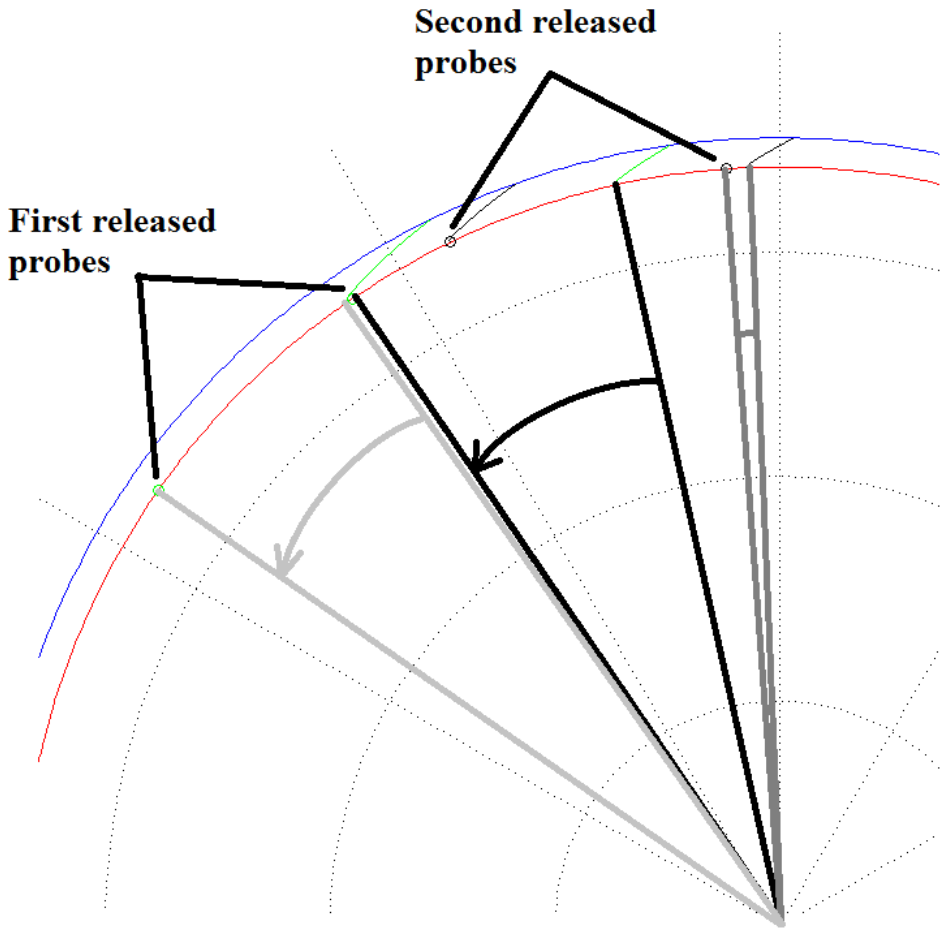

Figure 5.28: The landing area of the probes, including the rotational drift on the surface of Mars due to their different arrival times

In this design stretch YoYos will be used. A typical structure of a strech YoYo can be seen in figure 5.29. The stretch YoYo will be attached to two walls of the instrument box. The wire and spring will be rolled up on a small reel. At the end of the spring a small mass will be attached. When the mass gets released, it will be accelerated to the outside, which will result in deceleration.

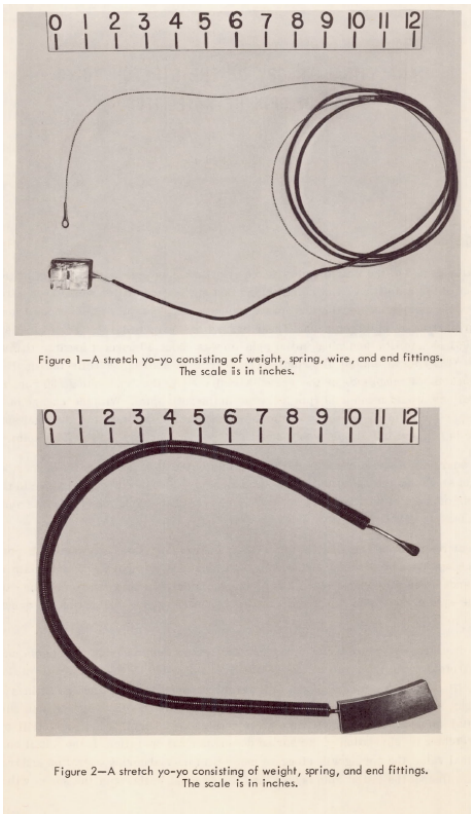

Figure 5.29: Typical designs of stretch YoYos [41]

Polar Moment of Inertia

In order to find the optimal size and design of a stretch Yoyo the polar moment of inertia (MOI) of the probe needs to be known. The dimensions of the probe can be found in figure 4.21. The probe is rotating about its longitudinal axis, which is referred to as the x-axis in this analysis.

In order to find MOI of the probe, the center of gravity will have to be computed first. Knowing the structure rotates about the x-axis and assuming symmetry about it, the *cog* will lie on the x-axis. Each part was separated and looked at individually when evaluating the MOI. This was done due to the different shapes of each sub part of the probe. The lander was divided into the following sub parts: inflatable heat shield, cone, outer crushable structure, tube, inner crushable structure, seismometer, instrument box and parachute.

Inflatable heat shield

The inflatable heat shield is 35 cm in diameter and as a height of 25 cm. The shape of the structure needs to be estimated between a hemisphere and a cone. A drawing of the heat shield, including the shapes to estimate the MOI is found in figure 5.30.

From figure 5.30 it can be seen that, taking the MOI of the average of, a hemisphere with a diameter of 46 cm and the cone of diameter 35 cm, will lead to a close approximation of the actual MOI contribution of the heat shield. The formula used for the contribution calculation was equation 5.41

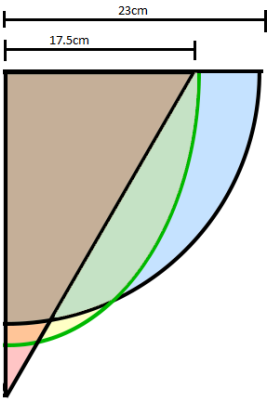

Figure 5.30: Estimation for the MOI for the heat shield

$$I_{heatshield} = \frac{\frac{2}{5}\ M_{heatshield}\ r^2_{heatshield} + \frac{3}{10}\ M_{heatshield}\ r^2_{cone}}{2} \tag{5.41}$$

Cone

The con of the lander is a solid cone with a height and diameter of 15 cm respectively and a mass of 17.76 kg. The MOI of the cone can be computed from formula 5.42

$$I_{cone} = \frac{3}{10}\ M_{cone}\ r^2_{cone} \tag{5.42}$$

Outer crushable structure

The outer crushable structure with a mass of 1.99 kg is 30 cm high, the outside of the crushable structure has the exact same parameters as the instrument box, whereas the inner side of the structure follows the arc of the cylinder of the penetrator. This can be seen in figure 5.43:

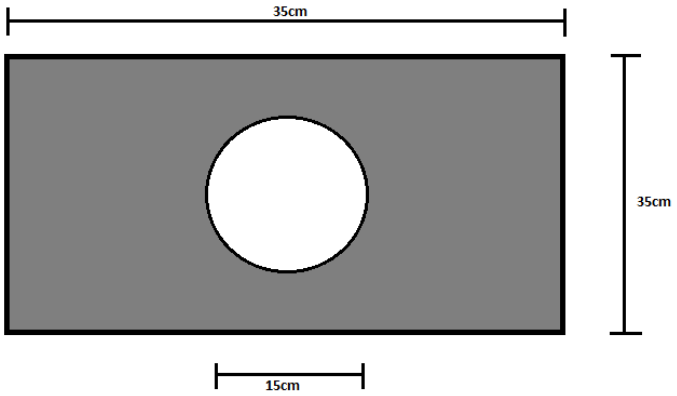

Figure 5.31: Top view of the outer crushables

In order to find the contribution of the outer crushable structure formula 5.43 was used:

$$I_{outercrush} = \frac{1}{12}\ (M_{outercrush} * M_{cylinder} * M_{seismo} * M_{inner\ crush})(a^2 + b^2) - \frac{1}{2}(M_{cylinder} * M_{seismo} * M_{inner\ crush})(r^2_{cone}) \tag{5.43}$$

Tube, Seismometer, Inner crushables

The penetrator consists of a tube with a wall thickness of 2.5 cm and a mass of 77.73 kg. Within the penetrator the seismometer and the inner crushable structure can be found. Their contribution to the MOI was found from formula 5.44, formula 5.45 and 5.46 respectively.

$$I_{tube} = \frac{1}{2}\, M_{tube}(r^2_{outer\ diameter} + r^2_{inner\ diameter}); \tag{5.44}$$

$$I_{seis} = \frac{1}{2}\, M_{seis}\, r^2_{seis} \tag{5.45}$$

$$I_{innercrush} = \frac{1}{2}\, M_{inner\ crush}\, r^2_{inner\ crush} \tag{5.46}$$

Instrumentation box

The instrumentation box is a box of length 35 cm, width 35 cm and height 15 cm. The MOI of the box can be computed from equation 5.47

$$I_{ib} = \frac{1}{12}\, M_{ib}(a^2 + b^2) \tag{5.47}$$

Parachute

The parachute, on top of the lander, is in a box of 35 cm length and 35 cm width. Here again, the formula for the MOI of a box can be used to find the contribution of the parachute. The contrribution was found from formula 5.48.

$$I_{para} = \frac{1}{12}\, M_{para}\, (a^2 + b^2) \tag{5.48}$$

Polar moment of inertia

Having found all the contributions of each sub part of the structure individually, they were then added up together to find the final polar moment of inertia from formula 5.49

$$I_{PMOI} = I_{heatshield} + I_{cone} + I_{outer\ crush} + I_{tube} + I_{inner\ crush} + I_{seis} + I_{ib} + I_{para} \tag{5.49}$$

The stretch YoYo

The exact mass contribution of the structure has been found,after which the dimensions of the stretch YoYo can be computed. First of all it it needs to be known how much the probe should be de-spun. De-spinning of the probe can not be done entirely but it should be de-spun to a major extend. Hereby attention needs to be paid that the probe will have such a slow rotational rate, that when the parachute is deployed, during the EDL, the wires are not entangling. Here the probe is being slowed to a rotational rate of 0.1 rpm. At 0.1 rpm the probe will turn approximately 60deg over the whole parachute phase. This is expected to be acceptable. Thus the desired spin reduction factor can be computed from formula 5.50.

$$r = \frac{\dot{\phi}_2}{\dot{\phi}_0} \tag{5.50}$$

Where $\dot{\phi}_2$ and $\dot{\phi}_0$ are the final spin rate and initial spin rate respectively.

Having found the de-spin factor, the actual elongation of the spring gets computed. The elongation is important to be known because it increases the de-spinning, dependent on how far it elongates. This, so called spin reduction stretch, can be evaluated from equation 5.51

$$\delta = \frac{r(l_0 + a_{probe})}{1 - r} \tag{5.51}$$

Where a_{probe}=17.5cm is the radius of the probe and l_0=2m is the initial length of the *stretch YoYo*.

Now the actual length of the construction at release can be evaluated from formula 5.52

$$l = l_0 + \delta \tag{5.52}$$

Having found the spin reduction factor, the length at release, the spin reduction stretch, knowing the MOI of the structure and knowing the radius of the probe(24.75 cm), the total mass can be computed from equation 5.53

$$M_{total} = \frac{I\ (1-r)}{(l + a_{probe})^2} \tag{5.53}$$

The radius of (24.75 cm) is based on the fact that, when the *stretch YoYo* is released it will act at the corners of the box. Thus it acts at one half of the diagonal of the box.

Spring mass

In order to find the weight contribution of the spring and its mass, the material of the spring needs to be determined. In this design *NS355 spring steel* was the material of choice, which has been used in other stretch YoYo applications. The material properties needed for the calculation of the spring weight are: The shear modulus of elasticity, the density, the mean helix radius and the wire diameter. Their values are listed below:

$$G = 7.92902 * 10^3\ [MPa] \tag{5.54}$$

$$rho = 7805.73\ \left[\frac{kg}{m^3}\right] \tag{5.55}$$

$$R_{helix} = 4.7625 * 10^(-3)\ [m] \tag{5.56}$$

$$d_{wire} = 1.5875 * 10^(-3)\ [m] \tag{5.57}$$

The spring constant is another important value that needs to be found in order to compute the actual weight and length of the spring. The spring constant is found from formula 5.58

$$k = \frac{\dot{\phi_2}^2 (1-r^3) I}{2\ r\ (l_0 + a_{probe})^2} \tag{5.58}$$

The forces that will act on the spring will be computed by equation 5.59

$$f = k\ \delta \tag{5.59}$$

The mass of the spring can then be found from equation 5.60

$$m_{spring} = \frac{G\ \rho\ \pi^2}{128\ k\ \left(\frac{R_{helix}}{d^3_{wire}}\right)^2} \tag{5.60}$$

Mass of the weight

From research it was found that the contribution of the weight of the spring and the mass attached to it, to the total mass of a stretch YoYo system, are 2/3 and and 2. Thus from formula 5.61

$$m_{total} = 2m_{mass} + \frac{2}{3} m_{spring} \tag{5.61}$$

Rearranging leads to the weight of the mass

$$m_{mass} = \frac{m_{total}}{2} - \frac{m_{spring}}{3} \tag{5.62}$$

Table 5.18: Structure Dimensions

length	35 cm
height	3 cm
width	3 cm

Concluding

From the model the dimension for the different spin-rates, of the two sets of probes, were found. Each probe will have two stretch YoYos attached at opposite sides of the instrument box. The primarily released probes, spinning at 10 rpm, will have a stretch YoYo with a spring length of 2 m and a mass attached to it of 0.2663 kg. The total system will weigh 0.5325 kg. The secondly released probes will have an initial spin rate of 15 rpm . They will have a spring length of 2 m and a mass attached to it of 0.2690 kg. The total system will weigh 0.5379 kg.

Dimensions of the reel

The spin and mass will be wound-up on a reel, that then is attached to two, opposite sides of the instrument box. The dimensions of the instrument box are 35 X 35 X 15 cm. The reel can thus have a maximum length of 35 cm and it may not extend 15 cm in height,which is the height of the box. The spring has a radius helix of 4.6 mm. Taking the reel to be 35 cm long and with a diameter of 10 cm, the spacing of the spring and mass onto the reel can be calculated. The amount of times the spring can be wounded around the reel can be calculated with equation 5.63

$$spacing = \frac{l_{reel}}{r_{helix}} \tag{5.63}$$

Thus the length of the spring that can be wounded around the length of the reel is found from formula 5.64

$$l_{wire\ on\ reel} = spacing * 2 * \pi * r \tag{5.64}$$

Where 2π r is the circumference.

The 2 m long spring can be wound around it at once. The dimensions of the structure attached to the box can be found in table 5.4.2.
The total design of the reel onto the instrument box, including the stretch YoYo, can be seen in drawing 5.32. Hereby only the instrument box is seen, not the whole probe. The mass at the end of the spring is colored in red.

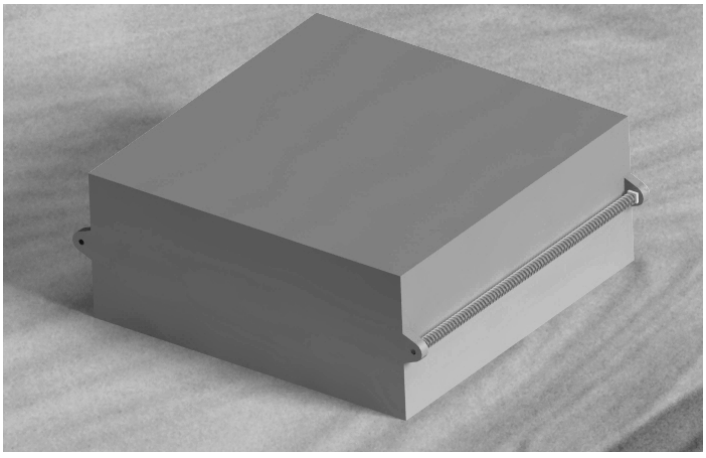

Figure 5.32: The instrument box including its de-spinning mechanism

5.4.3 Inflation of heat shield

After the probes have been despinned to nearly zero rpm, they need to inflate the heat shield before entering into the atmosphere. 100 s is budgeted to account for complete inflation, however an additional 40 s should be added for safety, leading to 140 s [58]. This means that the probe should be totally inflated before being at least 130 km above the surface of Mars. Again including a safety margin here, means that the probe should be inflated before being 200 km above the surface of Mars. The Aero-shells toroids are filled with Nitrogen which is being stored in the instrument box and released through inflation lines to the inflation system. Initially the Nitrogen tank will be kept at 207 Bar, with one control Valve leading to the inflation system [58]. The layout of the probe with the heat shield inflated can be seen in figure 5.33
The choice of this heat shield will be discussed in more detail in section 5.5.

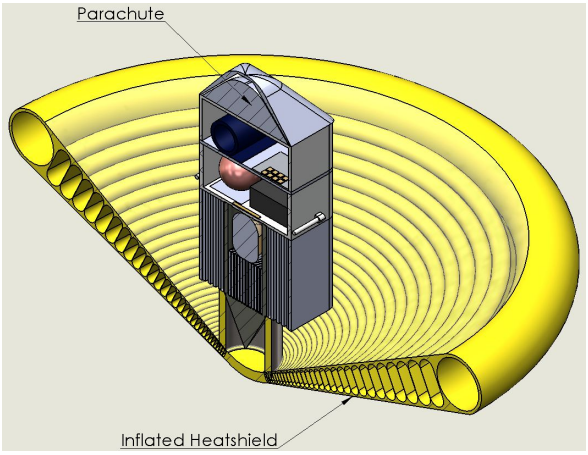

Figure 5.33: Probe with inflated heat shield

5.5 Entry, Descent and Landing

To land probes on the surface of Mars they first need to pass through the Martian atmosphere. The entry, descend and landing(EDL) procedure is often seen as the most critical part of a space mission and thus needs to be designed carefully. First of all the different subsystems of the EDL will be discussed, then the entry conditions will be stated. Thirdly the trajectory of the probe(s) is calculated, then the trajectory is optimized and the surface entry conditions are stated and finally the whole landing procedure is discussed.

5.5.1 Subsystems

The EDL consist of different subsystems that provide thermal control and stability and decelerate the probes. The most important subsystem is the heat shield, which has a large influence on the Ballistic coefficient(BC) and thus the impact velocity. A heat shield can be either solid or inflatable. Another important system is the parachute which will be triggered by an accelerometer. Also for the landing, a crushable structure needs to be designed in order too protect the instruments from to high g-loads. This structure will influence the EDL to a great extent, because it is closely correlated to the impact velocity and the angle at which the probe can enter the surface.

Heat-shield

The heat shield protects the lander from the extensive heat-loading during entry phase. Based on the shape and size of the entry vehicle high temperatures will occur while decelerating in the Martian atmosphere and so a heat shield is needed for thermal control. There are two main types of heat shields: solid or inflatable. Both will be evaluated in terms of applicability for this mission. However, either an inflatable or solid heat-shield will need to have a 70°cone shape, because this makes the probe statically stable and is a proven shape for entering into the Mars atmosphere.

- **Solid Heat-shield**
  In industry, solid heat shields are most commonly applied for thermal protection. The most widely used and accepted is an ablative heat shield, which burns away during descent. Another type of solid heat shield is a heat-sink, which is generally very heavy. Since the entry mass needs to be minimized in order to minimize the Ballistic Coefficient (BC), which is explained in the following subsection, a heat-sink is not a viable option. Also when looking at literature, it can be seen that every previous Mars mission performed by NASA had an ablative heat-shield [23]. The ablative heat-shields have been used and tested extensively until now. The material differs with different heat-shield designs. For this mission, the ablator applied for the Mars exploration Rover is used as reference [44]. It was invented for the Viking mission in 1970 and used in Mercury, Gemini and Apollo programs extensively [23]. The material consists of cork wood, silica, and phenolic micro spheres in a silicone binder, reinforced by a phenolic honeycomb [44]. The term ablative refers to the procedure that occurs during entry-phase: The outer layer of the surface melts and vaporizes, absorbing all substantial thermal energy. In order to calculate the total mass of the ablator, the reference heat-shield is scaled to the size of the probe characteristics. Regarding the Mars Exploration Rover, the heat shield is estimated to be 2.65 m in diameter, leading to a total Area of 5.5 m^2 and a mass of 78 kg [66]. Using a 70 degree cone that is needed for stability, and a diameter of 2.2 m, this leads to an area of 3.14 m^2. Scaling the mass of Mars Exploration Rover results into a total mass of 65 kg. The diameter is determined using a Matlab module that simulates the entry phase, which is discussed in section 5.5.3. The dimensions affect the aerodynamic properties and therefore the Ballistic coefficient, stability and physical loadings.

- **Inflatable Heat-shield**
  Investigating the possibility of inflatable heat shields already began in the seventies for the Viking mission. However, parachutes were back then considered the safer option and development came to a halt. Over recent years NASA started testing and developing inflatable decelerators again, with the IRVE 1, 2 and 3. IRVE-2 showed that an inflatable heat shield with a 60°cone was stable while decelerating into the atmosphere [58], while IRVE-3 showed that it will be stable during descent even with a higher heat peak rate [57] [33]. The main advantage of an inflatable heat shield over a solid one is weight. Using the same weight, the diameter of the inflatable can be many times bigger than the solid one, leading to a much lower peak deceleration and a lower impact velocity [81]. NASA plans to one day land humans on Mars using this very technique.
  Inflatable decelerators are however still in a testing phase and will lead to a high development and testing cost. For this mission, the inflatable heat shield will be based on the IRVE-3. The material lay up of the inflatable consist of three main layers: a thermal protection layer with Nextel 312 AF-14 and Kapton, a structural layer consisting of uncoated and Silicone coated Kevlar, and again a thermal protection layer with Kapton and Nextel 312 AF-14. The inner shells will have thicker Silicone coated Kevlar layers than the outer shells. Also the structure will be inflated by Nitrogen upto 0.2 Bar [57]. The weight of IRVE-3 was however hard to find, and only a total weight of 250 kg could be found [33]. Therefore the weight of the inflatable decelerator will be based on a different study of inflatable aerodynamic decelerators or IAD's. For a diameter of 7.5 m an IAD, structure, gas and inflation system included, weighs 71.1 kg [81]. Scaling this for a diameter of 2.2 m, leads to a weight of only 21 kg. The gas and inflation system together weigh 3 kg, leading to a weight of around 18 kg for the inflatable only, which is many times lighter than the ablative.

- **Trade-off and final heat-shield design**
  The weight of the probe without any EDL system equals 97 kg which is already pretty heavy, especially because of its small diameter of around 0.4 m. In order to bring the entry velocity of 5600 m/s back to 90 m/s at touchdown, the heat shield will need to be many times bigger than the diameter of the probe. This is very inconvenient for a solid heat shield but easily achievable for an inflatable heat shield. Also the lower weight of the inflatable will lead to a lower BC, which is preferred. It is thus obvious that the inflatable heat shield is the most viable option for this mission.
  The problem however is that it needs to be deployed before entering the atmosphere and thus needs to be packed on top or around the probe at the moment the probe is released from the bus. Again, scaling the not inflated volume of the inflatable to the IRVE-3, a volume of 0.03 m^3

is needed [33]. Having a probe where the largest diameter is that of the instrument box, which equals around 0.4 m, the inflatable will be packed 0.20 m on top of the crushable structure and widen the diameter around the penetrator to 5 m as can be seen in figure 5.34. But not only the inflatable needs to be packed on top of the probe, the gas tank and inflation systems also needs to be incorporated into the probe design. Since a gas tank is already present in the probe design to roll out the flexible solar panels, the volume of the instrument box will not be altered much. Again scaling the Nitrogen tank to the IRVE-3, a spherical tank with 13.5 cm diameter will be needed to inflate the heat shield and roll-out the solar panels [33]. The inflation system with pressure transducers, flow meters, regulators and control valves will be positioned between the penetrator and attached to the tip of the inflatable, with inflation lines going to the different departments of the aeroshell, but also one leading from the box to the inflation system. This inflation line will go through the crushable structure to connect the pressure tank with the inflation system.

Parachute

Every previous mission that was launched to Mars decelerated using an ablative heat shield and a parachute. The parachutes that have been used upto the Mars Curiosity mission, were all based on those tested for the Viking mission [23]. But why would the probes need an additional decelerator? Could the inflatable decelerator not be made large enough to ensure a landing velocity of 90 m/s? Well, it's a trade-off between weight and the angle of entry in the surface. Using only an inflatable will have the probe entering the surface at much steeper angles than when it is used in combination with a parachute. Furthermore an inflatable decelerator weighs much more and takes up much more space. Using the simulation that will be described later in this chapter, a parachute with a C_D of 0.41 needs a diameter of 4 m [23].
The parachute needs to be packed on top of the probe, which is opposite to the side where the inflatable is packed. It will be packed behind a shell which will open and a mortar will release the parachute when the accelerometer triggers the mechanism. The parachute will also take the shell off the solar panels and antenna. A chord will connect the probe to the shell, which is connected to the parachute. Using the Mars Viking parachute, the weight of disk-gap-band parachute with chord and mortar can be found to be around 10 kg. The parachute in the Viking was packed to a density of 640 kg/m^3, which leads to a volume of 0.015 m^3 [19]. Again using the diameter of the box to be around 0.4 m, the parachute box will extend the probe another 15 cm as can be seen in figure 5.34.

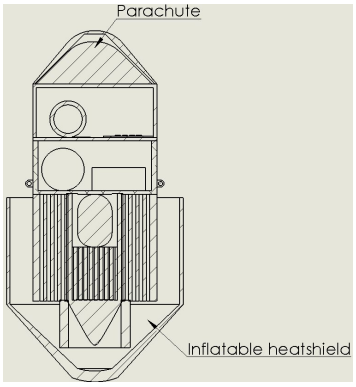

Figure 5.34: Packed probe

5.5.2 Entry Conditions

The entry conditions depend on the trajectory of the multi-probe bus. The bus is on a Hohmann-like transfer, from which the entry angle and velocity can be calculated. More specifically, it is on a direct orbit to Mars, meaning that it won't need additional ΔV to put it in an orbit around Mars. This means that the entry angle and speed directly follow from the transfer chosen. However the entry conditions need to be designed for descending into the atmosphere and not based on the trajectory. This means that the trajectory will be altered to comply with the entry conditions.

Every spacecraft that enters an atmosphere has an entry corridor [40]. Meaning that when the spacecraft goes beyond the borders of this corridor, the mission will fail. The entry angle and speed are closely correlated when looking at an entry corridor. These two values are also dependent on the kind of entry that the vehicle will perform. An entry vehicle can either perform a ballistic, lifting or skipping entry [76].
A ballistic entry is the most straightforward and easy of the three, but also is the least controllable together with the skipping entry. This means that the moment it enters the atmosphere, no more adjustments to its trajectory can be made other than with a propulsion system. This type of entry will thus have a very large landing footprint, ranging to hundreds of kilometres.
A lifting entry is more difficult than a ballistic entry, since the entry vehicle will also generate lift to extend its time in the atmosphere and slow down more for a soft landing. A lifting entry has a much smaller landing footprint ranging to tens of kilometres.
A skipping entry is the most difficult since it needs to skip once or multiple times on the atmosphere before performing either a ballistic or lifting entry. This will however slow down the vehicle and will allow softer landing for higher masses, but because of the dynamic atmosphere of Mars this is very hard to design and will lead to a huge landing footprint.

Since the probes designed for this mission will have a high impact velocity, a gliding entry is not necessary. Also since the EDL is such a critical part of the mission, it should be kept as simple as possible. Thus a ballistic entry is the preferred entry for this mission.
The faster the entry vehicle enters the atmosphere the more heat will be generated and the higher the impact speed. A steeper entry angle will have the same effects on the deceleration and landing. The upper limit of both entry velocity and entry angle are defined by the impact speed and the peak heat the heat shield can cope with. Since the probe are to land with a velocity of around 90 m/s to penetrate the ground deep enough and the inflatable heat shield can cope with temperatures up to 1260°, the upper limits can be easily simulated [47].
The lower limit of the entry angle and velocity is a bit harder to calculate and simulate. The upper limit for the angle is described by the entry angle and velocity at which the entry vehicle will skip back out of the atmosphere. The lower limit of the entry corridor will be based on previous missions, since the upper limit will constrain the probes the most and will be different from previous missions(higher impact velocity).
A large amount of Mars missions were all based on the Viking mission, which performed a ballistic entry with a 70°cone heat shield. They all entered the atmosphere with an angle between -11 and -17/degree and a velocity between 4.7 and 7.3 km/s [23]. The entry velocity will however only change marginally when altering the orbit for a different entry corridor and can thus be assumed constant and equal to 5.6 km/s. The lower limit of the entry angle will become -10°based on literature and the upper limit will follow from further simulation [23].
However, the probes need to land in a specific area around *Valles Marineris* and thus not only the entry angle and entry velocity will influence the landing area. The point of entry, given in latitude and longitude, and the heading of the entry vehicle will also define the landing footprint. These values will also be determined by simulation, which will be described in the following sections.

5.5.3 Entering Martian atmosphere: Ballistic trajectory

The ballistic entry will need to slow down the probe sufficiently for a safe landing, protect the vehicle from the heat generated by decelerating in Martian atmosphere and align the probe for a vertical penetration of the Martian surface. To protect the vehicle from the heat it will have an inflatable heat shield. Another advantage is that by deflating certain parts of the heat shield, it can change shape during descending, so that a good stable shape for both hypersonic and supersonic speeds can be achieved. During descending in the atmosphere the vehicle will first travel at hypersonic speeds for which the 70°cone shape is very stable, but once the probe enters the subsonic region of its flight the 70°cone shape becomes unstable. To stabilize the probe during subsonic flight, either the heat shield needs to be ejected or the inflatable heat shield could be deflated into a different more stable shape. However, because the probe is made pin heavy, ejecting the heat shield, will guarantee a stable subsonic flight. Recent inflatable designs can cope with a heat up to 1260°, thus limiting the entry angle range. This value will be used during simulation to determine the upper limit of the entry angle.
Another parameter that influences the trajectory and deceleration of the probe is the Ballistic coef-

ficient(BC). Equation 5.65 shows the formula for calculating BC [40].

$$BC = \frac{m}{C_D A} \tag{5.65}$$

Where m is the mass of the vehicle entering the atmosphere, C_D is the drag coefficient and A is the cross-sectional area of the vehicle.
The mass of the vehicle when entering the Mars atmosphere is around 121 kg, the diameter of a probe without heat shield is around 0.4 m and the C_D of a 70°blunted cone, similar to the ones used in previous missions, is always 1.7 for hypersonic speeds. This can easily be verified by using Newtonian flow to calculate the C_D, as can be seen in equation 5.66. However, this formula can only be used for hypersonic speeds [40].

$$C_D = (1 - sin^4\delta_c)\frac{r_n}{r_c} + 2sin^2\delta_c(1 - (\frac{r_n}{r_c})^2 cos^2\delta_c) \tag{5.66}$$

Where δ_c is the cone half angle, r_c is the cone radius and r_n is the blunted part radius.
For speeds lower than hypersonic($M < 5$), the 70°cone is not stable and thus either deflated or ejected. This will change the shape of the lander to a more stable geometry. The C_D of this design can then be based on literature to be between 0.6 and 0.8 [23].
At around Mach 2 the parachute will be deployed to decelerate the probe even further and align the probe perpendicular to the ground. The drag coefficient of the parachute will be based on the parachutes used in previous Mars mission. This leads to a drag coefficient of 0.41 for a parachute that can be released at Mach 1.77 [23]. The Ballistic coefficient after deploying the parachute can be found in equation 5.67.

$$BC = \frac{m}{(C_{D_2} A_2)(C_{D_{par}} A_{par})} \tag{5.67}$$

Where C_{D2} is 0.8, A_2 is the cross-sectional area of the shape of the vehicle after deflating the inflatable heat shield, C_{Dpar} is the drag coefficient of the parachute and A_{par} is the cross-sectional area of the parachute.

Decelerating into the atmosphere

After defining which inputs have an influence on the trajectory of the probe(s), the actual trajectory can be designed. First of all the free body diagram and kinetic diagram are shown in figures 5.35 and 5.36, from which the equations of motion can be derived as shown in equations 5.68 and 5.69.

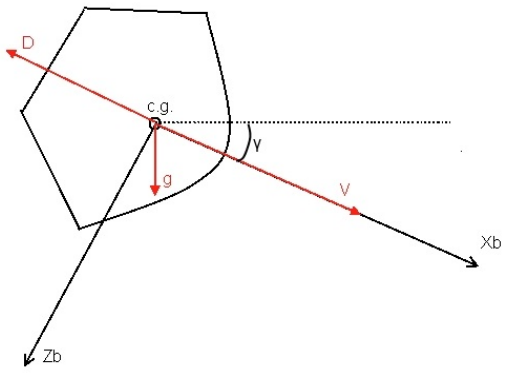

Figure 5.35: Free Body Diagram

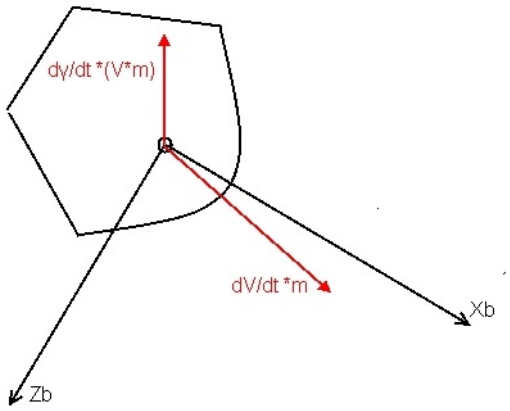

Figure 5.36: Kinetic Diagram

$$\frac{dV}{dt} m = -D - W sin\gamma \tag{5.68}$$

$$\frac{d\gamma}{dt} mV = -W cos\gamma \tag{5.69}$$

As can be seen from the equations of motions and figures, the lift, since the probe performs a ballistic entry, is negligible and the direction of the velocity can be assumed to coincide with the x-axis of the body frame. These equations can then be rewritten to calculate the acceleration (a) as shown in equation 5.70 and $\frac{d\gamma}{dt}$ in equation 5.71.

$$a = -\frac{D}{m} - gsin\gamma \tag{5.70}$$

$$\dot{\gamma} = -\frac{g}{V}cos\gamma \tag{5.71}$$

Where D is the drag, which can be calculated using equation 5.72, m is the mass of the entry vehicle, g is the gravitational acceleration at Mars, which varies with height as shown in equation 5.73 and γ is the entry angle or pitch angle.

$$D = -\frac{1}{2}C_D\rho V^2 S \tag{5.72}$$

$$g = \mu\frac{M}{R^2} \tag{5.73}$$

Where ρ is the atmospheric density, which is also dependent on the height as shown in equation 5.74, C_d is the drag coefficient, S is the cross-sectional area, V is the velocity at which the vehicle is travelling, μ is the universal gravitational constant, M is the mass of Mars and R is the radius of Mars summed with the height at which the vehicle is at that specific moment in time [35].

$$\rho = \rho_0 e^{(\frac{h}{H})} \tag{5.74}$$

Where ρ_0 is the density of the atmosphere at ground level and equals 0.02, h is the height of the vehicle above the surface of Mars and H is the atmospheric scale height, which equals around 11 km. However these equations only hold until the parachute is deployed. Then an extra drag force generated by the parachute is added to the free body diagram as can be seen in figure 5.37 and the kinetic diagram can be found in figure 5.38. This then results in the following equations of motion:

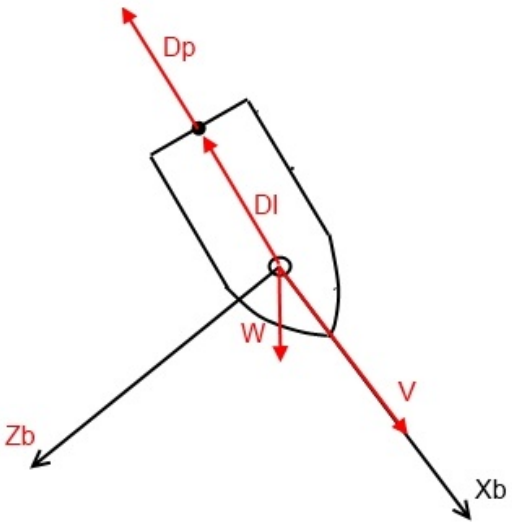

Figure 5.37: Free Body Diagram

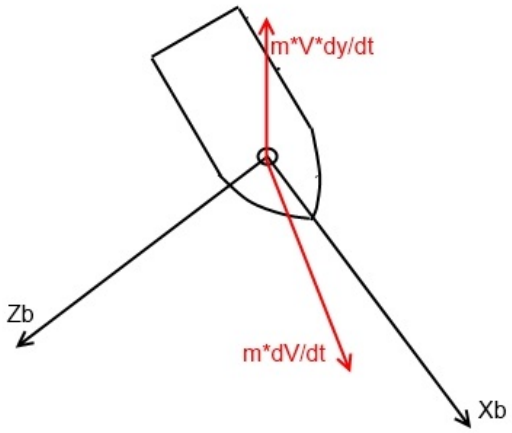

Figure 5.38: Kinetic Diagram

$$\frac{dV}{dt}m = -D_l - D_p - Wsin\gamma \tag{5.75}$$

$$\frac{d\gamma}{dt}mV = -Wcos\gamma \tag{5.76}$$

With the equations of motion known, the simulation can begin. Instead of integrating those equations over time, a while loop will be used in Matlab that ends when the height reaches the surface elevation

at which the probes should land. This requires some equations describing the change of the parameters over time. For these equations it is assumed that they are constant over a time dt, which is the time step of each iteration. The entry angle γ is always negative in the following formulas.

$$V_n = V_{n-1} + \Delta V \tag{5.77}$$

$$\gamma_n = \gamma_{n-1} + \Delta\gamma \tag{5.78}$$

$$h_n = h_{n-1} + \Delta h \tag{5.79}$$

$$x_n = x_{n-1} + \Delta x \tag{5.80}$$

$$\Delta V = a_{n-1}dt \tag{5.81}$$

$$\Delta\gamma = \dot{\gamma}_{n-1}dt \tag{5.82}$$

$$\Delta h = V_{n-1}sin\gamma_{n-1}dt - \frac{1}{2}a_{n-1}sin\gamma_{n-1}dt^2 - \frac{1}{2}g_{n-1}dt^2 \tag{5.83}$$

$$\Delta x = V_{n-1}cos\gamma_{n-1}dt - \frac{1}{2}a_{n-1}cos\gamma_{n-1}dt^2 \tag{5.84}$$

Heating in the atmosphere

Aerocapture, which is the deceleration of a vehicle due to the atmosphere, also heats the entry vehicle due to the flow of the air around it. The heat shield present on the probe must protect the delicate instruments that lie behind it. So the heat shields size is important for the deceleration, but also the type and material it is made of are important for heat protection. In order to design the heat shield, both the deceleration and heat generated should be known. Equation 5.85 shows the heating rate and equation 5.86 is the total heating load, increasing with ΔQ over the entire entry time [40].

$$\dot{q} = cV^3\sqrt{\frac{\rho}{r_{nose}}} \tag{5.85}$$

$$Q_n = Q_{n-1} + \Delta Q \tag{5.86}$$

$$\Delta Q = \dot{q}dt \tag{5.87}$$

Where c is a constant specific for a geometric shape(for a 70°cone this can be approximated to be $0.6E^{-4}$), $\dot{q}$ is the heating rate, Q is the total heat load and r_{nose} the radius of the nose of the heat shield [23].

Aligning probes vertically

A part of the mission is to provide a better understanding of the surface layers of Mars. In order to do this the probes will penetrate the ground to buffer the surface noise. In an ideal situation the probe will land vertically, penetrating the ground 0.6 m. Also a penetrating landing has many advantages over a soft landing, the major being a simple and straightforward EDL strategy.
Due to the gravity of Mars and the drag of the vehicle, the pitch angle will slowly increase during descent. However, only these two forces may not be enough to align the probe for a vertical penetration and other systems need to be used in order to achieve a landing perpendicular to the surface.
Either solid rocket motors, a parachute or a skycrane can be used to align the probes in a vertical way. A skycrane would add to much weight to the entry vehicle and would complicate the whole EDL a great deal, this option is thus not viable for this mission. Solid rocket motors would add to the landing accuracy, but would also add weight and complicate the EDL. A parachute however is already in the EDL design to slow the probes down sufficiently and can thus be designed to align the probes. This will not add much weight to the probe, nor will it complicate the EDL. The additional drag force of the parachute will help to align it vertically. Simulation will show that this suffices.

5.5.4 Verification and Validation

After all inputs, outputs and equations are defined, a simulation of the entire entry trajectory was made. This tool must of course be verified and validated before it is ready to be used for the actual simulation and optimization of the mission at hand.

Verification

It needs to be verified that the simulation model represents the actual model correctly, this is done by comparing each code module separately to hand calculated values or existing models. If differences occur, they need to be explained or correction to the program need to be made. Since it is hard to define code modules other than the atmospheric density and the gravitational acceleration, which are verified by running the program at different heights and comparing them to other models, only a verification of the whole model will be discussed in more detail by using a simplified problem.

Verification with simplified problem

After the most important subsections of the model are checked, the full model can be verified by using a simplified model. The first assumption is that the gravitational acceleration is constant and equals 3.5 m/s. The atmospheric density is also assumed to be constant and equal to $0.03E^{-2}$ which is an average value. It will also be assumed that there is only one stage, meaning no parachutes or additional decelerators will be deployed or ejected during descent. The vehicle will enter and land with a 70°cone heat shield attached, which means a drag coefficient of 1.7. It will weigh 100 kg. The diameter of the heat shield is taken to be 1 m and it is assumed that the vehicle enters the atmosphere with an entry angle of 90°and with a speed of 0 m/s for the first case and 5600 m/s for the second one. Using equation 5.68, where all parameters are now constant, the tool can be verified.
Running the tool for the first case gives a velocity of 276.8 m/s at no surface elevation. Assuming the height to be 0 m, the time it took to be 300 s and the height at which the probe entered the atmosphere to be 130000 m, using equation 5.88 the velocity is found to be 289 m/s, which is very similar to one that was found by simulation.

$$0 = 130000 - Vt - \frac{1}{2}at^2 \tag{5.88}$$

Where a equals Vt. Implementing this and solving for V, then gives us 289 m/s.
Running the tool for the second case gives a velocity of 1241 m/s. Using equation 5.68 the acceleration was found to be 251.2 m/s. Implementing this in equation 5.88 and a descending time of 27 s, gives a velocity of 1423 m/s, which is again similar to the value found by simulation. Thus the tool is verified.

Validation

In order to validate the tool, the data that comes out of the simulation will be compared to the data measured by previous Mars missions like Mars Pathfinder and Viking. However, since they all had soft landings and used rocket boosters or other landing strategies than penetration, only the part up until the parachute deployment can be validated.
Table 5.19 gives a small overview of a couple of previous missions.

Table 5.19: Previous missions [23]

	Mars Pathfinder	Mars Phoenix	Mars Viking 1
Diameter of heat shield	2.65 m	2.65 m	3.5 m
Angle of entry	-14.06°	-12.5°	-17°
Velocity at entry	7.26 km/s	5.67 km/s	4.7 km/s
Entry mass	584 kg	600 kg	992 kg
Heating rate	100 W/cm^2	58 W/cm^2	26 W/cm^2
Parachute deploy. Mach no.	1.57	1.6	1.1
Parachute deploy. altitude	9.4 km	9 km	5.8 km

Running the Descending tool, gives for the Mars pathfinder configuration a parachute deployment height of 3.5 km and a peak heat rate of 82 W/cm^2. For the Mars Phoenix a deployment height of 4 km was found with a heat rate of 37 W/cm^2. Finally for the Viking 1 the height for releasing the parachute and peak heat rate was found to be 2.2 km and 21 W/cm^2.
Comparing these values to the ones in the table shows that there are some differences, although not that large. These differences are mainly due to the assumptions made. First of all a very simple atmospheric model was used which will differ from the actual Martian atmosphere and secondly the model was linearised in order to simplify the whole problem. These two will have the biggest contribution to the differences found.

5.5.5 Landing

After the probes have decelerated sufficiently for a safe landing and the parachute has been ejected, the probe free-falls pin down to the surface. The probes will need to enter the surface of Mars at an entry angle between 70^o and 110^o as defined in section 4.6 and with a speed of 90 m/s as defined in section 4.4. At impact the pin will punch through the inflatable heat shield top, deflating the inner inflated part. At impact the straps, holding the inflatable in a bullet like shape, will be cut. The probe will thus pop back into its initial 70°cone shape, with four inflated parts, separated by four deflated parts. Since the inflated heat shield was designed to withstand high speeds and deceleration, it will not bounce on impact but stay rigid. Even if one or two are penetrated by a rock and deflated at impact, the other two will still make sure the inflatable heat shield does not cover the instruments. The same mechanism that deflated the heat shield during flight will then after landing deflate the other parts, so that the solar panel can be safely deployed. Since the heat shield covers the probe at landing and then creates a 2.2 m diameter blanket over the surface of Mars, no or little debris or dust will fall on the antenna and solar panels, thus not requiring an extra dust or debris protection system. After the probe has penetrated the inflatable, it penetrates the ground at least 45 cm deep, delivering the seismometer into the crust it is designed to map.

5.5.6 Trajectory Optimization

The trajectory simulation can be used to optimize the trajectory. The inputs that can be changed in order to achieve an optimized trajectory are listed in table 5.20. The range of the different inputs can also be found in the table.

Table 5.20: Changeable Inputs of the System

Inputs	Range
Diameter of inflatable heat shield (d_i)	0.6 m< d_i <3 m
Diameter of parachute (d_p)	2 m< d_p <7 m
Angle of Entry (γ)	-10°< γ <-90°

Where the minimum angle of entry was already set to be -10°, the minimum value of the diameter of the inflatable heat shield equals the diameter of the probe multiplied by a safety factor and the diameter of the parachute mainly depends on its weight and size. The parachute should not enlarge the probes that are released from the bus too much. The upper limit of the inflatable heat shield is also based on weight and size for the same reasons. The upper limit of the angle of entry is -90°because this equals an entry perpendicular to the surface of Mars.
By altering these values an optimized trajectory can to be found.

The optimized trajectory however should first of all apply to multiple probes because they are released simultaneous a couple of days before entering the atmosphere. They will thus all have a different angle of entry, meaning some will decelerate faster than others and some will impact at higher velocities than others. A new *safe* range of the angle of entry thus needs to be defined by iteration.
Secondly also the angle at which the probes penetrate the ground cannot cross certain boundaries. It was defined in chapter 4 that the probe needed at least a range of -70°to -110°, but since angles greater than 90°are not likely to occur since the entry vehicle will undergo a fairly stable descent, the range can be defined as -70 to -90°. However, the surface of Mars can also be under a certain angle. In order to compensate for this a safety factor is applied, leading to the following range: -80°to -90°.

Thirdly, also the impact velocity influences the design a great deal. The penetrators not only need to slow the probes down sufficiently, but also need to deliver the seismometers 0.6 m into the surface of Mars. This then puts a constraint on the impact velocity. The velocity should be large enough to penetrate the ground 0.6 m in every circumstance(soft and hard ground), but small enough in order to provide a safe landing for the instruments that are carried by the probes. The velocity at impact, already including safety margins, was then set to be around 90 m/s.
Fourthly, the inflatable heat shield should be able to cope with the generated heat. An inflatable heat shield at the moment can cope with up to 1260°C, which corresponds to a peak heat rate of about 46 W/cm^2. Finally, the g-loads generated by deceleration should not exceed a certain maximum. However, g-loads won't be a big issue because they are relatively small compared to the loads created at impact. Only the g-loads generated by releasing the parachute should not harm the instrument box.

These five outputs are closely correlated and an optimized trajectory will be found using iteration. Iteration, however, only optimizes the design to such an extent as the iterator is willing to go since it is a time consuming method. Using iterations a couple of optimized designs were found, which can be found in the table 5.21. The probes will land at an average surface elevation of 3000 m.

Table 5.21: Changeable Inputs of the System

	Concept 1	**Concept 2**	**Concept 3**
d_i	2.4 m	2.2 m	2 m
d_p	3.7 m	4 m	4.3 m
γ_e	-10°to -52	-10°to -40°	-10°to -32°
γ_l	88.5°to 80.6°	88.2°to 80.2°	87.8°to 79.7°
V	90.6 m/s to 92.6 m/s	90 m/s to 91.4 m/s	88.7 m/s to 90 m/s
T	384°C to 986°C	575°C to 1017.5°C	630°C to 1054°C
g	12 to 42	12 to 35	13 to 29

It can be seen from table 5.21 that the angle at which the vehicle enters the surface of Mars limits the angle of entry the most, but also the peak heat influences the design a lot. The impact velocity, however does not change considerably when changing the angle over a few degrees, which is due to the parachute deployment.
Now it can be seen that the bigger the heat shield, the bigger the range for the angle of entry. However, there are a couple of limits placed on the size of the heat shield. The inflatable heat shield will, at the time of the probe release from the bus, be packed around the penetrator as can be seen in figure 5.34. It should not exceed certain limits. It can be seen that the smaller the inflatable, the lower the angle at which the probe enters the surface. Concept 3 will not be an option, since a better vertical alignment is preferred. However, the angle of entry of concept 2 and 1 do not differ much. The only difference between the two concepts is the angle at which they can enter the atmosphere, but both have a sufficiently large range of entry angles. Then it comes down to weight and size. Concept 2 has a 0.2 m smaller inflatable and a 0.3 m larger parachute than concept 1. Since the parachute is lighter and smaller in packing size, concept 2 is considered the better of the two.

Perturbations

The above optimization was performed for a simplified case. To make the outcome more realistic, wind speeds up to 30 m/s are added, which was the fastest wind speed recorded by the Viking mission [45]. For speeds above Mach 1.77, so before the parachute is deployed, the wind does not influence the trajectory much, because the speed is still around 400 m/s. But after the heat shield is deployed the wind will also influence the parachute. It could either help align the parachute vertically or keep it from aligning itself vertically. In the latter case, the wind blows in the same direction as the horizontal velocity. The probe will thus land a bit further than without wind, but since it already has a very large footprint, this will not influence the design much. However, it does influence the angle of penetration into the surface. Adding the maximum wind speed of 30 m/s to the horizontal velocity does influence the angle but still only marginally because of the large vertical speed. In a worst case scenario, the angle of entry into the surface will be 3°off, of the above calculated range.

The optimized trajectory

The probes enter the atmosphere with an inflatable heat shield of 2.2 m already deployed. This heat shield will slow the probe down to Mach 1.77 at which the parachute will be deployed. Then by deflating certain parts of the inflatable decelerator and straps pulling it into a more bullet shaped design, a better aerodynamic shape is achieved for subsonic speeds. Then about hundred meters above the surface the parachute will be ejected and the probe will start its free-fall. At impact it will penetrate the heat shield, releasing the straps, because the heat shield is still partially inflated, it will keep its shape and fall in a wide circle around the probe, not covering it. The trajectory of the probe at an entry angle of 10°is shown in figure 5.39. The deceleration of the probe can be seen in figure 5.40. Figure 5.41 shows the acceleration to time, and figure 5.42 the acceleration to height. Finally the heat peak rate can be found in figure 5.43. As can be seen from figure 5.42 after 90 s

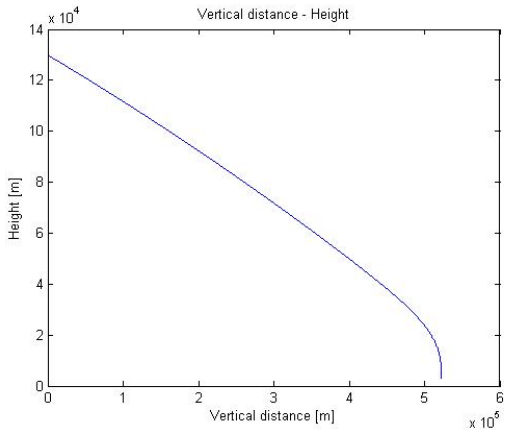

Figure 5.39: Vertical Distance to Height

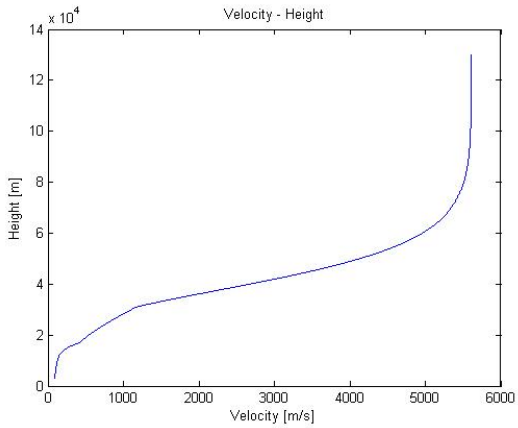

Figure 5.40: Velocity to Height

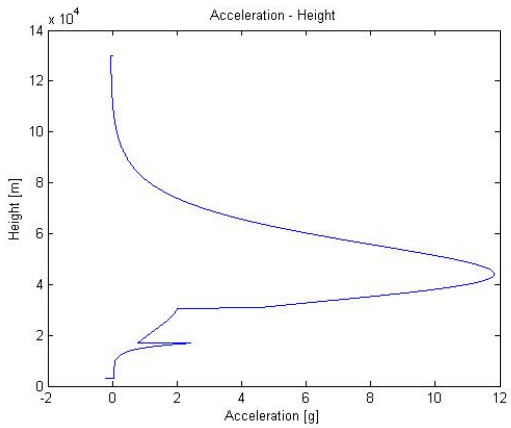

Figure 5.41: Acceleration to Height

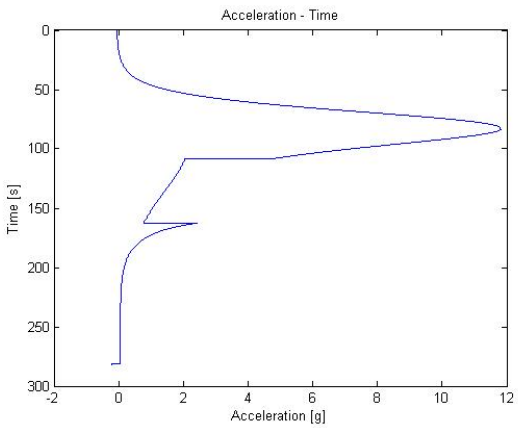

Figure 5.42: Acceleration to time

the probe reaches its peak acceleration, after 160 s the parachute is released and 280 s after entering the atmosphere at a height of 130 km the probe penetrates the surface. Especially the parachute deployment has a big influence on both the speed and trajectory. As can be seen in figure 5.39 the parachute makes the slope steeper, which shows that the parachute aligns the probes perpendicular to the surface. Also figure 5.40 shows a rapid decrease in velocity when the parachute is deployed. Figure 5.43 shows that the inflatable heat shield can cope with the generated heat. The simulated heat peak rate is about 21 W/cm^2 while the inflatable can cope with a heat peak rate of 46 W/cm^3. Figure 5.44 shows the EDL starting from probe release to penetration, clearly indicating the different phases the probe goes through.

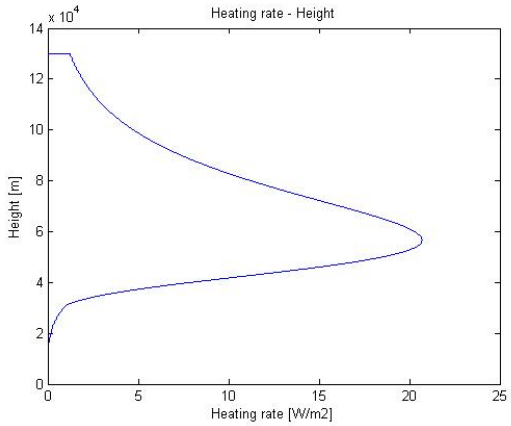

Figure 5.43: Heating Rate to Height

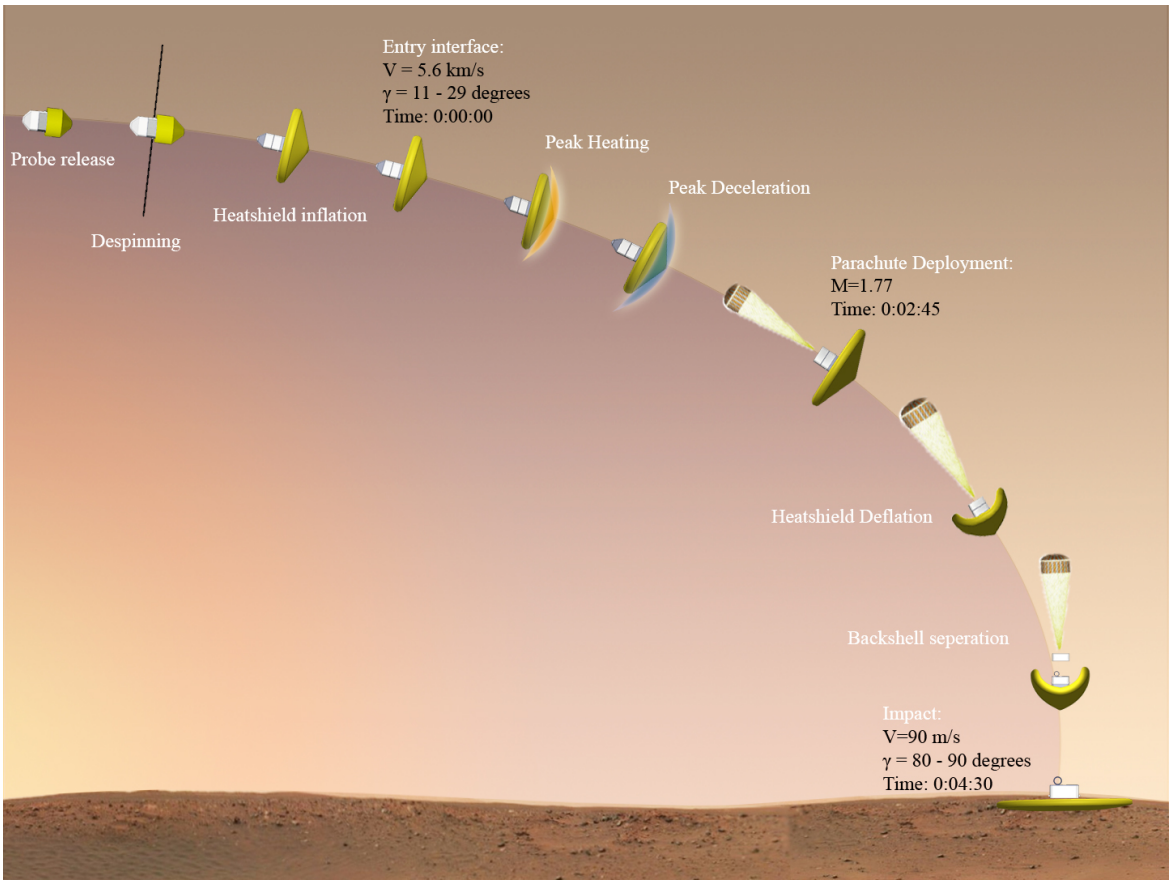

Figure 5.44: Entry, Descent and Landing

Chapter 6

System Analysis

6.1 Risk Assessment

When designing a mission there are always risks involved. Therefore the risk assessment of the Ancile mission is described in this section. It will help the developing team to add redundancy and fail-safe or safe life systems to the design. Every phase of the mission is discussed and assessed on the probability of failure and the consequence of failure on the mission. The consequence of failure can be marginal, minor, critical or catastrophic, while the probability of failure goes from very low to high. The Risk map for the Ancile mission can be found in figure 6.1, where mission phases in the red area are the most critical.

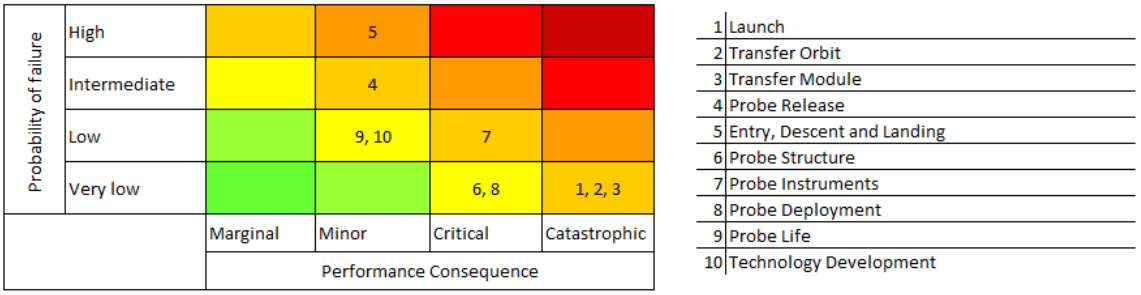

Figure 6.1: Risk map for the Ancile mission

1. **Launch**
   Only one launch will be performed to deliver the multi-probe bus into a direct transfer orbit to Mars. Failure of the launch thus means complete failure of the mission, making this a *catastrophic* event. However, the Ariane 5 has proven itself one of the most reliable launchers, with 63 out of 67 launches being successful. The probability of failure can thus be described as *very low*.

2. **Transfer Orbit**
   The transfer to Mars takes several months, during which orbital manoeuvres will need to be performed to accurately control the transfer. Small structural deviations, thruster failure or insufficient fuel could cause the transfer orbit to be inaccurate. This could either lead to the probes landing only on one side of *Valles Marineris* or the multi-probe bus missing Mars entirely. Failure of the orbital manoeuvring systems will thus be *catastrophic* for the mission. The probability of failure on the other hand is *very low*, because orbital manoeuvring has been performed by many previous mission either to Mars or other planets.

3. **Transfer Module**
   The transfer module does not only contain manoeuvring systems, but also trajectory sensing and power systems. If the solar panels attached to the bus fail, the batteries of the probes won't charge, which will lead to failure of the EDL, because no power is present to trigger the different phases. On the other hand if the star and sun sensors fail, the orbital manoeuvring could still send the bus on a wrong trajectory. However, many critical components, like sun and star sensors, have been made redundant. Therefore, if one or more of them fails, the transfer module still functions. The chance of failure is thus *very low*, but the consequence again *catastrophic*.

4. **Probe Release**
   The probe release is one of the most critical parts of the mission, because it will determine how the probes will enter the atmosphere and thus descent and land on the surface of Mars. After the probes are released, no additional manoeuvring can be performed to align the probes in the

right angle. The probes are released by a releasing mechanism, which consist of a mechanical and magnetic clamp. If either of those fail and one or more probes stay attached to the bus the first probe release stage will still be accurate enough, but the second probe release stage will fail. The change in the center of gravity will make the bus unstable leading to failure. The consequence of failure on the mission can thus be described as *critical*, because most likely some probes will still enter the atmosphere correctly, but it is unsure that there will be enough to perform the measurements. Probability of failure is *intermediate* because it is an entirely new probe release system with many different components that could fail.

5. **Entry, Descent and Landing**
   The Entry, Descent and Landing phase of any (re)entry mission is seen as very critical. NASA called the EDL phase of the Mars Curiosity rover '7 minutes of terror'. However, the EDL system, although being just as innovative as the Curiosity's is a lot more simple. No retro-boosters, sky-crane or airbags are used to land the probes. Instead they will just deploy a parachute, as performed by all previous Mars missions from NASA, and eject it before hitting the ground. The inflatable heat shield on the other hand has not been used in any mission, but is undergoing some extensive testing, also making it a fairly safe system to use. The high impact landing is only been performed by NASA's deep impact, which landed on an asteroid. This will need extensive testing to assure a safe landing. If the probe however lands on a slope steeper than 10°, the crushable structure will not damp the structure sufficiently or if the probe hits a rock or is deflected by one, the penetration could fail. NASA has landed 7 out of 8 Mars landers successfully on the surface [10], proving the EDL, if designed right, to be reliable. However, due to the additional risks described, the probability of failure is considered *high*. Redundancy by doubling the amount of probes is added to account for the high failure probability, making the consequence of failure of one or more probes *minor*.

6. **Probe Structure**
   The box of the probe could collapse due to manufacturing errors weakening the structure of the box. Calculations for the stress of the worst possible case incorporated a 50% safety factor. Therefore probability is considered *very low*, because manufacturing errors will be marginal and will not affect the structural integrity of the box to a large extent. The consequence of failure, however, is *critical*, since there is no redundancy or fail safe system to account for this.

7. **Probe Instruments**
   Inside and on top of the box and in the pin, there are instruments that will also experience the high loading during the impact. For the seismometer, located in the pin, which is the most sensitive instrument on board, a crushable honeycomb structure will damp the high loads and therefore protect the instrument. The other instruments were chosen to withstand the high impact. A flexible solar panel that rolls out after touchdown and a phased array antenna are designed to withstand the high loads created by the impact. These instruments, together with their dust removal system, need to be extensively tested in a desert environment. When extensively tested, the failure probability can be considered *low* and the consequence of failure *critical*.

8. **Probe Deployment**
   Deployment mechanism would not be able to cope with the high impact landing. Therefore the whole probe was designed to only have one deployment mechanism, that of the solar panel. This mechanism is not mechanical, it will be rolled out by Nitrogen gas being pumped through inflation lines, making it more fail safe for high load landings. Probability and consequence of failure is considered *very low* and *critical*, since probes cannot function without power.

9. **Probe Life**
   After the probes have successfully landed, (partial) system failure can still occur throughout their lifetime. The on-board computer could fail, communication with the satellite could be lost and the seismometer could stop working. However, if the instruments are properly tested by the manufacturer, the probability and consequence of failure will be *low* and *minor*.

10. **Technology Development**
    Some of the technology used in this mission still needs to be developed. More specifically, the heat shield and dust removal system are the ones that still need extensive developing and

testing. Since the launch date is set for the year 2018, there are 5 years available for developing and production of these systems. In comparison, the Mars Pathfinder rover was developed in 3 years [64]. Thus the probability of failure is considered *low* and its consequences *minor*. If extra development is needed, the mission will need to be postponed for at least two years, because the preferred launch window only occurs every two and a half year. This will increase costs, but since a big part of the budget is not used, enough money is available to account for it.

6.2 Sensitivity Analysis

The design setup is an iterative process. Most of the parameters are correlated. Adjusting or changing some input values has a significant effect on the whole design output. This section describes the impact on certain components by the modification of one parameter. Characteristics that are considered within this analysis are: mass, power, EDL, payload dimensions and costs.

Mass

The mass is one of the most critical parameters since it affects and is affected by all other components. Especially the EDL approach is influenced. Is the weight changed, the heat shield and the parachute need to be re-sized. That again might lead to a significant increase or decrease in mass and the iteration process for calculations starts over. Next to that, the launch vehicle depends on the total payload mass as well since the rocket can only bring a certain amount of weight into an heliocentric orbit.

Power

The power supply is crucial in every stage of the mission time-line. If the power requirement changes due to additional instruments or environmental aspects, the space-bus has to be adjusted in size. For example, additional solar cells are needed in order to cover an increase in demand. This has an impact on the cost and mass unit again and all other compartments that are linked to it.

EDL

The EDL-phase needs to be able to land the probes safely on Mars. If there are changes in the EDL procedure or systems it affects the mass, cost and payload dimensions. The whole design needs to be revised.

Payload Dimensions

The dimensions have mainly a consequence on the transfer module and the launcher selection. A change in size of the probe leads to a revision of the transfer module. Also another launcher might need to be chosen as soon as the transfer module becomes too large.

Costs

The financial budget is mainly claimed by the probe design. Modifying parameters to change the design will lead to redesigning or re-sizing of many parts. In addition there is extensive testing required in order to ensure the success of the mission. Costs are therefore depending on the complexity of the design as well as on elaborateness. If the budget tends to run out and no additional funds are obtained, the project might not be realizable.

6.3 Resource Allocation

This section will provide the resource allocation for this project. The costs will be split into three parts. The first part will deal with the launcher. The second part will be allocated to the transfer module, and the third part will provide the details for the probes. The section will be concluded with a small summary of the total resource allocation.

6.3.1 Launcher

For this mission, a commercially available launcher (Ariane V) will be used. The costs of this launcher are 120 million dollar [21] (Fiscal Year (FY)2001) which equals, after taking inflation into account, 120 million euro (FY 2013). No further costs are assigned to this section. This money will be spent in 2018, since buying the launcher earlier will increase the costs as money has to be spent on storage and maintenance.

6.3.2 Transfer Module

The transfer module for the Ancile mission will be different from other transfer vehicles used in previous Mars missions. The only transfer module ever used that slightly looks like the one used in this mission is the Venus Pioneer Multiprobe (VPM) [29].
The costs for this mission were 250 million dollar (FY 1980) which equals 550 million euro (FY 2013). It is assumed that 40% of this budget was spent on the transfer module, that is 220 million euro. Since the transfer module used in this concept is technically more complicated when compared to the VPM transfer module, a higher budget will be available. Therefore 300 million euro will be allocated to the transfer module. From literature [94], it is estimated that 60% of the budget will be spent on non-recurring costs (research and development, etc.), and 40% is spent on recurring costs (manufacturing etc.). Therefore 180 million euro will be spent on non-recurring costs. This money will be spent between 2013 and 1016. 120 million euro will be spent on recurring costs. This will be spent between 2017 and 2018.

6.3.3 Probes

The probes used in this mission are quite similar when compared to the landers used in the Mars pathfinder mission. Therefore the costs for the landers will be derived from the costs of this mission. The cost for the lander in the Pathfinder mission equaled 170 million dollar (FY 1992) which corresponds to 210 million euro (FY 2013). Just as for the transfer module, 60% of this budget will be spent on non-recurring costs, between 2013 and 2015, which equals 126 million euro. A difference between the Pathfinder mission and the Ancile mission is that this mission will use 16 probes. The recurring costs for the theoretical first unit in this mission equal 40% of 210 million euro, that is 84 million euro.
A learning curve will be applied to calculate the budget for the remaining landers. The learning curve factor (L) for the space and aerospace industry is usually between 0.87 and 0.96 [94]. L was picked as 0.95 because of the innovative design. Now the total costs of the probes can be computed using equation 6.1.

$$costs = 126 + \sum_{n=1}^{16} 84 \cdot L^{n-1} \tag{6.1}$$

The total cost equals 1065 million euro. From this value, 939 million euro is reserved for the production of the probes.

6.3.4 Total Costs

The total costs of this mission can be computed by adding the cost of the launcher, the cost of the cruise stage and the cost of the probes. The total cost equals 1485 million euro. This implies that the total mission costs will be a billion less then the maximum budget. This will make it far more likely for this mission to be carried out. The distribution of when the budget will be spent can be found in figure 6.3.4. For this mission, operation after launch are assumed to come from a different budget. Therefore they are not included in this resource allocation.

6.4 Sustainable Development Strategy

In recent years sustainability has become a major issue, not only here on Earth, but also in Space. Debris within the Earth orbit pose a growing threat to spaceflight, with millions of parts which could collide with future missions. By all cost, additional space debris and the creation of a similar problem around Mars need to be avoided. Furthermore the Earth and Mars environments need to be

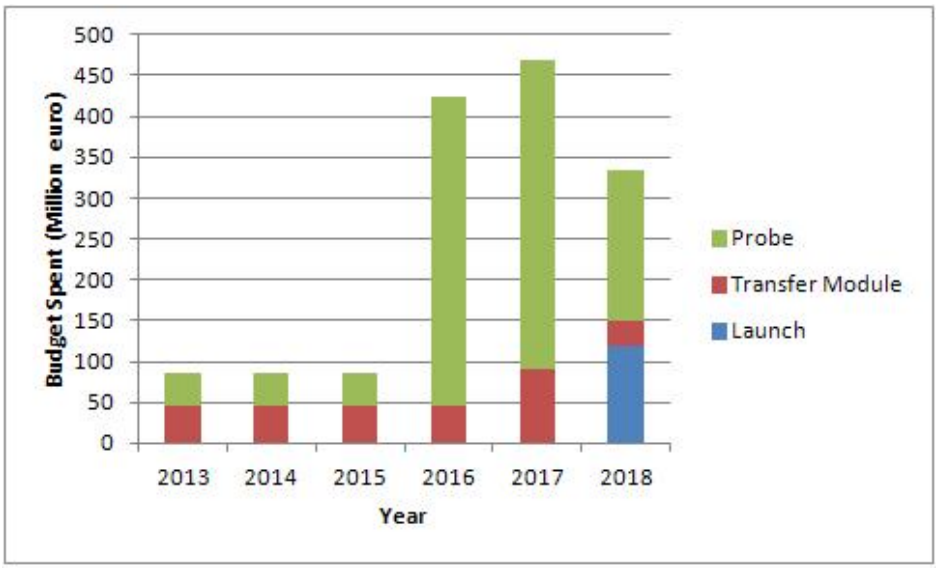

Figure 6.2: Budget spent per year

protected. This section discusses the sustainable strategy for the Ancile-mission, starting at launch and finishing with the landing of the probes on the Martian surface.

6.4.1 Launch

To put the multi-probe space bus into a direct transfer to Mars, it needs to be launched from an Earth based station. If the launch should fail, contamination of the environment should be minimized. The launcher itself has a large amount of propellant on board, which could possibly pollute large areas, but since the mission will be using an existing rocket systems no sustainable changes can be made to the launcher. The payload of the launch-vehicle, however, is a different case. The payload will consist of the space-bus with sixteen small probes on board. These probes will need a power-source to take measurements over a period of five years. It was designed such that the probes will carry flexible solar panels to provide power. It can thus be said that the multi-probe bus will only contaminate the environment marginally more than the launcher would have done on its own. However, if instead RTG's were used as a power source and the launch failed, an environmental disaster can be a consequence.

No matter what launcher is chosen, stages of the launcher will crash into desert areas or oceans. However, this will not have a big environmental impact and every stage that crashes into earth does not become space debris.
The launch will be performed with the Ariane 5, which has had thirty-five consecutive successes. Two solid boosters will burn for 130 s before separation over a designated zone of the Atlantic. The main cryogenic stage is commanded to reenter the atmosphere for an ocean splashdown after completing its propulsive mission. The upper composite, composing of ESC-A cryogenic upper stage, a vehicle equipment bay and a 3936 cone, will be de-orbiting after payload separation to crash into the Pacific. Thus not leaving any stages behind in space and limiting space debris. The separate stages can be recycled and reused.

6.4.2 Earth-Mars Transfer

Once the payload has been separated from the launcher, the multi-probe bus is on a direct transfer to Mars. During this phase of the mission only manoeuvring for orbit adjustment will be performed, which does not leave any stages in space. The rockets will stay attached to the bus and will need to perform orbital manoeuvres multiple times.

34 hours before entering the Martian atmosphere the probes will need to be released from the space bus to create a large enough landing area. The shell, protecting the probes from the harsh space

environment, is ejected just before releasing the probes. Since the space bus is heading directly to Mars, the ejected covers will still travel at the same velocity towards Mars as the bus travelled at the time they were released. Since the probes are designed to hit the atmosphere of Mars in a circle with a diameter of about 1200 km, compared to a 7000 m diameter of the atmosphere of Mars, and the shields are released just before the probes, they will land no further than 1000 km from Vallis Marineris, thus not missing Mars and becoming space debris.

The Venus Pioneer multi-probe bus released its small probes twenty days before entering the atmosphere with spring accelerated clamps. The clamps were immediately ejected from the bus, becoming space debris. For the same reasons as the covers that protected the probes, the clamps would not be left in space but crash into the surface of Mars. However, the useless debris landed on the surface of Mars should also be minimized. Therefore a new release system was designed for this mission. First mechanical clamps are retracted and then magnetic clamps release the probes, leaving everything but the probes attached to the bus.
By accurately controlling the spin rate and velocity of the space bus, the probes do not need additional attitude control in the form of rocket boosters, thus not leading to additional useless debris that lands on the surface of Mars.

The probes need to be protected from the generated heat, meaning that they will all have an inflatable heat shield. The inflatable heat shield is packed around the probe when released. Before entering the atmosphere the cover of the inflatable is ejected and the heat shield is inflated. The inflatable covers will also crash into the surface of Mars like the covers of the space bus did, but will burn up completely.

6.4.3 Entry, Descent and Landing

The multi-probe bus, covers and probes will enter the atmosphere of Mars and perform a ballistic entry.
The bus and covers will not have any heat-shield or protection, and will thus burn up slightly in the atmosphere of Mars. Especially the probe bus will lose only little of its material during descent, the covers however will have become considerably smaller. Not providing any protection during descent will thus limit the amount of useless landed mass on Mars, thus polluting the surface of Mars to a lesser extent.

The probes will also perform an EDL, but much more complicated than the bus or covers. With the heat shield already inflated, they enter the atmosphere of Mars. The heat shield slows the entry vehicle down to Mach 1.77 at which the parachute will be deployed. The probe will further decelerate the probe and at hundreds of meters above the surface the parachute will be ejected from the bus, carrying with it the shield that covered the antenna and solar panel.
The parachute will thus become useless debris that lands on the surface of Mars and could possibly interfere with future missions. However, using a parachute instead of solid rocket boosters to align the probes, is the more sustainable option. Rocket boosters require fuel, that needs to be carried by the probes and will impact the ground of Mars at a high speed, possibly scattering the boosters in every direction, creating a debris area. Also the fuel would penetrate the soil, contaminating it to a large extent for that specific area.

After the parachute is ejected, the probe free-falls to the surface, penetrating the heat shield at impact. The heat shield will thus not be ejected and become another useless piece of debris. Instead it will function as a shield against dust and debris thrown into the air by penetrating the surface.
If the whole EDL would fail, then no more debris would land on the surface of Mars then if the EDL was a success, although all landed mass will now be useless. However, if RTG's were chosen as a power source, then an EDL failure could have catastrophic consequences for the local environment of the impact area.

6.4.4 End of Life

Eventually the mission will either be terminated or stop working on itself, reaching its End of Life (EOL). The probes will be using an existing satellite to communicate with Earth, meaning that no

additional satellite will be in an orbit around Mars. A satellite would have a chance at becoming space debris when control is lost after several years or not enough fuel is left for de-orbiting. If however the satellite can be controlled to enter Martian atmosphere, it will most likely be to big to burn up entirely in the atmosphere of Mars, creating landed debris. By using existing satellites, extra debris is thus avoided.
When the probes stop functioning on their own or are terminated, they become useless landed debris. The design aimed to land the least amount of probes on the ground, while still be able to measure the existence of plate tectonics. This leads to sixteen dead masses at EOL.

6.5 Compliance Matrix

Figure 6.3: Compliance Matrix

No.	Requirement	Compliance	Note
	Top level requirements		
1.1	The system shall detect the possible existence of plate tectonics	full	The system is capable of detecting possible plate tectonics movement within 1mm per year
1.2	The system shall image the internal structure and composition of Mars	full	Seismometers within the penetrator measure seismic activities caused by natural impacts/noise
1.3	The mission shall limit the generation of space debris	unknown	A sustainable strategy is accomplished for all mission phases
1.4	The Landers shall survive Mars environment for a period of 5 years	full	The system is designed to survive a mission duration for at least 5 years time including safety margins
1.5	The Mission shall not cost more than 2.5 billion euro	full	The total cost of the mission is calculated to be 1.485 billion euro
	Launch sequence requirements	full	
2.1	The system shall launch within the near future	full	The system is going to launch on 1st of May 2018
2.2	The system shall fit within the launcher	full	The system is 2.2m in diameter and 4.5m in height and therefore fits within the Areane 5
2.3	The Launcher shall lift the payload into the transfer orbit	full	Ariane 5G is able to lift more than 3 tons to Mars trajectory, the system weighs 2867 kg
2.4	The System shall survive the launch sequence	full	The system is designed to resist the high g - loads
	Earth - Mars Transfer requirements		
3.1	The system shall get to Mars	full	The Ancile-module uses an Hohmann-like transfer and will arrive at Mars in a time of 258 days
3.2	The system shall survive the transfer	full	The system is equipped with shielding, thermal control and power generation systems
	EDL - requirements		
4.1	The probe needs to despin	full	The probe uses a stretch YoYo with a spring of 2m length and a mass of
4.2	The probe needs to inflate the heatshield	full	The heatshield is inflated within 100s by a nitrogen gas
4.3	The probe enters Mars within constraints	full	The probes enter Mars atmosphere with 5.6 km/s and an angle of 11 - 29 degrees
4.5	The probe has to be protect against heat	full	Heatshield covers and protects the probe against the generated heat of around 1000 degrees Celsius
4.4	The probe shall decelerate	full	Ejects parachute and decelerates to 90 m/s
4.6	The probe has to survive the landing	full	The probe penetrates the ground with 90 m/s in an angle of 80 - 90 degrees and is damped by a honeycomb structure
4.7	The probe grid need to be around Valles marineris	full	In total 16 probes will land within range of 2900 and 3100 km

No.	Requirement	Compliance	Note
	Transfer module requirements		
	Power		
5.1	The module shall generate sufficient power	full	The module uses 2.84 m^2 and generates 312.8 W including safety margin
	Probe needs to be charged at arrival	full	The module charges the batteries of the probes during the transfer phase
	ADCS		
5.2	The system shall determine its attitude	full	The transfer module uses 8 sun-sensors and 2 star-trackers
	Communications		
5.3	The system shall communicate with Earth	full	The system uses a C-Band horn-antenna to communicate
	Structures & mechanism		
5.4	The probes shall fit within the transfer module	full	the probes fit into the transfer module
5.5	The structure shall protect internal components	full	The shell is layered with a gold-foil and accomplishes electromagnetic and thermal isolation
	Propulsion		
5.6	The system shall provide thrust to adjust trajectory	full	There are 8 small thrusters with 5 N and one big thruster with 667 N for trajectory corrections
5.7	The system needs to store propellant	full	There are 4 fuel tanks with diameter of 43.4 cm and filled with monopropellant hydrazine
	Payload subsystems		
5.8	The system shall fix the probes during transfer	full	The probes are fixed with mechanical clamps
5.9	The system shall spin up to a certain rpm	full	An electro-motor spins up the module to 10 and 15 rpm
5.10	The system shall release probes	full	The system removes first the shells and then the probes by opening the clamps
	Thermal control		
5.11	The system shall have efficient thermal control	full	Sensors detect temperature and radiators, heaters and louvers are installed to control the temperature
	Probe		
	Power		
6.1	The probe shall generate power	full	A Solar panel of 30 X 270 cm provides 25 W on average
6.2	Probe needs to store sufficient energy	full	A battery stores up to 442 Wh
	Communications		
6.3	The system shall communicate with Earth	full	The probe uses an antenna that uses a X-Band signal with 7.51 GHz
6.4	The probe shall receive the Signal from DSN network	full	The phased - array antenna can achieve a gain of 19.5 dBe
	Structures and mechanisms		
6.5	The solarpanel needs to be deployed	full	2 tubes with 1.2 cm in diameter are inflated with nitrogen
6.6	The probe shall be damped to touch-down	full	The outer honeycomb structure damps up to 56.7 kJ and the seismometer honeycomb structure damps up to 2.3 kJ
6.7	The instrument box shall not plastically deform	full	The wall thickness and material provides enough structural strength to withstand landing up to 92 m/s
6.8	The penetrator shall penetrate the ground sufficiently	full	The penetrator gets at least 45 cm deep into the soil
	Payload		
6.9	The clock has to measure time and have a very stable frequency	full	The probe uses multiple atomic frequency standard that generates a signal with an Allan Deveation of 1*10^(-11) per hour
6.10	The seismometer needs to measure seismic activities effectively	full	The VBB-Seismometer can measure seismic activities due to natural impacts and Wind noise
	Command & Data Handling		
6.11	Computer has to store 7.2 GB Data between communication windows	full	The hard-drive can save up 256 GB
6.12	Validate and process commands	full	A processor deals with the data housekeeping
6.13	Code/decode data	full	A decoder is implemented
6.14	provide error checking	full	Software/ fault detection program deals with error checking

Figure 6.4: Compliance Matrix

Chapter 7
Conclusion

In this section the report is reviewed by concluding the resulting design and looking at recommendations. The conclusion looks into the requirements of the mission and how the design fulfills them. The recommendations focuses on future research and further detailing to the design.

7.1 Conclusion

The Mission Need Statement was formulated as *"gather conclusive evidence for the possible existence of plate tectonics on Mars"* in the beginning of the project. Using proven technology in combination with sufficient risk mitigation is an indication that the MNS is met by the current design.

The VLBI principle is a good foundation to perform ranging measurements and has been successfully used on Earth. Therefore, it is a suitable solution to the requirement to measure movement over large distances. The accuracy of this method can even be increased by using multiple measurements, which makes the mission feasible in that respect.

Using an penetrating concept with a seismometer, next to the primary mission that simply utilizes the communication subsystem, is a selling point of the design. It significantly increases the cost effectiveness of the mission. However, this unusual landing method places high risks on the mission and decreases the likelihood of the feasibility.

For the scientific community, the *Ancile* mission can be of high value. Providing conclusive evidence to the formation origin of Mars, including accurate images on the internals of Valles Marineris, is an important advancement in science.

7.2 Recommendations

The main areas in which the design is not fully completed should be the focus of further research. This includes more detailed analyses on risks, costs and feasibility. The probability of failure and the contingencies available are of high importance for the new concepts used in this design. A cost estimation based on references is limited in its accuracy, so further research in the available technology and production costs is useful. Finally, feasibility is dependent on multiple factors of the design and becomes more accurate as the design becomes more detailed.

After *Ancile* is accepted by the customer, extensive testing of the design is required. As mentioned above, the unusual concepts used on this mission will need to be proved to work under all mission circumstances. The main areas of focus should be the transfer details, the probe release procedure, the inflatable heat shields, the landing method and the seismometer utilization.

Appendix A: Project Organization and Design & Development Logic

The Project Organization and Design & Development Logic explains how the team was generally divided, and how the project developed by moving around the resources that are available. The group comprises of nine aerospace students, and there are three general design teams, i.e. the *probe design team*, the *EDL design team* and the *transfer module design team*.
The task of the probe team is to design the probe, consisting of the scientific payload, the structural integrity and all the supporting systems, e.g. power and thermal control. The team also modeled the maximum stresses experienced by the structure of the probe during the high impact loading. Ultimately, the goal was to achieve the mission objectives and generated the requirements for the other design teams. Hence the probe was the first design that needed to be finalized.

The EDL team details the systems that are needed to comply with the requirements set by the probe design team, e.g. the landing angle and the impact velocity. The EDL team programmed a descending tool to model the entire entry, descent and landing the probe will experience once it reaches the Martian atmosphere.

The transfer module team designed the Hohmann transfer orbit and its launch window, specified the subsystems on the transfer module and the calculated the probe release mechanics. The team also modeled the trajectory from the moment the transfer module enters the sphere of influence of Mars till it reaches the Martian atmosphere.

Appendix B: Gantt Chart

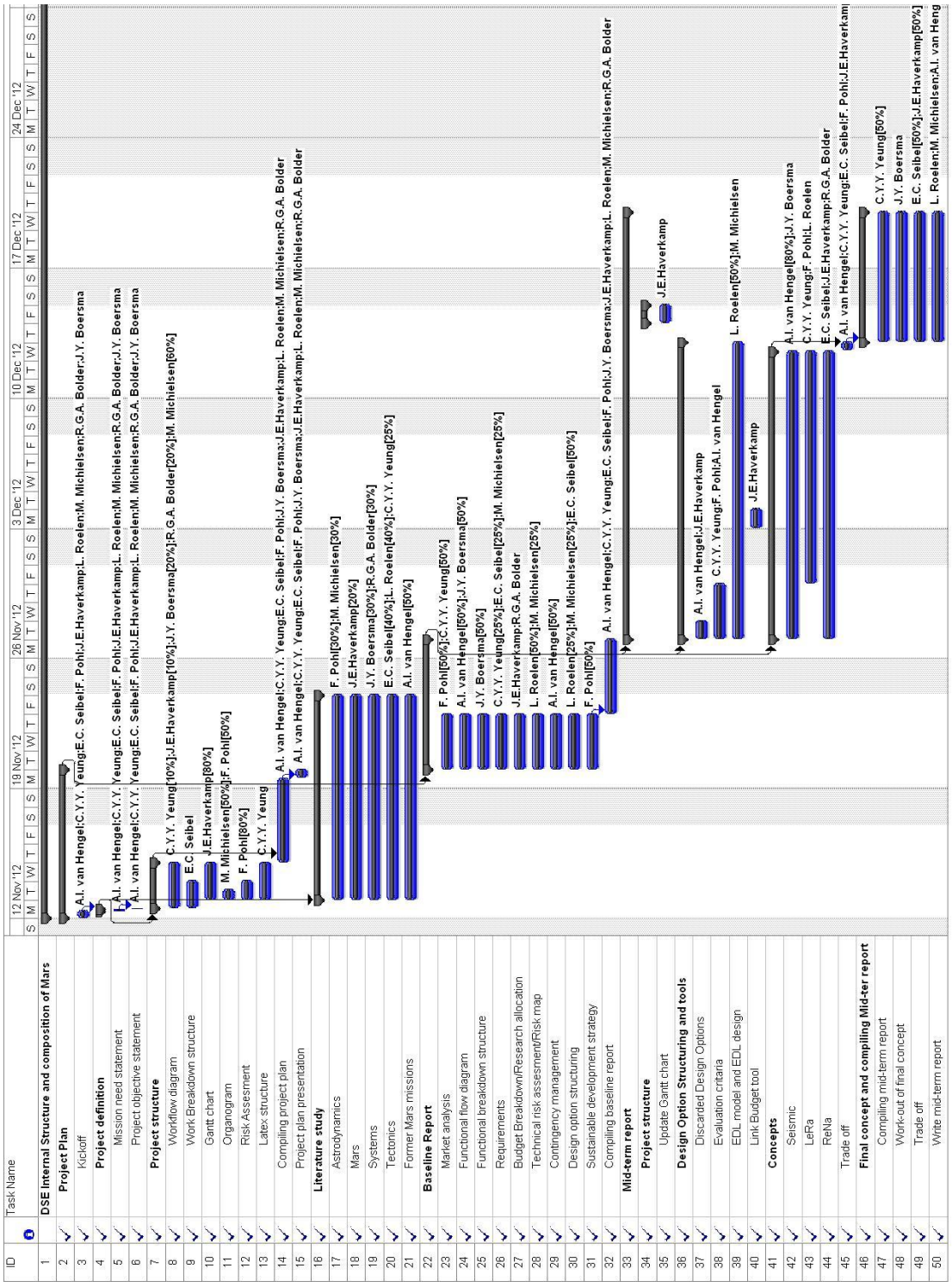

Figure 7.1: Gantt chart, part 1

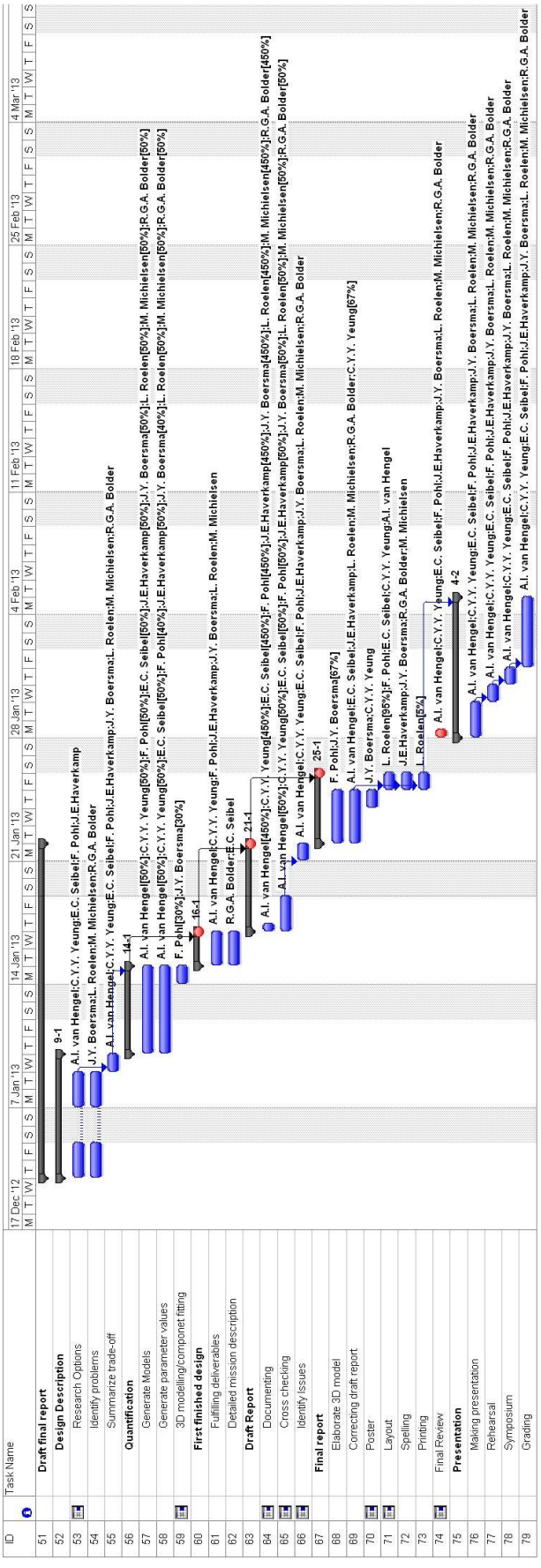

Figure 7.2: Gantt chart, part 2

Appendix C: List of Authors

Chapter	Section		Author
		Front Page	Chee
		Preface	Franz
		Summary	Emily
1		**Introduction**	Marijn
2		**Mission description**	
	2.1	Scientific goals	Emily & Robin
	2.2	Functional Flow Diagram	Emily
	2.3	Functional Breakdown Structure	Emily
	2.4	Market Analysis	Franz
	2.5	Mission Description	Emily
3		**Mission Operations**	
	3.1.1	Primary Mission	Robin
	3.1.2	Secondary Objectives	Emily
	3.2	Scenario Analysis	Robin & Emily
	3.3.1	Accuracy - Primary Objectives	Robin
	3.3.2	Accuracy - Secondary Objectives	Emily
4		**Probe**	
	4.1	Probe Design Description	Chee & Marijn
	4.2	Communications	Jorn
	4.3.1	Atomic Frequency Standard	Jorn
	4.3.2	Seismometer	Emily
	4.4	Penetration Depth and Pin Design	Jorn
	4.5.1	Requirements	Liselot
	4.5.2	Solar Panel Design	Liselot
	4.5.3	Effects of Wind	Liselot
	4.5.4	Electrodynamic Dust Shield	Liselot
	4.5.5	Energy Storage	Jorn
	4.5.6	Power Regulation	Jorn
	4.6	Crushable Honeycomb Structure	Chee
	4.7	Thermal Control	Liselot & Jorn
	4.8.1	Command and Data Handling System	Liselot & Jorn
	4.8.2	Hardware - Software Block Diagram	Robin
	4.8.3	Data Handling Block Diagram	Robin
	4.9	Layout	Liselot & Jorn
	4.10	Instrument Box	Chee
5		**Earth-Mars Transfer**	
	5.1	Launch	Franz
	5.2	Transfer Module	Anita
	5.3	Transfer Orbit	Franz
	5.4.1	Probe Release	Jelle
	5.4.2	Despinning	Emily
	5.4.3	Inflation of Heat Shield	Marijn
	5.5.1	Subsystems	Franz & Marijn
	5.5.2	Entry Conditions	Marijn
	5.5.3	Entering Martian Atmosphere	Marijn
	5.5.4	Verification and Validation	Marijn
	5.5.5	Landing	Marijn
	5.5.6	Trajectory Optimisation	Marijn

Chapter	Section	Author
6	**System Analysis**	
6.1	Risk Assesment	Liselot & Marijn
6.2	Sensitivity Analysis	Anita
6.3	Resource Allocation	Jorn
6.4	Sustainable Development Strategy	
6.5	Compliance Matrix	Franz
7	**Conclusion**	Jelle
A	**Project Organisation**	Chee
B	**Gantt Chart**	Jorn
C	**List of Authors**	Robin & Jorn

Other Contributions	**Author**
3D Model Transfer Module	Jelle
3D Model Probe	Franz
Poster Design	Chee

Bibliography

[1] Electrodynamic dust shield technology. URL: http://physics.ksc.nasa.gov/CurrentResearch/ElectrodynamicScreen/Electrodynamic.htm.

[2] Encyclopedia astronautica atlas v. URL: http://www.astronautix.com/lvs/atlasv.htm.

[3] Esa die europische weltraumorganisation. URL: http://www.fundus.org/pdf.asp?ID=12666.

[4] Keeping the rover warm through heaters. URL: http://marsrover.nasa.gov/mission/sc_rover_temp_heaters.html.

[5] Mars, facts and information about the planet mars. URL: http://www.space.com/47-mars-the-red-planet-fourth-planet-from-the-sun.html.

[6] Seismometers. URL: http://www.guralp.com/product-range/seismometers/.

[7] Solar radiation in space. URL: http://pveducation.org/pvcdrom/properties-of-sunlight/solar-radiation-in-space.

[8] Spiral orbits using electric thrust. URL: http://forum.nasaspaceflight.com/index.php?topic=25045.5;wap2.

[9] Wind effects on mars. URL: http://cseligman.com/text/planets/marswind.htm.

[10] Historical log, 2011. URL: http://mars.jpl.nasa.gov/programmissions/missions/log/.

[11] Fiscal year 2013 budget estimates, 2012. URL: http://www.nasa.gov/pdf/622986main%5C_FY%5C_13%5C_summary%5C_Budget%5C_Briefing%5C_Master%5C_Files%5C_final%5C_2%5C_14%5C_12.pdf.

[12] Technology brief single cell, December 2012. URL: http://www.altadevices.com/pdfs/single_cell.pdf.

[13] Flexible solar cells: Rollable series, 2013. URL: http://www.flexsolarcells.com/Rollable_Series.php.

[14] M. Alexander. Mars transportation environment definition document. 2001.

[15] U. L. Alliance. *Delta IV Guide*. United Launch Alliance, 2007.

[16] D. Anderson, W. Miller, G. Latham, Y. Nakamura, M. Toksoz, A. Dainty, F. Duennebier, A. Lazarewicz, R. Kovach, and T. Knight. Seismology on mars. *Journal of geophysical Research*, 82(28):4524–4546, 1977.

[17] J. Anderson. *Fundamentals of Aerodynamics*. Mc Graw Hill, fourth edition, 2007.

[18] J. Beish. A trend analysis for predicting dust storms on mars. URL: http://www.alpo-astronomy.org/jbeish/MetTrendDust.htm.

[19] R. Bendura, E. K. Huckings, and L. C. Coltrane. Performance of a 19.7-meter-diameter disk-gap-band parachute in a simulated martian environment. *National Aeronautics and Space Administration*, 1968.

[20] S. Bernard. Depth and motion prediction for earth penetrators. Technical report, U.S. Army Engineer Waterways Experiment Station Soils and Pavements Laboratory, 1978.

[21] P. Blau. Ariane 5-eca launch vehicle. URL: http://www.spaceflight101.com/ariane-5-eca.html.

[22] P. R.-M. Bonnet and P. J.-P. Swings. *The Aurora Program*. ESA, 2004.

[23] R. D. Braun and R. M. Manning. Mars exploration entry, descent and landing challenges. *American Institute of Aeronautics and Astronautics*, 2010.

[24] D. Byrnes, J. Longuski, and B. Aldrin. *Cycler Orbit Between Earth and Mars*. AIAA, 1993.

[25] C. Calle, C.R.Buhler, M.R.Johansen, M.D.Hogue, and S.J.Snyder. Active dust control and mitigation technology for lunar and martian exploration. *Acta Astronautica*, 69:7, 2011.

[26] C. Calle, M. Mazumder, C. Immer, C. Buhler, J. Clements, P. Lundeen, A. Chen, and J. Mantovani. Controlled particle removal from surfaces by electrodynamic methods for terrestrial, lunar, and martian environmental conditions. *Journal of Physics: Conference Series*, 142:7, 2008.

[27] C. e. a. Calle. Electrodynamic dust shield for solar panels on mars. *Lunar and Planetary Science*, 35:2, 2004.

[28] B. Campbell, editor. *So You Want to Do VLBI*. JIVE, 1999. URL: `http://www.jive.nl/~campbell/jvs2.pdf`.

[29] L. Colin. The pioneer venus program. *Journal of Geophysical Research*, 85:7575–7598, 1980.

[30] A. Curtis, P. Gerstoft, H. Sato, R. Snieder, and K. Wapenaar. Sismic interferometry-turning noise into signal. URL: `http://geodus1.ta.tudelft.nl/PrivatePages/C.P.A.Wapenaar/4_Journals/The_Leading_Edge/tle_06.pdf`.

[31] P. M. Davis. Meteoroid impacts as seismic sources on mars. URL: `http://www.sciencedirect.com/science/article/pii/S0019103583711425`.

[32] J. DeNatale, R. Borwick, C. Tsai, P. Stupar, Y. Lin, R. Newgard, R. Berquist, and M. Zhu. Compact, low-power chip-scale atomic clock. *IEEE Xplore*, 3:67–70, 2008.

[33] R. Dillman, N. Cheatwood, S. Hughes, J. D. C. R. Bodkin, and A. Olds. Planned flight of the inflatable re-entry vehicle experiment 3 (irve-3). *8th International Planettary Probe Workshop*, 2011.

[34] doengi. Lander shock-alleviation techniques. URL: `http://www.esa.int/esapub/bulletin/bullet93/DOENGI.pdf`.

[35] A. M. Dwyer. *Modeling the Mars Atmosphere for Monte Carlo Simulations of the Mars 2001 Odyssey Aerobreaking Mission*. PhD thesis, George Washington University, 2001.

[36] C. D. Eagle. *The Hohmann Orbit Transfer*. CDeagle, 2012.

[37] ESA. *ESA budget for 2010*. ESA, 2009.

[38] ESA. *ESA Programmes with Czech participation*. ESA, 2009.

[39] ESA. Die esa: Fakten und zahlen. ESA, 2012. URL: `http://www.esa.int/ger/ESA_in_your_country/Germany/Die_ESA_Fakten_und_Zahlen`.

[40] FAA. Returning from space: Re-entry. URL: `http://www.faa.gov/other_visit/aviation_industry/designees_delegations/designee_types/ame/media/Section%20III.4.1.7%20Returning%20from%20Space.pdf`.

[41] J. V. Fedor. Analyticaltheoryof the stretch for de-spin of satellites. page 19, April 1963.

[42] J. Frank and J. Richards. *Radar Handbook*. Mc Graw Hill, 2008.

[43] L. George and L. Kos. *Interplanetary Mission Design Handbook:*. Nasa, 1998.

[44] R. Grabow. Ablative heat shielding for spacecraft re-entry, December 2006. URL: `http://courses.ucsd.edu/rherz/mae221a/reports/Grabow_221A_F06.pdf`.

[45] E. Grayzeck. Mars fact sheet, 2010. URL: `http://nssdc.gsfc.nasa.gov/planetary/factsheet/marsfact.html`.

[46] e. a. Green, M. A. Solar cell efficiency tables (version 40). *Progress in Photovoltaics: Research and Applications*, 2012.

[47] M. Green. The heat is on, 2012. URL: `http://www.nasa.gov/offices/oct/stp/game_changing_development/HIAD/heat-is-on.html`.

[48] C. Guiar. Antenna pointing systematic error model derivations. *TDA progress report*, 1:42–88, 1986.

[49] L. Gurvits. Personal conversation with mr. l. gurvits, January 2013.

[50] R. Haas and A. Nothnagel. Crustal motion in europe determined with geodetic very long baseline interferometry. 1998.

[51] J. Henry J. Cornille. A method of accurately reducing the spin rate of a rotating spacecraft. page 7, 1962.

[52] G. Holtkamp. *Space budgets*. Scilogs, 2010.

[53] S. Interplanetary. Star sensor. URL: `http://www.sinclairinterplanetary.com/startrackers`.

[54] S. Interplanetary. Sun sensor. URL: `http://www.sinclairinterplanetary.com/digitalsunsensors`.

[55] E. Jung, J. Lee, T. Lee, and W. Lee. Siw-based array antennas with sequential feeding for x-band satellite communication. *IEEE transactions on antennas and propagation*, 60:3632–3639, 2012.

[56] A. R. Lazarewicz, D. L. Anderson, K. Anderson, A. M. Dainty, F. K. Duennebier, N. R. Goins, T. C. D. Knight, R. L. Kovach, G. V. L. W. F. Miller, Y. Nakamura, G. H. Sutton, and M. N. Toksoz. The viking seismometry final report. Technical report, NASA, 1981. URL: `http://ntrs.nasa.gov/archive/nasa/casi.ntrs.nasa.gov/19810013458_1981013458.pdf`.

[57] M. C. Lindell, S. J. Hughes, M. Dixo, and C. E. Willey. Structural analysis and testing of the inflatable re-entry vehicle experiment (irve). *American Institute of Aeronautics and Astronautics*, 47th Structures, Structural Dynamics and Materials Conference, 2006.

[58] D. Litton, D. Bose, A. Olds, S. Hughes, and S. Derry. Inflatable re-entry vehicle experiment (irve) - 4 overview. *American Institute of Aeronautics and Astronautics*, 21st AIAA Aerodynamic Decelerator Systems Technology Conference and Seminar, 2011.

[59] M. Lombardi. *Fundementals of Time and Frequency*. CRC Press LLC, 2002.

[60] K. Masters. How much money is spent on space exploration?, 2005. URL: `http://curious.astro.cornell.edu/question.php?number=684`.

[61] Mastervolt. *Lithium-Ion battery*.

[62] D. J. McCleese. *Robotic Mars Exploration strategies*. Nasa, 2006.

[63] M. MOONS. Review of the dynamics in the kirkwood gaps. URL: `http://download.springer.com/static/pdf/332/art%253A10.1007%252FBF00048446.pdf?auth66=1360323444_ec12ed7702b5f2c576b1eec9804e5131&ext=.pdf`.

[64] NASA. Mars pathfinder nasa facts. URL: `http://www.jpl.nasa.gov/news/fact_sheets/mpf.pdf`.

[65] NASA. Nozomi. URL: `http://solarsystem.nasa.gov/missions/profile.cfm?MCode=Nozomi&Display=ReadMore`.

[66] NASA. What is the spacespace? URL: `http://marsrovers.jpl.nasa.gov/mission/spacecraft.html`.

[67] NASA. What is the temperature of space? NASA. URL: `http://www.nasa.gov/pdf/379068main_Temperature_of_Space.pdf`.

[68] NASA. Mars science laboratory: Curiosity rover, 2012. URL: `http://mars.jpl.nasa.gov/msl/mission/spacecraft/cruiseconfig/`.

[69] U. Nations. 1472 (xiv). international co-operation in the peaceful uses of outer space, 1959. URL: `http://www.unoosa.org/oosa/SpaceLaw/gares/html/gares_14_1472.html`.

[70] Newsat. *Die europische Weltraumorganisation ESA: Ihre Mitglieder und Mitarbeiter, ihr Budget.* ESA, 2007.

[71] H. Nicolson, A. Curtis, B. Baptie, and E. Galetti. Seismic interferometry and ambient noise tomography in the british isles. URL: `http://www.geos.ed.ac.uk/homes/acurtis/Nicolson_etal_PGA_2012.pdf`.

[72] R. Noomen. Flight and orbital mechanics. Lecture Notes, October 2010.

[73] M. Okutsu and J. M. Longuski. *Mars Free Returns via Gravity Assist from Venus.* Purdue University, 2002.

[74] Panasonic. *Overview of Lithium Ion Batteries*, Januari 2007.

[75] F. Pecal, N. Paulin, D. Mimoun, and G. Pont. Mechanical design of a multi-axis martian seismometer. page 17, 2006.

[76] D. A. Pechev. Reentry dynamics. Powerpoint.

[77] P. A. Penzo. *Mission Design for Mars Missions Using the Ariane ASAP Launch Capability.* AIAA, 1999.

[78] E. Perez. *Ariane 5 Users Manual.* Arianespace, 2011.

[79] J. Poco. Labs aerogel sets world record, October 2003. URL: `https://www.llnl.gov/str/October03/NewsOctober03.html`.

[80] D. Rapp. *Solar Energy on Mars*, volume 1. Jet Propulsion Laboratory California Institute of Technology, 2004.

[81] S. Reza, R. Hund, F. Kustas, W. Willcockson, J. Songer, and G. Brown. Aerocapture inflatable decelerator (aid) for planetary entry. *American Institute of Aeronautics and Astronautics*, 19th Aerodynamic Decelerator Systems Technology Conference and Seminar, 2007.

[82] J. Romney. *Very long baseline interferometry and the VLBA.* San Francisco: Astronomical Society of the Pacific, 1995.

[83] J. D. I. Ronald Greeley. *Wind as a geological process.* Cambridge Planetary Science series.

[84] M. D. Sacchi. Introduction to seismic imaging (refraction and reflection seismology). URL: `http://www.ualberta.ca/~msacchi/GWS2012/seismic_introduction.pdf`.

[85] P. Sarti, M. Negusini, and C. Abbondanza. Improved geodetic european very-long-baseline interferometry solution using models of antenna gravitational deformation. *Annals of Geophysics*, 53(5-6):13–23, 2011. URL: `http://www.annalsofgeophysics.eu/index.php/annals/article/view/4739`.

[86] R. Scheid. Precsion pointing compensation for dsn antennas with optical distance measuring sensors. *TDA progress report*, 1:42–97, 1989.

[87] B. Schutz, B. Tapley, and G. Born. *Statistical orbit determination.* Academic Press, 2004.

[88] M. Seibert, H. J., and D. ElDeeb. Operations strategies for the mars exploration rovers during the 2007 martian global dust storm. *Aerospace conference*, 1:1–7, 2009.

[89] Sercel, 16 rue de Bel-Air, B.P. 30439. 44474 CARQUEFOU Cedex. *Analog Seismic Sensors*, 2012.

[90] S. Steward and G. Valiant. Martian subsurface properties and crater formation processes inferred from fresh impact crater geometries. *Meteoritics & Planetary Science 41*, 10:1509–1537, 2006.

[91] S.Tillier, S. de Raucourt, P. Lognonn, T. Nbut, O.Robert, T.Gabsi, B.Lecomte, O.Pot, J. Gagnepain-Beyneix, and D.Mimoun. A martian and lunar very broad band seismometer. page 8, 2011.

[92] I. The Aluminum Association. Aluminum standards and data 2000. URL: http://asm.matweb.com/search/SpecificMaterial.asp?bassnum=MA7075T6.

[93] A. Thompson, J. Moran, and G. Swenson Jr. *Interferometry and synthesis in radio astronomy*. Wiley-Vch, 2004.

[94] J. R. Wertz and W. J. Larson. *Space Mission Analysis and Design*. Space Technology Library, 1999.

[95] M. Wilkins. *Atlas V Launch Services Users Guide*. United Launch Alliance, 2010.

[96] Y. Xu and F. Guan. Structure design and mechanical measurement of inflatable antenna. *Acta Astronautica*, 76:13–25, 2012.

[97] A. Yin. Structural analysis of the valles marineris fault zone: Possible evidence for large-scale strike-slip faulting on mars. *Lithosphere*, 4(4):286–330, 2012. URL: http://www.lithosphere.geoscienceworld.org/content/4/4/286.short.